

The Natural Rate of Interest in the Euro Area: Evidence from Inflation-Indexed Bonds

Jens H. E. Christensen[†]

&

Sarah Mouabbi[‡]

Abstract

The natural rate of interest, widely known as r_t^* , is a key variable used to judge the stance of monetary policy. We offer a novel euro-area r_t^* estimate based on a dynamic term structure model estimated directly on the prices of bonds with cash flows indexed to the euro-area harmonized index of consumer prices with adjustments for bond-specific risk and real term premia. Despite a recent increase, our estimate indicates that the natural rate in the euro area had fallen about 2 percentage points on net in the 2002-2021 period. We also devise a related measure of the stance of monetary policy, which suggests that monetary policy in the euro area was not accommodative at the height of the COVID-19 pandemic.

JEL Classification: C32, E43, E52, G12

Keywords: affine arbitrage-free term structure model, financial market frictions, convenience premium, monetary policy, rstar

We thank participants at the Second ESM Workshop on Economic Modelling in Policy Institutions, the 13th Bundesbank Term Structure Workshop, and the European Commission Workshop on the Monetary and Fiscal Policy Mix in a Changing World for helpful comments, including our discussants Peter Hördahl, Daniel Monteiro, and Andreea Vladu. Furthermore, we thank seminar participants at the Swiss National Bank, the Banque de France, the European Banking Authority, the European Central Bank, the Danish National Bank, the National Bank of Belgium, the Bank of England, the Board of Governors, Aarhus University, and Universidad Técnica Federico Santa María for helpful comments. Moreover, we thank Jean-Paul Renne and Timo Reinelt for helpful comments and suggestions. Finally, we thank Gus Kmetz and Caroline Paulson for excellent research assistance. The views in this paper are solely the responsibility of the authors and should not be interpreted as reflecting the views of the Federal Reserve Bank of San Francisco or the Federal Reserve System, or those of the Banque de France or the Eurosystem.

[†]Corresponding author: Federal Reserve Bank of San Francisco, 101 Market Street MS 1130, San Francisco, CA 94105, USA; phone: 1-415-974-3115; e-mail: jens.christensen@sf.frb.org.

[‡]Banque de France; e-mail: sarah.mouabbi@banque-france.fr.

This version: October 30, 2025.

1 Introduction

The so-called natural rate of interest, widely known as r_t^* , is a key variable in finance and macroeconomic theory. For investors, the steady-state level of the real short-term interest rate serves as an anchor for projections of the future discount rates used in valuing assets (e.g., Clarida 2014). For policymakers and researchers, the natural rate of interest is a policy lodestar that provides a neutral benchmark to calibrate the stance of monetary policy: Monetary policy is expansionary if the real short-term interest rate lies below the natural rate and contractionary if it lies above. A good estimate of the natural rate is also necessary to operationalize popular monetary policy rules such as the Taylor rule. For fiscal policy, the natural rate of interest is instrumental to assessing the sustainability of public finances in the long run. More broadly, in the decades prior to the COVID-19 pandemic, the possibility of a lower new normal for interest rates was at the center of key policy debates about bond market conundrums, global saving gluts, and secular stagnation.¹ More recently, the post-pandemic spike in interest rates globally has given rise to intense policy debates about whether interest rates will hold steady at the new higher levels or revert back towards their pre-pandemic lows.² In short, the natural rate of interest is a variable of immense importance.

Unfortunately, despite its importance, the natural rate of interest is not directly observable. Instead, it has to be inferred from economic data. In the literature, most estimates of the natural rate are drawn from *macroeconomic* models and data, including the widely cited Laubach and Williams (2003) model. In this paper, we follow Christensen and Rudebusch (2019, henceforth CR) and use *financial* models. Specifically, we rely on bond prices denominated in euros and indexed with the harmonized index for consumer prices (HICP) for our analysis and therefore offer a euro-area perspective on recent trends in the natural rate of interest.

To further motivate our focus on the euro area, we note that euro-area yield data are unique in that the European Central Bank (ECB) is a major central bank that has gone far in exploring the true lower bound for its key policy rate. One relevant policy question is therefore whether this extreme policy choice has caused the natural rate to be lower in the euro area than in other advanced economies. Alternatively, the causation could run in the other direction, namely that the ECB was forced to pursue what might appear to be an extremely accommodative stance of monetary policy *because* the natural rate in the euro area was already really low. We will attempt to provide an answer to this important question, which is likely to also have major implications for what to expect going forward in the post-pandemic world.

¹See, for example, Greenspan (2005), Bernanke (2005), and Summers (2014, 2015), respectively, on these three debates.

²See, for example, Blanchard (2023) and Summers (2023).

The bonds we consider have coupon and principal payments indexed to the HICP (ex tobacco) and provide compensation to investors for the erosion of purchasing power due to price inflation in the euro area as a whole.³ Therefore, their prices can be expressed directly in terms of real yields. The basic premise of our analysis is that the longer-term expectations embedded in these bond prices reflect financial market participants' views about the steady state of the euro-area economy, including its natural rate of interest.

To provide the cleanest possible read on investors' expectations for the natural rate in the euro area, we limit our focus to bonds issued by the French government. In principle, we could have included bonds indexed to HICP (ex tobacco) issued by other euro-area countries such as Germany, Italy, or Spain,⁴ but it would complicate the analysis in terms of accounting for differences in credit and liquidity risks across these different markets and with few apparent benefits, in particular it would *not* provide us with a longer sample for our analysis.

The French government first issued bonds indexed to the HICP (ex tobacco), known as OAT€, in October 2001. However, given that we need at least two bonds to be trading, we start our analysis in October 2002. This long sample allows us to provide a 20-year perspective on the components that have influenced euro-area real yields in recent decades. Besides its length, this sample choice offers additional advantages. First, France has deep and liquid markets for government debt. Second, with maturities of up to 33 years, the OAT€ market contains the farthest forward-looking information among all the inflation-indexed bond markets in the euro area and hence is likely to provide the clearest evidence for the question at hand. Third, by relying on inflation-indexed bonds, we avoid any issues related to the effective lower bound that applies to the ECB's policy rate and other nominal interest rates. Furthermore, as the underlying factors affecting long-term interest rates are likely global in nature—such as worldwide demographic shifts or changes in productivity trends—the euro-area government bond market in general, and the French government bond market specifically, may well be as informative as any other major sovereign bond market. Finally, the French government held a AA credit rating from all major rating agencies during our sample period, which ends in December 2022. Hence, there is a minimum of credit risk to account for in our French bond price data.

Despite all these advantages the use of inflation-indexed bonds for measuring the natural rate of interest entails its own empirical challenges. One problem is that inflation-indexed bond prices include a real term premium. Given the generally upward slope of the OAT€ yield curve, the real term premium is presumably usually positive. However, little is known with certainty about its size or variability. In addition, despite the fairly large notional amount

³HICP is the price index targeted by the ECB for monetary policy purposes, but for historical reasons the HICP-indexed bonds issued in the euro area reference HICP (ex tobacco); see Ejsing et al. (2007).

⁴See Christensen et al. (2025) for an analysis of the limited universe of German inflation-linked government bonds indexed to the HICP (ex tobacco).

of outstanding OAT€s, these securities face unique market risks due to high demand from institutional investors such as pension funds and life insurance companies.⁵

To estimate the natural rate of interest in the presence of market risk and real term premia, we use an arbitrage-free dynamic term structure model of real yields augmented with a bond-specific risk factor. The identification of the bond-specific risk factor comes from its unique loading for each individual bond security as in Andreasen et al. (2021, henceforth ACR). Our analysis uses prices of individual bonds rather than the more usual input of yields from fitted synthetic curves. The underlying mechanism assumes that, over time, an increasing proportion of the outstanding inventory is locked up in buy-and-hold investors’ portfolios. Given forward-looking investor behavior, this lock-up effect means that a particular bond’s sensitivity to the market-wide bond-specific risk factor will vary depending on how seasoned the bond is and how close to maturity it is. In a careful study of nominal U.S. Treasuries, Fontaine and Garcia (2012) find a pervasive bond-specific factor that affects all bond prices, with loadings that vary with the maturity and age of each bond. By observing a cross section of bond prices over time—each with a different time-since-issuance and time-to-maturity—we can identify the overall bond-specific risk factor and each bond’s loading on that factor. This technique is particularly useful for analyzing inflation-indexed debt when only a limited sample of bonds may be available, for example early in our sample.⁶

The theoretical arbitrage-free formulation of the model also provides identification of a time-varying real term premium in the pricing of OAT€s. Identifying the bond-specific risk premium and real term premium allows us to estimate the underlying frictionless real rate term structure and the natural rate of interest, which we measure as the average expected real short rate over a five-year period starting five years ahead—consistent with the longer-run perspective emphasized by Laubach and Williams (2016). Our preferred estimate of the natural rate of interest, r_t^* , is shown in Figure 1 along with ten-year nominal and real yields.⁷ Both nominal and real long-term yields in the euro area trended down together during the 2002-2021 period, and this concurrence suggests little net change in inflation expectations or the inflation risk premium during that 20-year period. The estimated natural rate fell from above 1.5 percent to below -1.5 percent by the end of 2021, before retracing some of that decline during 2022. Accordingly, our results show that more than 75 percent of the 4-percentage-point decline in longer-term yields by the end of 2021 represents a reduction in the natural rate of interest. Our model estimates also indicate that about 75 percent of

⁵OAT€s also provide protection against net deflation over the life of each bond. However, the value of this protection is likely to be low and is therefore not considered; see Christensen and Mouabbi (2023).

⁶Finlay and Wende (2012) examine prices from a limited number of Australian inflation-indexed bonds but do not account for bond-specific liquidity or convenience premia.

⁷These yields are constructed using a model of French standard nominal government bonds, known as OATs, and a separate model of French OAT€ prices, each estimated directly on the observed bond prices as advocated by Andreasen et al. (2019).

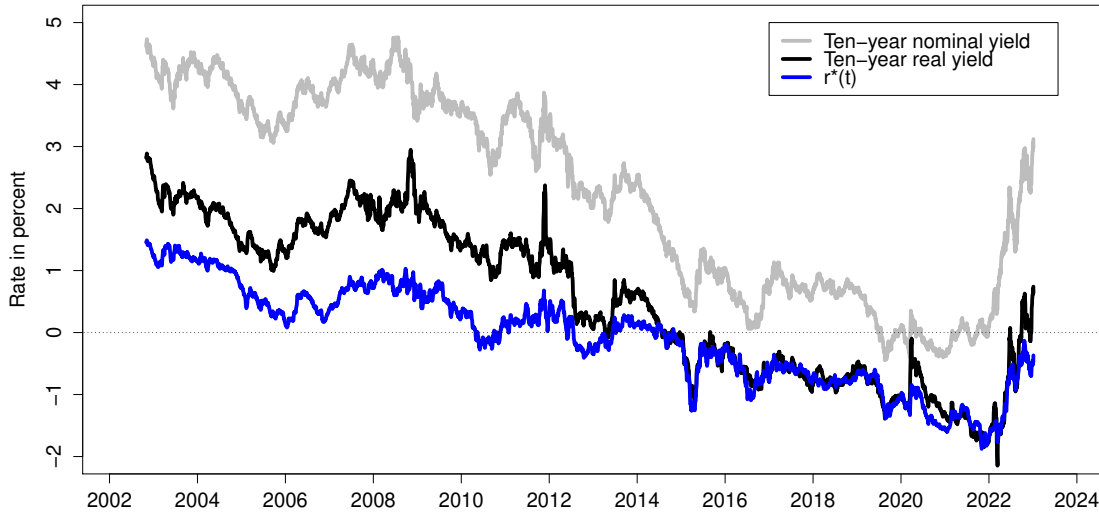


Figure 1: **Long-Term Nominal and Real Yields and an Estimate of r^***

Ten-year nominal and real yields and our preferred AFNS-R model estimate of the equilibrium real short rate, r_t^* , i.e., the 5- to 10-year risk-neutral real rate.

the interest rate increases the last year of our sample reflect increases in the natural rate of interest. However, model projections suggest that the natural rate of interest is likely to revert only very gradually towards its old mean in the years ahead. Thus, policy rates in the euro area may return to levels close to the effective lower bound during economic downturns once the economy moves past the recent spell of high inflation. Finally, to evaluate the model more fully, we note that we perform our analysis using daily data. This allows us to examine the impact of specific events and policy announcements relying on established high-frequency event-study technology for identification, e.g. as in Christensen and Rudebusch (2012), with two applications described in the following.

In the literature, it is an unsettled question whether monetary policy can affect the level of the natural rate. In many standard macro models such as the widely used three-equation New Keynesian model, r_t^* is a conditioning variable unaffected by the decisions of the monetary authority. Empirically, though, there is evidence to suggest that monetary policy may be able to affect the level of long-term real rates; see Hanson and Stein (2015) and Hillenbrand (2025) for examples. In turn, this evidence has motivated macro models with mechanisms through which monetary policy can affect long-term real rates in a persistent manner.⁸ To speak to this question, we replicate the analysis in Hillenbrand (2025), who study the impact on

⁸For example, Beaudry et al. (2025) analyze a heterogenous-agent model with workers saving for retirement in which monetary policy can persistently affect long-term real rates.

long-term U.S. Treasury yields around FOMC meetings since the early 1980s and document persistent declines in long-term interest rates during those narrow event windows. Using our daily r_t^* estimate for the euro area, we find that about half of its decline in the twenty years since 2002 has occurred during those narrow FOMC windows. We interpret this as evidence of international spillover effects from U.S. monetary policy to euro-area financial markets. We then use the same approach, but focus on narrow windows around the meetings of the governing council of the ECB. Surprisingly, we detect no persistent effects, and this conclusion applies to both short one-day event windows and longer three-day event windows. Based on this evidence, we conclude that the monetary policy of the ECB does not appear to have had any lasting impact on the natural rate in the euro area, unlike its U.S. counterpart.

In a recent paper, Somogyi et al. (2025) highlight the role of the demand for safe assets for long-term interest rates as revealed through the outcomes of U.S. Treasury auctions. Specifically, they find that a significant part of the decline in U.S. long-term interest rates since the mid-1990s has occurred during narrow windows around U.S. Treasury note and bond auctions. We replicate their exercise using our r_t^* estimate for the euro area and find that about two thirds of its decline in the 2002-2021 period occurred during their set of narrow auction windows. This points to safe-asset demand as another likely factor depressing long-term real rates in the euro area. However, we leave it for future research to examine that relationship further.

As a separate contribution and to further demonstrate the applicability of our model for economic analysis, we use it to devise market-based measures of the stance of monetary policy in the euro area. This is achieved by deducting our r_t^* estimate from observed measures of one-year real yields. We consider the latter to be a reasonable proxy for the theoretically ideal, but unobserved, instantaneous real short rate r_t appearing in textbook formulas of the stance of monetary policy measured as the gap between the current real short-term interest rate and its natural level. The results indicate that it took significant time for monetary policy in the euro area to reach an accommodative stance during both the Global Financial Crisis (GFC) and the COVID-19 pandemic.

We further validate our estimate of the stance of monetary policy by comparing it with a text-based measure introduced by Hubert and Portier (2024), who use machine learning techniques to analyze the statement and transcript of the press conference following each ECB governing council meeting since 2001. Although similar most of the time, the market- and text-based measures of the policy stance deviate during three key periods, namely the European Sovereign Debt Crisis, the COVID-19 pandemic, and the post-pandemic economic reopening characterized by highly elevated inflation. During the first and last of these three episodes, text-based analysis points to a hawkish posture among policymakers, while our market-based measure suggests that monetary policy was in fact quite accommodative. In

contrast, policymakers clearly tried to achieve an accommodative stance for policy through their communications in response to the COVID-19 pandemic. However, our market-based measure suggests that policy did not become accommodative until into 2021. Thus, our results underscore the challenges of central bank communication during times of crisis. At the same time, though, our market-based measure of the stance of monetary policy offers a way to examine in real time to what extent investors’ and financial market participants’ perceptions about the stance of monetary policy is aligned with the one communicated by policymakers. Hence, we see our measure as a potentially important complement to existing policy tools going forward, but we leave it for future research to examine its usefulness for this purpose.

Our analysis focuses on a real term structure model that only includes the prices of inflation-indexed bonds. This methodology contrasts with most previous term structure research in two ways. First, previous term structure models are almost universally estimated not on observed bond prices but on synthetic zero-coupon yields obtained from fitted yield curves. Fontaine and Garcia (2012) argue that the use of such synthetic yields can erase useful information on bond-specific price effects, and they provide a rare exception of the estimation of a term structure model with bond prices. More generally, the use of interpolated yield curves in term structure analysis can introduce arbitrary and unnecessary measurement error.⁹ A second difference is that past analysis of inflation-indexed bonds has jointly modeled both the real and nominal yield curves, e.g., Christensen et al. (2010), Abrahams et al. (2016), and D’Amico et al. (2018) for the United States and Joyce et al. (2010) and Carriero et al. (2018) for the United Kingdom. Such joint specifications can also be used to estimate the steady-state real rate—though this earlier work has emphasized only the measurement of inflation expectations and risk premia.¹⁰ Relative to our procedure of using just inflation-indexed bonds to estimate the natural rate, including both real and nominal yields has the advantage of being able to estimate a model on a much larger sample of bond yields. However, a joint specification also requires additional modeling structure—including specifying more pricing factors, an inflation risk premium, and inflation expectations. The greater number of modeling elements—along with the requirement that this more elaborate structure remains stable over the sample—raises the risk of model misspecification, which can contaminate estimates of the natural rate and model inference more generally. In particular, if the inflation components are misspecified, the whole dynamic system may be compromised, a valid concern in the recent high-inflation environment. Furthermore, during the 2009-2021

⁹Dai et al. (2004) found notable differences in empirical results across four different yield curve interpolation schemes. For further discussion of these issues; see Andreassen et al. (2019).

¹⁰Joyce et al. (2012) use dynamic term structure models of U.K. index-linked government bond yields to study long-term real rate expectations while accounting for real term premia though not bond-specific risk or liquidity premia.

period when the ECB kept its policy rate close to its effective lower bound, the dynamic interactions of short- and medium-term *nominal* yields were likely affected. Such a constraint is very difficult to include in an empirical term structure model of nominal yields (see Swanson and Williams 2014 and Christensen and Rudebusch 2015 for discussions). By relying solely on real yields, which are not subject to a lower bound, we avoid this complication altogether.

The analysis in this paper relates to several important literatures. Most directly, it speaks to the burgeoning literature on measurement of the natural rate of interest. Moreover, by offering an associated market-based measure of the stance of monetary policy, our analysis may have implications for the voluminous literature on that topic. Second, our estimates of the real yield curve that would prevail without trading frictions have implications for asset pricing analysis on the true slope of the real yield curve. Furthermore, our results relate to research on financial market liquidity and convenience premia. Finally, the paper contributes to the rapidly growing literature on the economic consequences of the COVID-19 pandemic.

The remainder of the paper is organized as follows. Section 2 contains a description of the French OAT€ bond data, while Section 3 details the no-arbitrage term structure models we use and presents the empirical results. Section 4 describes the estimated real bond-specific premia, while Section 5 analyzes our OAT€-based estimate of the natural rate and compares it with other measures. Finally, Section 6 introduces our market-based measure of the stance of the ECB’s monetary policy before Section 7 concludes. Appendices available online contain additional technical details on the pricing of OAT€s and the model estimation.

2 The French OAT€ Bond Data

This section briefly describes the available data downloaded from Bloomberg for the market for French inflation-indexed bonds referencing the harmonized index for consumer prices (HICP) (ex tobacco) and known as OAT€s.

To give a sense of the size of the French government bond market, we note up front that, as of the end of December 2022, the total outstanding notional amount of marketable bonds issued by the French government was €2,28 trillion. In terms of medium- and long-term debt, the outstanding notional amount was €2,13 trillion of which €262 billion, or 12.3 percent, represented inflation-indexed securities, and out of this amount OAT€s represented €183.7 billion, or 70.1 percent.¹¹ Despite the large size of the French government bond market, the French government still held a AA rating from all major rating agencies during our sample period. As a consequence, there is essentially no credit risk to account for in our bond price data, as also suggested by measures of the credit risk premia of French government bonds

¹¹This information is available at https://www.aft.gouv.fr/files/medias-aft/7_Publications/7.2_BM/392_Monthly%20bulletin%20january%202023.pdf

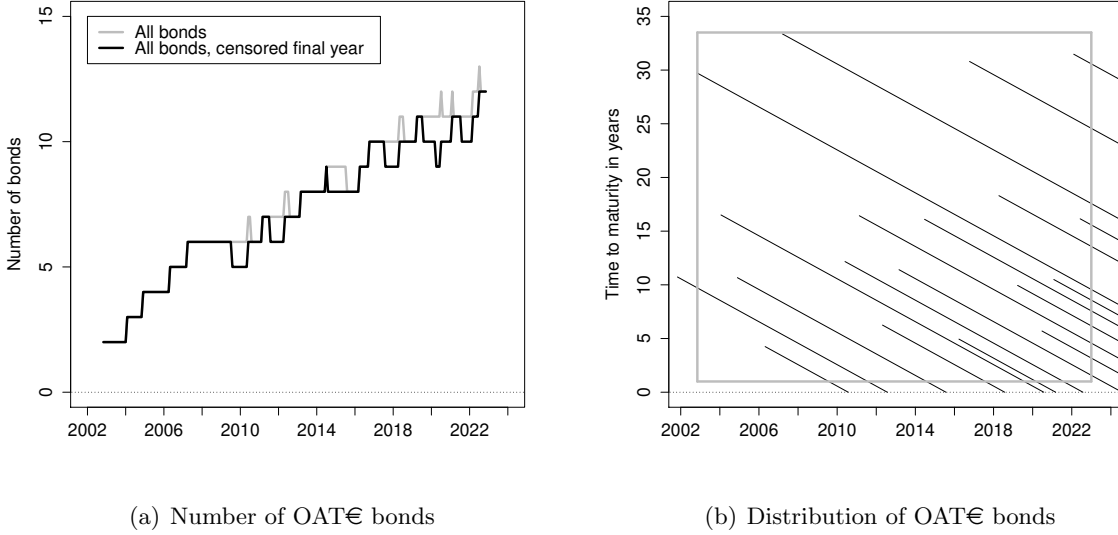


Figure 2: Overview of the French OAT€ Bond Data

Panel (a) reports the number of outstanding OAT€ bonds at a given point in time. Panel (b) shows the maturity distribution of all French OAT€ bonds issued since October 2001. The solid gray rectangle indicates the sample used in our analysis, where the sample is restricted to start on October 31, 2002, and limited to bond prices with more than one year to maturity after issuance.

examined in Section 2.2.

The French government issued its first inflation-indexed bond referencing HICP on October 31, 2001. At the end of December 2022, the outstanding amount of French OAT€s was €184 billion as already noted. Thus, this is a large market in a European context. The total number of such bonds outstanding over time in our sample is shown as a solid gray line in Figure 2(a). At the end of our sample, 12 French OAT€s were outstanding. However, as noted by Gürkaynak et al. (2010) and ACR, prices of inflation-indexed bonds near their maturity tend to be somewhat erratic because of the indexation lag in their payouts. Therefore, to facilitate model estimation, we censor the prices of OAT€s from our sample when they have less than one year to maturity. Using this cutoff, the number of OAT€s in the sample is modestly reduced, as shown with a solid black line in Figure 2(a). We stress that we examine the effect of the cutoff choice on our results.

Figure 2(b) shows the distribution of the available universe of French OAT€s, where we note that a repeated, although somewhat infrequent, issuance of ten-, fifteen-, and thirty-year OAT€s implies that there is a fairly wide range of available maturities in the data going back to the start of our sample in October 2002. It is this cross-sectional dispersion that provides the econometric identification of the factors in our models, including the inflation-indexed bond-specific risk factor. Finally, Table 1 contains the contractual details of all 19 French OAT€s in our data as well as the number of daily observations for each in our sample.

OAT€ bond	No. obs.	Issuance		Total uplifted amount
		Date	amount	
(1) 3% 7/25/2012	2,278	10/31/2001	787	14,494
(2) 3.15% 7/25/2032	5,258	10/31/2002	587	12,098
(3) 2.25% 7/25/2020	4,045	1/22/2004	298	20,310
(4) 1.6% 7/25/2015	2,522	11/23/2004	3,527	14,052
(5) 1.25% 7/25/2010	849	4/25/2006	3,634	9,325
(6) 1.8% 7/25/2040	4,119	3/14/2007	347	12,929
(7) 1.1% 7/25/2022	2,910	5/25/2010	2,883	19,928
(8) 1.85% 7/25/2027	3,094	2/16/2011	418	23,433
(9) 0.25% 7/25/2018	1,370	2/16/2011	2,520	11,257
(10) 0.25% 7/25/2024	2,566	2/26/2013	2,320	14,644
(11) 0.7% 7/25/2030	2,225	6/18/2014	429	17,232
(12) 0.1% 3/1/2021	1,029	3/21/2016	2,290	7,566
(13) 0.1% 7/25/2047	1,629	10/5/2016	556	13,027
(14) 0.1% 7/25/2036	1,233	4/6/2018	416	12,747
(15) 0.1% 3/1/2029	984	3/21/2019	2,128	17,772
(16) 0.1% 3/1/2026	660	6/18/2020	3,044	12,736
(17) 0.1% 7/25/2031	505	1/24/2021	2,370	11,741
(18) 0.1% 7/25/2053	239	2/1/2022	217	6,447
(19) 0.1% 7/25/2038	153	6/1/2022	549	7,089

Table 1: **Sample of French OAT€ Bonds**

The table reports the characteristics, first issuance date and amount, and total amount issued in millions of euros either at maturity or as of December 31, 2022, for the sample of French OAT€ bonds. Also reported are the number of daily observation dates for each bond during the sample period from October 31, 2002, to December 31, 2022.

Figure 3 shows the yields to maturity for all French OAT€ bonds in our sample at daily frequency from October 31, 2002, to December 30, 2022. Note the following regarding these yield series. First, the significant persistent decline in real yields over this 20-year period is clearly visible. Long-term real yields in the euro area were close to 3 percent in late 2002 and had dropped below -1 percent by late 2021 before retracing some of that decline during 2022. The empirical question we are interested in is to what extent these persistent fluctuations represent changes in the natural rate or are driven by other factors such as term or other bond-specific risk premia. Second, business cycle variation in the shape of the yield curve is pronounced around the lower trend. The yield curve tends to flatten ahead of recessions and steepen during the initial phase of economic recoveries. These characteristics are the practical motivation behind our choice of using a three-factor model for the frictionless part of the euro-area real yield curve, adopting an approach similar to what is standard for U.S. and U.K. nominal yield data; see Christensen and Rudebusch (2012).

Figure 4 shows the inflation index ratios for all 19 French OAT€s in our sample. We note that none of the bonds have been exposed to any prolonged period of deflation, defined

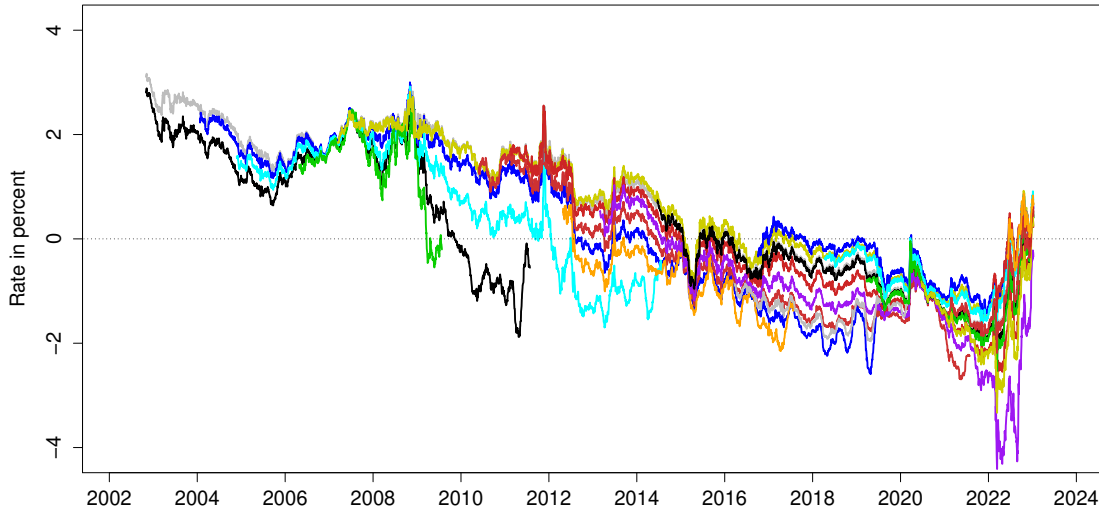


Figure 3: **Yield to Maturity of French OAT€ Bonds**

as periods with inflation index ratios below one. Indeed, thanks to the generally positive inflation environment in the euro area, the ratios tend to relatively quickly become significantly positive. This suggests that their offered deflation protection is likely to be of modest value, similar to what Christensen and Mouabbi (2023, henceforth CM) find for French government bonds indexed using the French CPI and known as OATi's. We therefore disregard this component in our analysis and leave it for future research to assess its value.

2.1 Holdings of French OAT€ Bonds

In this section, we exploit euro-area security holdings data at the sector level, for the available period (2013Q4 to 2024Q3), to better understand the demand for French OAT€ bonds. Note that this dataset covers the universe of holders of euro-area securities, thus providing a complete overview for the demand of such assets. In Table 2, we observe that, on average, throughout the period 2013Q4 to 2024Q3, banks, non-money market investment funds, insurance companies and pension funds are the largest holders of French OAT€ bonds, with respective average holdings of about 36 percent, 26 percent, 24 percent and 8 percent. Notably, for bonds whose tenor is up to 20 years, banks have the largest holdings (45 percent), followed by non-money market investment funds (Non-MMFs) and insurance companies. Conversely, for bonds whose tenor is above 20 years, we observe that the average ownership share of insurance companies is the largest (about 40 percent), followed by Non-MMFs, banks and pension funds. Moreover, on average about 65 percent of these bonds are held by French

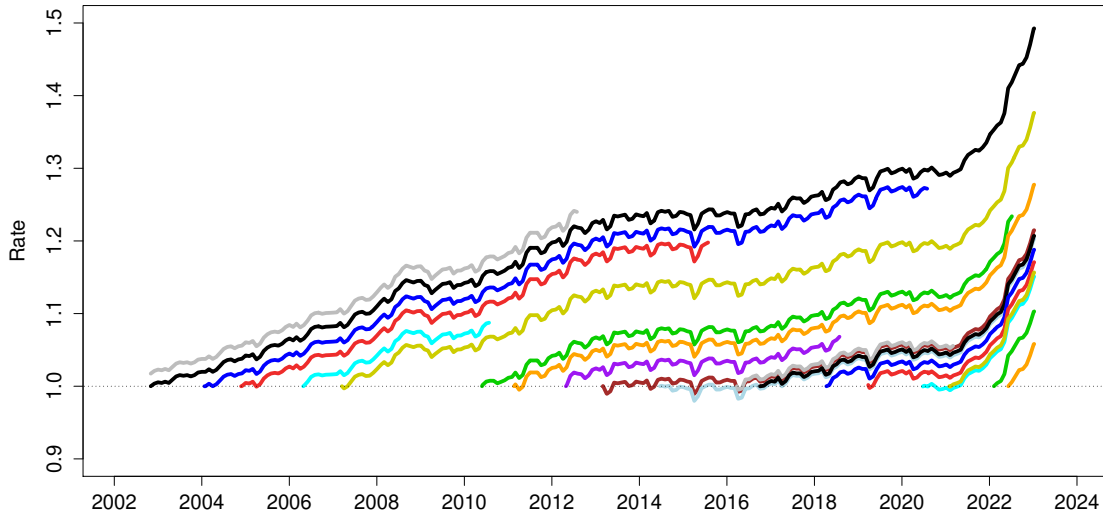


Figure 4: **Inflation Index Ratios of French OAT€ Bonds**

Bond Tenor	Banks	Government	Households	Insurance	NFCs	Non-MMF	Pension	Other
Below 10Y	46.34	1.72	0.97	12.31	0.24	34.24	3.67	0.51
11Y-20Y	44.43	1.54	0.25	19.18	0.27	25.36	7.33	1.64
Above 20Y	17.22	2.79	0.22	41.37	1.62	19.69	14.30	2.79

Table 2: **Sectoral Holdings of French OAT€ Bonds**

The table reports the average share of holdings (in percent) of French OAT€ bonds, across sectors, by tenor segment. These statistics are produced using Eurosystem SHSS data for the period 2013Q4-2024Q3. NFCs are non-financial corporations and Non-MMFs are non-money market investment funds.

investors, with the rest being held abroad. Prominent investors outside of France include the Netherlands (12 percent), Ireland (6 percent), Luxembourg (5.5 percent) and Germany (4 percent).

2.2 The Credit Risk of French Government Bonds

In this section, we assess whether there are any material credit risk issues to consider in modeling French OAT€ bond prices.

First, we examine rates on so-called credit default swap (CDS) contracts. They reflect the annual rate investors are willing to pay to buy protection against default-related losses on these bonds over a fixed period of time stipulated in the contract. Such derivatives have been used to price the credit risk of many countries, including France, since the early 2000s.

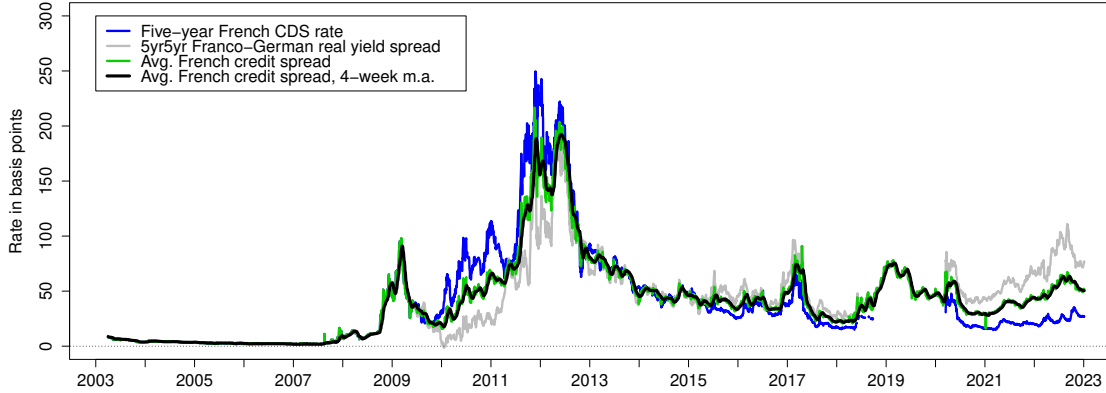


Figure 5: Measures of the Credit Risk of French Government Bonds

In Figure 5, we plot the available series downloaded from Bloomberg for the five-year French CDS rate shown with a solid blue line. In addition to occasionally missing values, the five-year CDS rate is missing entirely between September 24, 2018, and March 11, 2020. As a consequence of the missing data, we consider an alternative measure of the credit risk of French government bonds. Specifically, we include the five-year forward yield spread between French and German inflation-indexed bond yields for a period starting five years ahead. Due to the late launch of the German inflation-indexed government bond program, we can only construct the 5yr5yr Franco-German real yield spread starting June 12, 2009, when the third such German bond was issued; see Christensen et al. (2025) for details. The available series since then through the end of our sample is shown with a solid grey line in Figure 5. Similar to regular German bunds, German inflation-indexed government bonds trade at a convenience premium as documented by Christensen et al. (2025). However, given their lower liquidity, we refer to these premia as safety premia; see Christensen and Mirkov (2022). For the same reason we interpret the 5yr5yr Franco-German real yield spread as mainly reflecting differences in credit risk premia rather than differences in liquidity risk premia.

In light of the incomplete sample histories for both credit risk measures, we construct a composite measure of the credit risk of French government bonds by averaging the two measures. To further smooth out idiosyncratic noise, we calculate the four-week moving average of this composite series, which is shown with a solid black line in Figure 5. This series is available daily from April 1, 2003, to December 30, 2022, and we take it to be a representative proxy for the credit risk premium of French government bonds.

We note that, beyond being elevated around the European sovereign debt crisis in the 2010-2013 period, our composite measure of credit risk has remained fairly stable fluctuating

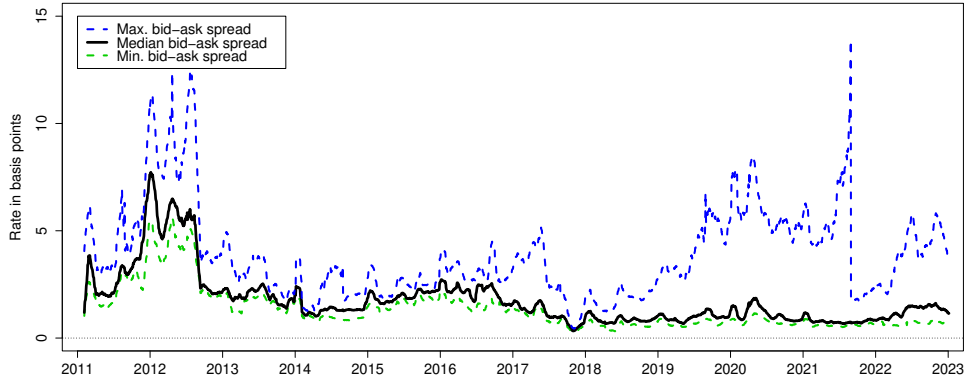


Figure 6: **Bid-Ask Spreads of OAT€ Bonds**

around 50 basis points. Thus, the main takeaway for our analysis is that changes in credit risk premia cannot account for the persistent trends in the OAT€ bond yields during our sample period. Furthermore and importantly, if anything, given the modest positive net change in the composite credit risk measure from April 2003 to December 2022, the credit risk component should have *pushed up* French real yields. Instead, French real yields of all maturities have experienced a persistent significant net *decline* since 2003. Thus, we feel that we can rule out with great confidence credit risk components as an important driver of French real yields during our sample period.

2.3 Bid-Ask Spreads of OAT€ Bonds

In this section, to shed light on the trading frictions in the market for French OAT€ bonds, we examine their bid-ask spreads.

To begin, we note that reliable bid-ask spreads for individual OAT€ bonds are available from Bloomberg starting in 2011.¹² In Figure 6, we show the smallest and largest observed bid-ask spread for each observation date as well as the median bid-ask spread. Although elevated during the European sovereign debt crisis in 2011 and the first half of 2012, the median bid-ask spread since then has followed a stable and declining trend that has left it close to 1 basis point by the end of our sample. This points to high, and even improving, liquidity in the market for OAT€s during the last decade of our sample. That said, we still want to account for any bond-specific effects tied to liquidity in our analysis, in particular in light of the fact that there is one or more OAT€s that face challenging trading conditions on an on-going basis as evidenced by the elevated maximum bid-ask spreads observed for

¹²Speck (2021) reports bid-ask spreads for French inflation-indexed bonds back to 2006, but his data comes from a different source.

extended periods in Figure 6.

A key purpose of the remainder of the paper is to quantify the importance of these bond-specific risk premia in the pricing of OAT€ bonds and what adjustments for them may imply about bond investors' underlying real short-rate expectations and associated real term premia.

3 Model Estimation and Results

In this section, we first describe how we model yields in a world without any frictions to trading. This model of frictionless dynamics is fundamental to our analysis. We then detail the augmented model that accounts for the bond-specific premia in inflation-indexed yields. This is followed by a description of the restrictions imposed to achieve econometric identification of this model and its estimation. We end the section with a brief summary of our estimation results.

3.1 A Frictionless Arbitrage-Free Model of Real Yields

To capture the fundamental or frictionless factors operating the OAT€ real yield curve, we choose to focus on the tractable affine dynamic term structure model introduced in Christensen et al. (2011).¹³

In this arbitrage-free Nelson-Siegel (AFNS) model, the state vector is denoted by $X_t = (L_t, S_t, C_t)$, where L_t is a level factor, S_t is a slope factor, and C_t is a curvature factor. The instantaneous risk-free real rate is defined as

$$r_t = L_t + S_t. \quad (1)$$

The risk-neutral (or \mathbb{Q} -) dynamics of the state variables are given by the stochastic differential equations¹⁴

$$\begin{pmatrix} dL_t \\ dS_t \\ dC_t \end{pmatrix} = \begin{pmatrix} 0 & 0 & 0 \\ 0 & -\lambda & \lambda \\ 0 & 0 & -\lambda \end{pmatrix} \begin{pmatrix} L_t \\ S_t \\ C_t \end{pmatrix} dt + \Sigma \begin{pmatrix} dW_t^{L,\mathbb{Q}} \\ dW_t^{S,\mathbb{Q}} \\ dW_t^{C,\mathbb{Q}} \end{pmatrix}, \quad (2)$$

where Σ is the lower triangular constant covariance (or volatility) matrix.¹⁵ Based on this specification of the \mathbb{Q} -dynamics, real zero-coupon bond yields preserve the Nelson-Siegel factor

¹³Although the model is not formulated using the canonical form of affine term structure models introduced by Dai and Singleton (2000), it can be viewed as a restricted version of the canonical Gaussian model; see Christensen et al. (2011) for details.

¹⁴As discussed in Christensen et al. (2011), with a unit root in the level factor, the model is not arbitrage-free with an unbounded horizon; therefore, as is often done in theoretical discussions, we impose an arbitrary maximum horizon.

¹⁵As per Christensen et al. (2011), $\theta^{\mathbb{Q}}$ is set to zero without loss of generality.

loading structure as

$$y_t(\tau) = L_t + \left(\frac{1 - e^{-\lambda\tau}}{\lambda\tau} \right) S_t + \left(\frac{1 - e^{-\lambda\tau}}{\lambda\tau} - e^{-\lambda\tau} \right) C_t - \frac{A(\tau)}{\tau}, \quad (3)$$

where $A(\tau)$ is a convexity term that adjusts the functional form in Nelson and Siegel (1987) to ensure absence of arbitrage (see Christensen et al. (2011)).

To complete the description of the model and to implement it empirically, we will need to specify the risk premia that connect these factor dynamics under the \mathbb{Q} -measure to the dynamics under the real-world (or physical) \mathbb{P} -measure. It is important to note that there are no restrictions on the dynamic drift components under the empirical \mathbb{P} -measure beyond the requirement of constant volatility. To facilitate empirical implementation, we use the essentially affine risk premium specification introduced in Duffee (2002). In the Gaussian framework, this specification implies that the risk premia Γ_t depend on the state variables; that is,

$$\Gamma_t = \gamma^0 + \gamma^1 X_t,$$

where $\gamma^0 \in \mathbf{R}^3$ and $\gamma^1 \in \mathbf{R}^{3 \times 3}$ contain unrestricted parameters.

Thus, the resulting unrestricted three-factor AFNS model has \mathbb{P} -dynamics given by

$$\begin{pmatrix} dL_t \\ dS_t \\ dC_t \end{pmatrix} = \begin{pmatrix} \kappa_{11}^{\mathbb{P}} & \kappa_{12}^{\mathbb{P}} & \kappa_{13}^{\mathbb{P}} \\ \kappa_{21}^{\mathbb{P}} & \kappa_{22}^{\mathbb{P}} & \kappa_{23}^{\mathbb{P}} \\ \kappa_{31}^{\mathbb{P}} & \kappa_{32}^{\mathbb{P}} & \kappa_{33}^{\mathbb{P}} \end{pmatrix} \left(\begin{pmatrix} \theta_1^{\mathbb{P}} \\ \theta_2^{\mathbb{P}} \\ \theta_3^{\mathbb{P}} \end{pmatrix} - \begin{pmatrix} L_t \\ S_t \\ C_t \end{pmatrix} \right) dt + \Sigma \begin{pmatrix} dW_t^{L,\mathbb{P}} \\ dW_t^{S,\mathbb{P}} \\ dW_t^{C,\mathbb{P}} \end{pmatrix}.$$

This is the transition equation in the Kalman filter estimation.

3.2 An Arbitrage-Free Model of Real Yields with Bond-Specific Risk

In this section, we augment the frictionless AFNS model introduced above to account for any bond-specific risk premia embedded in the OAT€ prices. To do so, let $X_t = (L_t, S_t, C_t, X_t^R)$ denote the state vector of the four-factor AFNS-R model with bond-specific risk premium adjustment. As in the non-augmented model, we let the frictionless instantaneous real risk-free rate be defined by equation (1), while the risk-neutral dynamics of the state variables used for pricing are given by

$$\begin{pmatrix} dL_t \\ dS_t \\ dC_t \\ dX_t^R \end{pmatrix} = \begin{pmatrix} 0 & 0 & 0 & 0 \\ 0 & \lambda & -\lambda & 0 \\ 0 & 0 & \lambda & 0 \\ 0 & 0 & 0 & \kappa_R^{\mathbb{Q}} \end{pmatrix} \left[\begin{pmatrix} 0 \\ 0 \\ 0 \\ \theta_R^{\mathbb{Q}} \end{pmatrix} - \begin{pmatrix} L_t \\ S_t \\ C_t \\ X_t^R \end{pmatrix} \right] dt + \Sigma \begin{pmatrix} dW_t^{L,\mathbb{Q}} \\ dW_t^{S,\mathbb{Q}} \\ dW_t^{C,\mathbb{Q}} \\ dW_t^{R,\mathbb{Q}} \end{pmatrix},$$

where Σ continues to be a lower triangular matrix.

In the augmented model, OAT€ yields are sensitive to bond-specific risks because the net present value of their future cash flow is calculated using the following discount function:

$$\bar{r}^i(t, t_0^i) = r_t + \beta^i(1 - e^{-\lambda^{R,i}(t-t_0^i)})X_t^R = L_t + S_t + \beta^i(1 - e^{-\lambda^{R,i}(t-t_0^i)})X_t^R. \quad (4)$$

CR show that the net present value of one unit of consumption paid by OAT€ i at time $t + \tau$ has the following exponential-affine form

$$\begin{aligned} P_t(t_0^i, \tau) &= E^{\mathbb{Q}} \left[e^{-\int_t^{t+\tau} \bar{r}^i(s, t_0^i) ds} \right] \\ &= \exp \left(B_1(\tau)L_t + B_2(\tau)S_t + B_3(\tau)C_t + B_4(t, t_0^i, \tau)X_t^R + A(t, t_0^i, \tau) \right). \end{aligned}$$

This result implies that the model belongs to the class of Gaussian affine term structure models. Note also that, by fixing $\beta^i = 0$ for all i , we recover the AFNS model.

Now, consider the whole value of OAT€ i issued at time t_0^i with maturity at $t + \tau^i$ that pays an annual coupon C^i . Its price is given by¹⁶

$$\begin{aligned} \bar{P}_t(t_0^i, \tau^i, C^i) &= C^i(t_1 - t)E^{\mathbb{Q}} \left[e^{-\int_t^{t_1} \bar{r}^i(s, t_0^i) ds} \right] + \sum_{j=2}^N C^i E^{\mathbb{Q}} \left[e^{-\int_t^{t_j} \bar{r}^i(s, t_0^i) ds} \right] \\ &\quad + E^{\mathbb{Q}} \left[e^{-\int_t^{t+\tau^i} \bar{r}^i(s, t_0^i) ds} \right]. \end{aligned}$$

There are only two minor omissions in this bond pricing formula. First, it does not account for the lag in the inflation indexation of the OAT€ bond payoff. The potential error from this omission should be modest (see Grishchenko and Huang 2013), especially as we exclude bonds from our sample when they have less than one year of maturity remaining. Second, we do not account for the value of deflation protection offered by OAT€s, as already noted. However, CM find these values to be very small for French OATi bonds indexed to the French consumer price index, and, given that HICP inflation has run quite a bit above French CPI inflation during our sample, the value of this protection for OAT€ bonds is likely to be entirely negligible.

Finally, to complete the description of the AFNS-R model, we again specify an essentially affine risk premium structure, which implies that the risk premia Γ_t take the form

$$\Gamma_t = \gamma^0 + \gamma^1 X_t,$$

where $\gamma^0 \in \mathbf{R}^4$ and $\gamma^1 \in \mathbf{R}^{4 \times 4}$ contain unrestricted parameters. Thus, the resulting unre-

¹⁶This is the clean price that does not account for any accrued interest and maps to our observed bond prices.

stricted four-factor AFNS-R model has \mathbb{P} -dynamics given by

$$\begin{pmatrix} dL_t \\ dS_t \\ dC_t \\ dX_t^R \end{pmatrix} = \begin{pmatrix} \kappa_{11}^{\mathbb{P}} & \kappa_{12}^{\mathbb{P}} & \kappa_{13}^{\mathbb{P}} & \kappa_{14}^{\mathbb{P}} \\ \kappa_{21}^{\mathbb{P}} & \kappa_{22}^{\mathbb{P}} & \kappa_{23}^{\mathbb{P}} & \kappa_{24}^{\mathbb{P}} \\ \kappa_{31}^{\mathbb{P}} & \kappa_{32}^{\mathbb{P}} & \kappa_{33}^{\mathbb{P}} & \kappa_{34}^{\mathbb{P}} \\ \kappa_{41}^{\mathbb{P}} & \kappa_{42}^{\mathbb{P}} & \kappa_{43}^{\mathbb{P}} & \kappa_{44}^{\mathbb{P}} \end{pmatrix} \left(\begin{pmatrix} \theta_1^{\mathbb{P}} \\ \theta_2^{\mathbb{P}} \\ \theta_3^{\mathbb{P}} \\ \theta_4^{\mathbb{P}} \end{pmatrix} - \begin{pmatrix} L_t \\ S_t \\ C_t \\ X_t^R \end{pmatrix} \right) dt + \Sigma \begin{pmatrix} dW_t^{L,\mathbb{P}} \\ dW_t^{S,\mathbb{P}} \\ dW_t^{C,\mathbb{P}} \\ dW_t^{R,\mathbb{P}} \end{pmatrix}.$$

This is the transition equation in the Kalman filter estimation.

3.3 Model Estimation and Econometric Identification

Due to the nonlinear relationship between the state variables and the bond prices, the model cannot be estimated with the standard Kalman filter. Instead, we use the extended Kalman filter as in Kim and Singleton (2012); see CR for details. Furthermore, to make the fitted errors comparable across bonds of various maturities, we scale each bond price by its duration. Thus, the measurement equation for the bond prices takes the following form

$$\frac{P_t^i(t_0^i, \tau^i)}{D_t^i(t_0^i, \tau^i)} = \frac{\hat{P}_t^i(t_0^i, \tau^i)}{D_t^i(t_0^i, \tau^i)} + \varepsilon_t^i, \quad (5)$$

where $\hat{P}_t^i(t_0^i, \tau^i)$ is the model-implied price of bond i and $D_t^i(t_0^i, \tau^i)$ is its duration, which is calculated before estimation. See Andreasen et al. (2019) for evidence supporting this formulation of the measurement equation.

Furthermore, since the bond-specific risk factor is a latent factor that we do not observe, its level is not identified without additional restrictions. As a consequence, we let the second OAT€ bond, which was issued right at the start of our sample, have a unit loading on this factor, that is, the 30-year OAT€ bond issued on October 31, 2002, and maturing on July 25, 2032, with 3.15 percent coupon has $\beta^i = 1$. This choice implies that the β^i sensitivity parameters measure bond-specific risk sensitivity relative to that of the 30-year 2032 OAT€ bond.

Finally, we note that the $\lambda^{R,i}$ parameters can be hard to identify if their values are too large or too small. As a consequence, we follow ACR and impose the restriction that they fall within the range from 0.0001 to 10, which is without practical consequences, as demonstrated by CM. Also, for numerical stability during model optimization, we impose the restriction that the β^i parameters fall within the range from 0 to 250, which turns out to be a binding constraint for two of the 19 bonds in our sample, but it is again the case that these two constraints are without practical consequences.

OAT€ bond	Pricing errors				Estimated parameters			
	AFNS		AFNS-R		AFNS-R			
	Mean	RMSE	Mean	RMSE	β^i	SE	$\lambda^{R,i}$	SE
(1) 3% 7/25/2012	0.32	4.29	0.55	3.00	249.9962	1.3687	0.0022	0.0001
(2) 3.15% 7/25/2032	1.09	4.24	0.85	2.62	1	n.a.	9.9999	1.3562
(3) 2.25% 7/25/2020	-0.88	4.81	0.58	2.90	45.4290	1.2766	0.0024	0.0001
(4) 1.6% 7/25/2015	-4.88	9.16	-5.75	12.86	58.6938	0.8397	0.7940	0.0444
(5) 1.25% 7/25/2010	1.14	4.33	0.94	2.59	0.5500	0.1740	9.9941	1.3542
(6) 1.8% 7/25/2040	-1.19	4.70	0.72	2.81	0.9419	0.0669	9.9945	1.3535
(7) 1.1% 7/25/2022	-0.94	4.23	-0.58	3.13	2.9259	0.3679	0.1050	0.0222
(8) 1.85% 7/25/2027	2.10	4.23	1.53	2.91	0.8847	0.0254	10.0000	1.3522
(9) 0.25% 7/25/2018	-2.19	4.99	0.45	2.06	4.6753	0.1780	1.9798	0.6843
(10) 0.25% 7/25/2024	0.26	5.24	0.65	2.59	1.4392	0.0439	9.2613	1.3507
(11) 0.7% 7/25/2030	-1.76	4.73	-0.16	2.28	3.7724	1.0018	0.0481	0.0155
(12) 0.1% 3/1/2021	8.07	9.44	2.17	3.45	1.2439	0.0401	1.0239	0.1341
(13) 0.1% 7/25/2047	3.11	5.01	0.11	2.17	249.9910	1.3611	0.0028	0.0001
(14) 0.1% 7/25/2036	-0.30	2.98	0.31	2.14	1.0284	0.0538	10.0000	1.3318
(15) 0.1% 3/1/2029	2.65	3.65	1.32	2.48	143.6258	1.3572	0.0014	0.0000
(16) 0.1% 3/1/2026	14.87	16.24	1.30	3.25	35.0249	1.3548	0.0100	0.0006
(17) 0.1% 7/25/2031	-4.07	7.19	0.47	2.14	1.8264	0.1884	0.6665	0.1139
(18) 0.1% 7/25/2053	1.98	7.38	0.41	3.89	29.8711	1.3287	0.2621	0.0169
(19) 0.1% 7/25/2038	3.39	4.95	0.04	2.99	1.3281	0.0781	9.9998	1.1221
All yields	0.23	5.61	0.20	4.25	-	-	-	-
Max \mathcal{L}^{EKF}	217,238.6		234,570.8		-		-	

Table 3: **Pricing Errors and Estimated Bond-Specific Risk Parameters**

This table reports the mean pricing errors (Mean) and the root mean-squared pricing errors (RMSE) of French OAT€ bonds in the AFNS and AFNS-R models estimated with a diagonal specification of $K^{\mathbb{P}}$ and Σ . The errors are computed as the difference between the French OAT€ bonds market price expressed as yield to maturity and the corresponding model-implied yield. All errors are reported in basis points. Standard errors (SE) are not available (n.a.) for the normalized value of β^2 .

3.4 Estimation Results

This section presents our benchmark estimation results. In the interest of simplicity, in this section we focus on a version of the AFNS-R model where $K^{\mathbb{P}}$ and Σ are diagonal matrices. As shown in ACR, these restrictions have hardly any effects on the estimated bond-specific risk premium for each inflation-indexed bond, because it is identified from the model's \mathbb{Q} -dynamics, which are independent of $K^{\mathbb{P}}$ and only display a weak link to Σ through the small convexity adjustment in the bond yields. Furthermore, we stress that we relax this assumption in Section 5 when we analyze estimates of r_t^* , which are indeed sensitive to the specification of the models' \mathbb{P} -dynamics.

Table 3 reports the summary statistics for the fitted errors of individual OAT€s as well as for all OAT€s combined. With the single exception of OAT€ number 4 in our sample, there is otherwise uniform improvement in model fit from incorporating the bond-specific risk factor into the AFNS model. Still, it is worth noting that the AFNS model is able to

Parameter	AFNS		AFNS-R	
	Est.	SE	Est.	SE
$\kappa_{11}^{\mathbb{P}}$	0.0194	0.0473	0.0441	0.0767
$\kappa_{22}^{\mathbb{P}}$	0.3754	0.2020	0.2522	0.1952
$\kappa_{33}^{\mathbb{P}}$	0.4188	0.2578	0.4964	0.2697
$\kappa_{44}^{\mathbb{P}}$	-	-	0.0876	0.1432
σ_{11}	0.0036	0.0000	0.0054	0.0000
σ_{22}	0.0129	0.0002	0.0117	0.0002
σ_{33}	0.0183	0.0003	0.0184	0.0003
σ_{44}	-	-	0.0189	0.0025
$\theta_1^{\mathbb{P}}$	0.0340	0.0322	0.0383	0.0248
$\theta_2^{\mathbb{P}}$	-0.0235	0.0120	-0.0211	0.0156
$\theta_3^{\mathbb{P}}$	-0.0096	0.0139	-0.0209	0.0126
$\theta_4^{\mathbb{P}}$	-	-	-0.0290	0.0426
λ	0.3860	0.0012	0.3245	0.0013
$\kappa_R^{\mathbb{Q}}$	-	-	7.5059	0.9816
$\theta_R^{\mathbb{Q}}$	-	-	0.0002	0.0000
σ_y	0.0006	7.4×10^{-7}	0.0003	1.14×10^{-6}

Table 4: **Estimated Dynamic Parameters**

The table shows the estimated dynamic parameters for the AFNS and AFNS-R models estimated with a diagonal specification of $K^{\mathbb{P}}$ and Σ .

deliver a root mean-squared fitted error of 5.6 basis points across all bonds combined, which in general could be characterized as a satisfactory fit, but obviously not as good as the RMSE of 4.3 basis points for all bonds combined achieved by the AFNS-R model, which represents a really good fit to the entire cross section of yields. Note also that neither the 15- nor 30-year bonds pose any particular challenges for the two models. Thus, both the AFNS and AFNS-R models are clearly able to fit those long-term bond yields to a satisfactory level of accuracy.

Table 4 contains the estimated dynamic parameters. Note that the dynamics of the first three factors are qualitatively very similar across the two estimations. Hence, the frictionless dynamics of the state variables within the AFNS-R model are essentially statistically indistinguishable from the corresponding dynamics in the simpler AFNS model. We take this as a sign of the robustness of our results. Furthermore, λ is smaller in the AFNS-R model. This implies that the yield loadings of the slope factor decays toward zero more slowly as the maturity increases. At the same time, the peak of the curvature yield loadings is located at a later maturity compared with its loading in the AFNS model. As a consequence, slope and curvature matter more for longer-term yields in the AFNS-R model. This helps explain part of the better fit to the entire cross section of bonds within that model.

The estimated paths of the level, slope, and curvature factors from the two models are shown in Figure 7. While the two models' slope factors are close to each other most of the

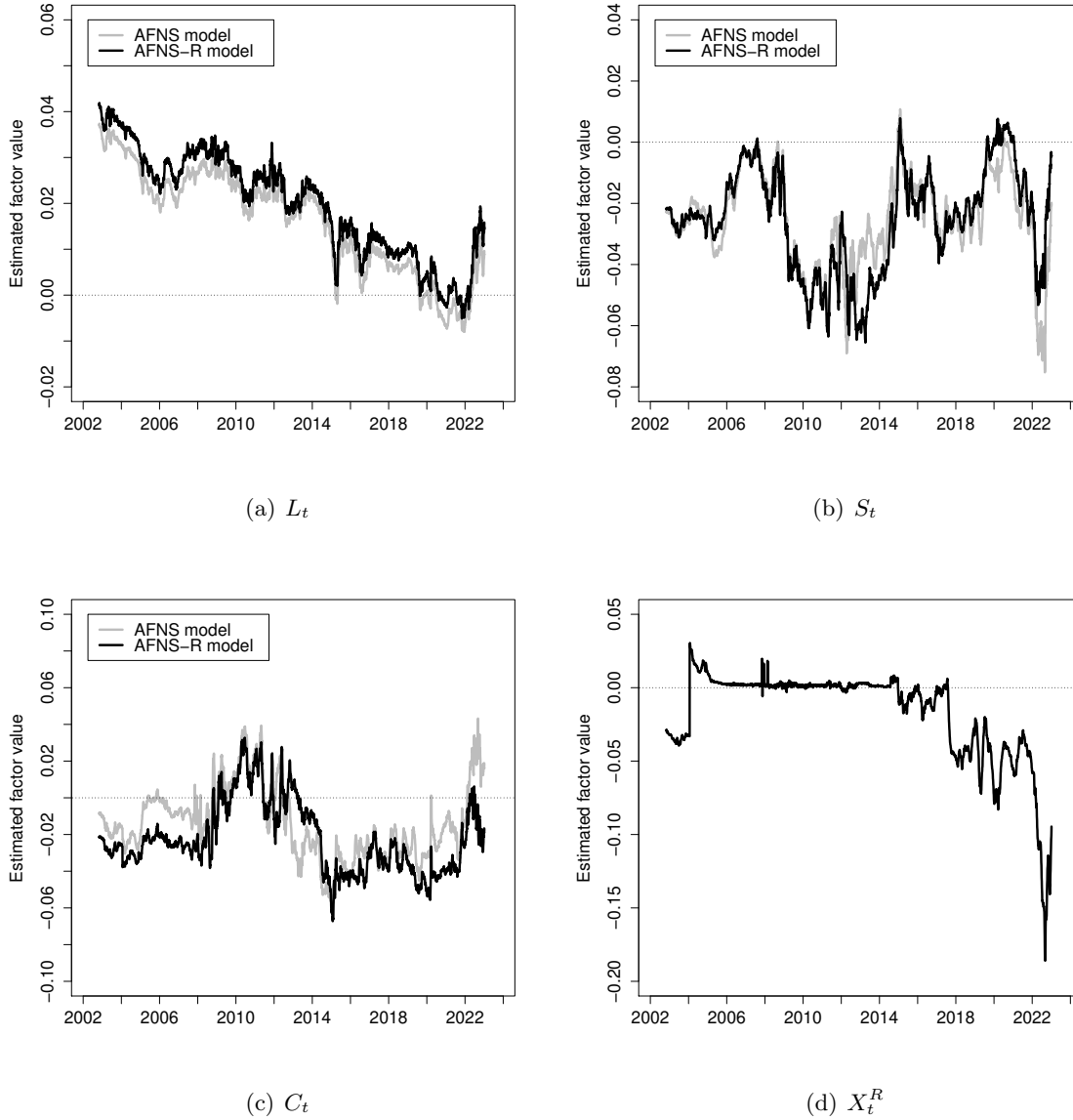


Figure 7: Estimated State Variables

Illustration of the estimated state variables from the AFNS and AFNS-R models.

time, their level factors have a wedge between them. However, they generally move in tandem, as both exhibit a persistent decline from 2002 through the end of 2021 that is partially offset by a sharp reversal during the last year of our sample. The lower path of the level factor in the AFNS model is offset by a mostly higher path of the curvature factor in that model compared to the AFNS-R model. Accordingly, the main impact of accounting for bond-specific risk premia in the pricing of the OAT€s is on the level and curvature factors of the frictionless real yield curve. As we demonstrate later, this affects the models' longer-run projections of real rates and hence the estimates of the natural rate. The fourth factor in the AFNS-R model,

the bond-specific risk factor, is shown in Figure 7(d). It follows a persistent process with a very stable path near zero for the first 15 years before it experiences a pronounced downward trend during the last 7 years of the sample that leaves it with a significantly negative value at the end of our sample.

4 The OAT€ Bond-Specific Risk Premium

In this section, we analyze the French OAT€ bond-specific risk premia implied by the estimated AFNS-R model described in the previous section. First, we formally define the bond-specific risk premium and study its historical evolution. We then briefly assess its robustness, including its sensitivity to the high-frequency daily data we use. We end the section with an examination of the determinants of the average estimated bond-specific risk premium using regression analysis.

4.1 The Estimated OAT€ Bond-Specific Risk Premia

We now use the estimated AFNS-R model to extract the bond-specific risk premia in the OAT€ market. To compute these premia, we first use the estimated parameters and the filtered states $\{X_{t|t}\}_{t=1}^T$ to calculate the fitted OAT€ prices $\{\hat{P}_t^i\}_{t=1}^T$ for all outstanding OAT€ securities in our sample. These bond prices are then converted into yields to maturity $\{\hat{y}_t^{c,i}\}_{t=1}^T$ by solving the fixed-point problem

$$\begin{aligned} \hat{P}_t^i &= C(t_1 - t) \exp \left\{ -(t_1 - t) \hat{y}_t^{c,i} \right\} + \sum_{k=2}^n C \exp \left\{ -(t_k - t) \hat{y}_t^{c,i} \right\} \\ &\quad + \exp \left\{ -(T - t) \hat{y}_t^{c,i} \right\}, \end{aligned} \quad (6)$$

for $i = 1, 2, \dots, n_{OATe}$, meaning that $\{\hat{y}_t^{c,i}\}_{t=1}^T$ is approximately the real rate of return on the i th OAT€ if held until maturity (see Sack and Elsassser 2004). To obtain the corresponding yields with correction for the bond-specific risk premia, we compute a new set of model-implied bond prices from the estimated AFNS-R model using only its frictionless part, i.e., using the constraints that $X_{t|t}^R = 0$ for all t as well as $\sigma_{44} = 0$ and $\theta_R^Q = 0$. These prices are denoted $\{\tilde{P}_t^i\}_{t=1}^T$ and converted into yields to maturity $\tilde{y}_t^{c,i}$ using equation (6). They represent estimates of the prices that would prevail in a world without any financial frictions or special demands for certain bonds. The bond-specific risk premium for the i th OAT€ is then defined as

$$\Psi_t^i \equiv \hat{y}_t^{c,i} - \tilde{y}_t^{c,i}. \quad (7)$$

Figure 8 shows the average estimated OAT€ bond-specific risk premium $\bar{\Psi}_t$ across the

outstanding OAT€s at each point in time. Note that a negative value means that the fitted OAT€ price is *above* the model-implied frictionless price, i.e., OAT€ prices are higher than they should be in a world without any frictions. Importantly, though, the mean of the series is -0.56 basis point, that is, less than 0.0001 in absolute size. Thus, on average, OAT€ prices are *not* biased by bond-specific risk premia unlike French OATi's, whose prices contain a large convenience premium as documented by CM. That said, there are clearly still some trends and time variation in the series, which explains the standard variation of 9.46 basis points. Furthermore, toward the end of our sample, the average bond-specific premium dropped significantly into negative territory, reaching a historic low of -41.94 basis points on August 31, 2022. Hence, at that point in time, the average OAT€ bond was trading at a significant price or convenience premium. When HICP inflation spiked sharply in 2022, one implication was that bonds like OAT€s, whose principal and cash flows adjust with the changes in the HICP, became very desirable and convenient assets to hold—so much so that investors were willing to give up 0.42 percent in annual return, or equivalently overpay a corresponding amount, to hold these securities. In contrast, it reached its maximum of 37.25 basis points in late 2007, coinciding with a few single-day large spikes. Notably, a large *positive* premium here means that the average OAT€ was trading at a liquidity discount, or at low prices. This is the typical pattern in fixed-income markets when investors are concerned about liquidity and their ability to sell a bond back to the market, and such spells of illiquidity tend to be fairly short lived. Thus, the single-day spikes driven by illiquidity events fit that historical pattern well.

Finally, we note the abrupt uptick on January 22, 2004, when the third OAT€ bond was issued and entered our sample. By having pricing information from three bonds instead of two, the model learns that the bond-specific risk premia in the early years of this market most likely were modestly positive. Hence, the estimated bond-specific risk premia prior to January 22, 2004, should be interpreted with caution. This contrasts with the later years in our sample, when our AFNS-R model has sufficient pricing information to identify all four state variables. This makes the bond-specific risk premia very robustly estimated as we demonstrate in Section 4.2.

In Figure 9, we show the individual estimated bond-specific risk premium series for each OAT€ bond. In general, these bonds start out with bond-specific risk premia very close to zero in the first many years of trading. However, as the bonds become seasoned and less traded because the majority of their outstanding notional amount is locked up in buy-and-hold investors' portfolios, their pricing starts to become rather sensitive to market conditions. To demonstrate this, two bonds are highlighted in Figure 9: the OAT€ 1.6% 7/25/2015 that reached maturity during our sample and OAT€ 0.25% 7/25/2024 that was approaching maturity by the end of our sample.

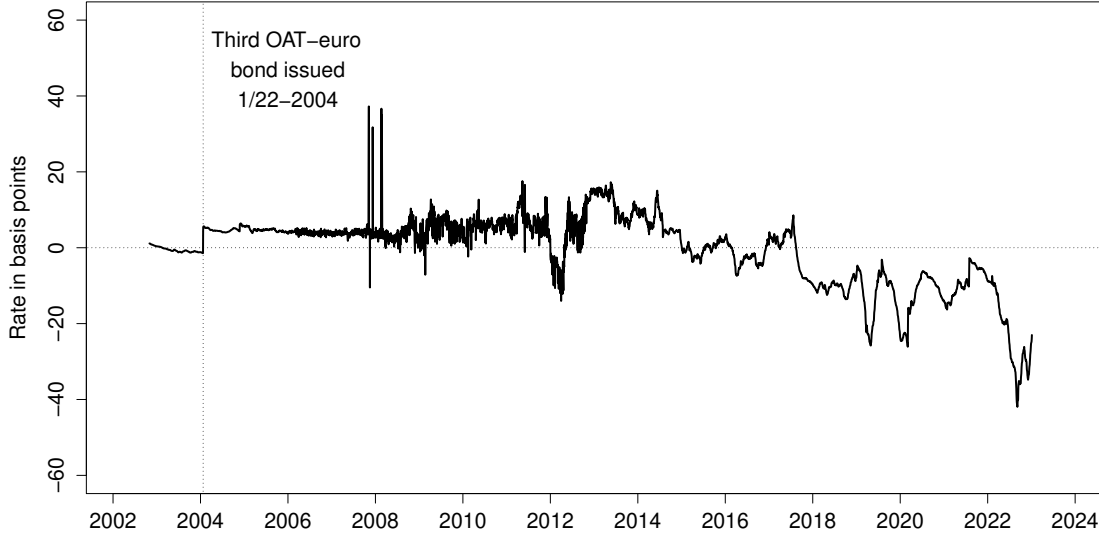


Figure 8: **Average Estimated OAT€ Bond-Specific Risk Premium**

Illustration of the average estimated bond-specific risk premium of French OAT€s for each observation date implied by the AFNS-R model. The bond-specific risk premia are measured as the estimated yield difference between the fitted yield to maturity of individual OAT€s and the corresponding frictionless yield to maturity with the bond-specific risk factor turned off. The data are daily and cover the period from October 31, 2002, to December 30, 2022.

For the OAT€ 1.6% 7/25/2015, which reached this critical phase during the European Sovereign Debt Crisis, we see a sizable and volatile *positive* bond-specific risk premium, meaning there was a material liquidity discount in its pricing in 2012 and 2013. As shown in Figure 6, market conditions for OAT€s as measured by bid-ask spreads were indeed challenging in 2012. Under those circumstances OAT€s approaching maturity are likely to trade at a liquidity discount similar to what the OAT€ 1.6% 7/25/2015 did at the time. Importantly, though, the remaining universe of OAT€s continued to trade with close to zero bond-specific risk premia even during this challenging period.

For the OAT€ 0.25% 7/25/2024, which was approaching maturity towards the end of our sample, we see the opposite outcome, namely a sizable and volatile *negative* bond-specific risk premium, meaning it was trading at a material price premium. That happened in the context of highly elevated inflation well above the ECB's 2 percent target. Under those conditions, inflation-indexed bonds become very convenient assets to hold. As a consequence, the entire outstanding universe of OAT€s was trading at a price premium towards the end of our sample.

As a final exercise and to put our average estimated bond-specific risk premium from the market for French OAT€s into an international context, we compare it to similar estimates

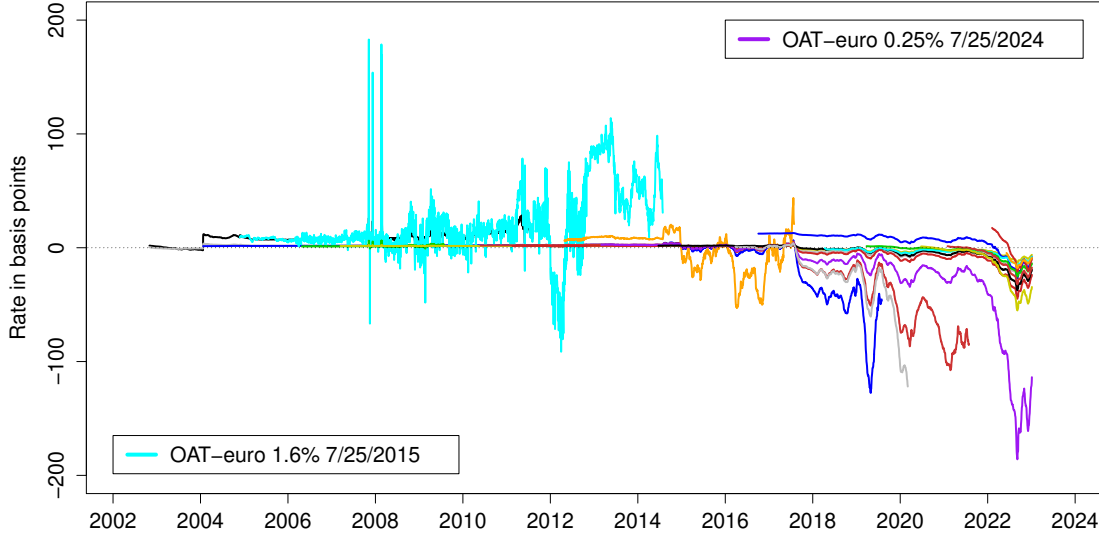


Figure 9: Individual Estimated OAT€ Bond-Specific Risk Premia

Illustration of the individual estimated bond-specific risk premia of French OAT€s for each observation date implied by the AFNS-R model. The bond-specific risk premia are measured as the estimated yield difference between the fitted yield to maturity of individual OAT€s and the corresponding frictionless yield to maturity with the bond-specific risk factor turned off. The data are daily and cover the period from October 31, 2002, to December 30, 2022.

from two other major inflation-indexed bond markets, specifically the market for French OATi's with cash flows adjusted to the French consumer price index examined by CM and the much larger market for U.S. TIPS with cash flows adjusted to the U.S. consumer price index examined by CR. Figure 10 shows the respective average estimated bond-specific risk premium series from all three markets.

We note that U.S. TIPS prices contain a sizable liquidity premium discount, which is well documented in the literature; see ACR, D'Amico et al. (2018), and Pflueger and Vi-ceira (2016), among many others. Cardozo and Christensen (2025) offer a rationale for the illiquidity of inflation-indexed securities like TIPS. By being protected against inflation, indexed securities are inherently less traded than nominal securities. In addition, foreigners not exposed to the domestic price index do not benefit from owning them. Combined this significantly reduces their trading volumes and makes the market for these securities be dominated by patient domestic buy-and-hold investors. This drives up the search frictions in the over-the-counter market for these bonds and leads to a steady-state outcome with their prices containing a large liquidity discount.

In contrast, CM document that French OATi's prices contain a sizable convenience pre-

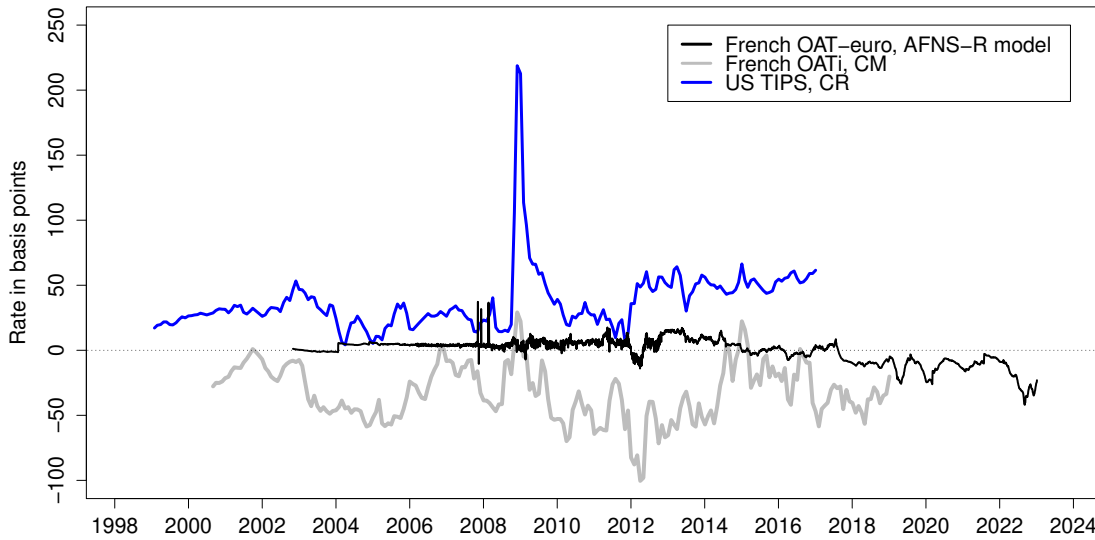


Figure 10: **Comparison of Average Estimated Bond-Specific Risk Premia**

Illustration of the average estimated bond-specific risk premium of French OAT€s implied by the AFNS-R model. Also shown are the average estimated bond-specific risk premium in French OATi yields reported by CM and the average estimated bond-specific risk premium in U.S. TIPS yields reported by CR.

mium averaging close to 0.40 percent. They explain this with the fact that French banks are obliged by law to offer their customers a special type of savings account, known as livret A, the interest of which is tied mechanically to French CPI through a somewhat complicated formula. This creates a regulatory-driven natural demand for OATi bonds as French banks need them to hedge the promised interest payments on these savings accounts.

Based on our average estimated bond-specific risk premium for French OAT€s, this market falls in between these two extremes. On the one hand, there does not seem to be any regulatory-driven benefits of holding OAT€s. As a consequence, there is little reason for them to trade at a convenience premium outside of unusual circumstances with highly elevated inflation when they are obviously convenient assets to hold. On the other hand, by being the largest safe euro-denominated market for bonds indexed to the HICP (ex tobacco), these bonds may be able to attract sufficient demand from non-French investors in the euro area to offset the otherwise negative price dynamics implied by the inherent illiquidity of inflation-indexed bonds.

Overall, our results suggest that the French OAT€ market is a rich and relatively unbiased source of information about bond investors' real rate expectations in the euro area that is not

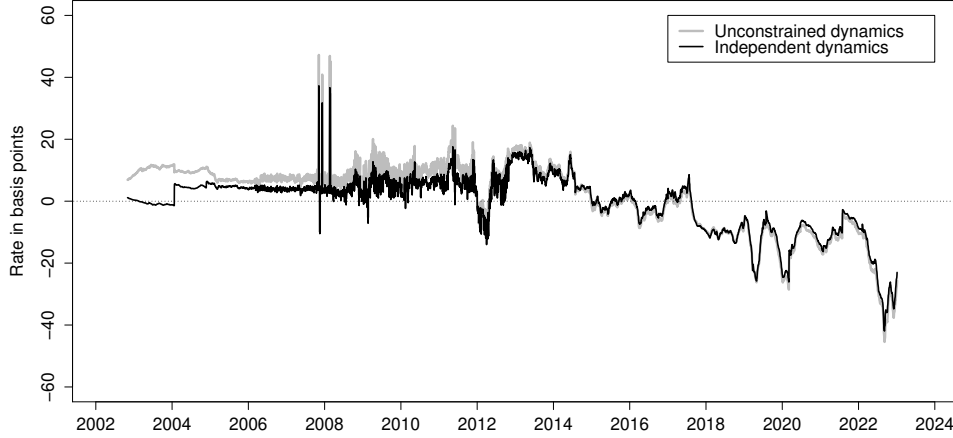


Figure 11: Average Estimated OAT€ Bond-Specific Risk Premium: Alternative \mathbb{P} Dynamics

Illustration of the average estimated bond-specific risk premium of French OAT€s for each observation date implied by the AFNS-R model when estimated with unconstrained dynamics as detailed in the text instead of independent factor dynamics. In both cases, the bond-specific risk premia are measured as the estimated yield difference between the fitted yield to maturity of individual OAT€s and the corresponding frictionless yield to maturity with the bond-specific risk factor turned off.

overly influenced by either liquidity discounts or flight-to-safety convenience premia. This makes it an ideal source for our purposes of understanding the trends in the natural rate in the euro area. Moreover, it makes it an ideal input for the construction of breakeven inflation for the euro area, but we leave that task for future research.

To summarize, we feel that the average estimated OAT€ bond-specific risk premium broadly follows a reasonable time series pattern. More importantly, these premia only constitute a minor distortion in the observed OAT€ prices. This provides support for our approach in which we rely on these bond prices for evidence on bond investors' outlook for future real rates in the euro area.

4.2 Robustness Analysis

This section examines the robustness of the average bond-specific risk premium reported in the previous section to some of the main assumptions imposed so far. Throughout the section, the AFNS-R model with diagonal $K^{\mathbb{P}}$ and Σ matrices serves as the benchmark.

First, we assess whether the specification of the dynamics within the AFNS-R model matters for the estimated OAT€ bond-specific risk premium. To do so, we estimate the AFNS-R model with unconstrained dynamics, that is, the AFNS-R model with unrestricted

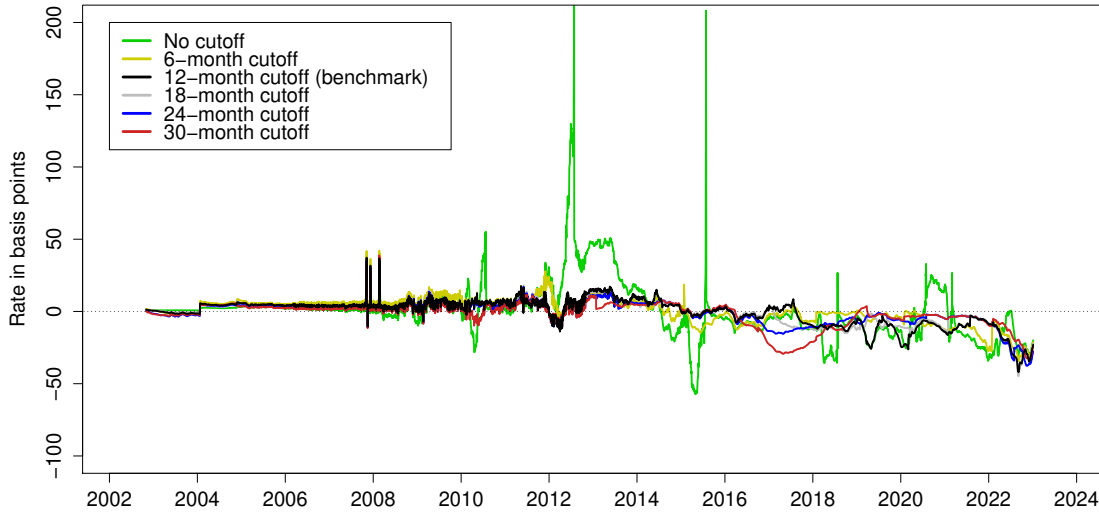


Figure 12: **Average Estimated OAT€ Bond-Specific Risk Premium: Data Cutoff**

Illustration of the average estimated bond-specific risk premium of French OAT€s for each observation date implied by the AFNS-R model when estimated using daily, weekly, monthly, and quarterly data. In all cases, the bond-specific risk premia are measured as the estimated yield difference between the fitted yield to maturity of individual OAT€s and the corresponding frictionless yield to maturity with the bond-specific risk factor turned off.

$K^{\mathbb{P}}$ and lower triangular Σ matrix. Figure 11 shows the estimated OAT€ bond-specific risk premium from this estimation and compares it to the series produced by our benchmark model. Note that they are barely distinguishable. Thus, we conclude that the specification of the dynamics within the AFNS-R model only play a very modest role for the estimated bond-specific risk premia, which is consistent with the findings of ACR in the context of U.S. TIPS.

Second, we assess whether the data censoring choice matters for our results. To do so, we estimate the AFNS-R model using alternative data cutoffs: No cutoff (i.e. 0 months), 6 months, 18 months, 24 months, and 30 months in addition to our benchmark choice of using 12 months as the censoring point for OAT€ bonds approaching maturity. We note that we perform this exercise for our preferred AFNS-R model to be described in Section 5.2, but we stress that the results are not sensitive to this choice as demonstrated by the results above. Figure 12 shows the average estimated OAT€ bond-specific risk premium series from all six estimations. In general, except when we do not impose any cutoff, the estimated risk premium series are very similar and close to each other. Furthermore, the cutoff choice matters little during the first 6-7 years of our sample as no bonds are approaching maturity early on in our

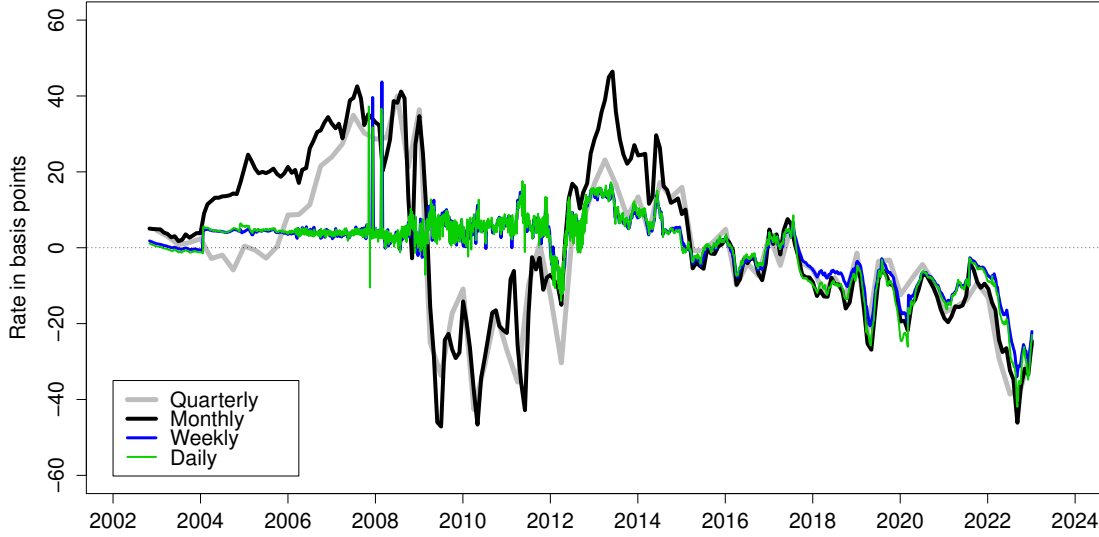


Figure 13: **Average Estimated OAT€ Bond-Specific Risk Premium: Data Frequency**

Illustration of the average estimated bond-specific risk premium of French OAT€s for each observation date implied by the AFNS-R model when estimated using daily, weekly, monthly, and quarterly data. In all cases, the bond-specific risk premia are measured as the estimated yield difference between the fitted yield to maturity of individual OAT€s and the corresponding frictionless yield to maturity with the bond-specific risk factor turned off.

sample. In choosing a preferred cutoff point, there is a tension between, on the one hand, keeping as much information as possible, and at the same time limit the impact of noisy observations on the estimation results. We think of our benchmark choice to use a 12-month cutoff similar to ACR as striking a sensible balance between these two considerations for our specific data sample.

Third, we assess whether the data frequency plays any role for our results. To do so, we estimate the AFNS-R model using daily, weekly, monthly, and quarterly data, and based on the results above it suffices to focus on the most parsimonious AFNS-R model with diagonal $K^{\mathbb{P}}$ and Σ matrices. Figure 13 shows the average estimated OAT€ bond-specific risk premium series from all four estimations. Note that they are barely distinguishable during the last decade of our sample, while there are some notable discrepancies during the first decade of our sample between the high-frequency daily and weekly series, on one hand, and the lower-frequency monthly and quarterly series, on the other.

As to the importance of these early discrepancies, we stress that, in explaining the large swings in OAT€ yields observed in Figure 3, the relatively minor differences between the high-

and low-frequency series during the first 10 years of the sample are clearly *not* the source of those declines.

At a technical level, the issue is that, at low frequency, some variation in the OAT€ yields gets ascribed to the nonfundamental bond-specific risk premia that, at higher daily or weekly frequency, the AFNS-R model is able to tell should go into the fundamental frictionless level, slope, and curvature factors. Given that the ideal is to have as much of the bond yield variation explained by the fundamental level, slope, and curvature factors rather than bond-specific risks, these findings provide one justification for us to prefer the implementation based on high-frequency daily data over the more conventional monthly data frequently considered in the literature, despite the significantly higher computational costs.

4.3 Determinants of the Bond-Specific Risk Premia

In this section, we explore which factors matter for the size of the bond-specific risk premia in the OAT€ prices. To explain the variation of the average estimated bond-specific risk premium series, we run regressions with it as the dependent variable and a wide set of explanatory variables that are thought to play a role for the bond-specific risk premia as explained in the following.

To begin, we are interested in the role of factors that are believed to matter for OAT€ market liquidity specifically or bond market liquidity more broadly as they could matter for the estimated bond-specific risk premia. First, we include the average OAT€ bond age and the one-month realized volatility of the 10-year OAT€ bond yield as proxies for OAT€ bond liquidity following the work of Houweling et al. (2005).¹⁷ Inspired by the analysis of Hu et al. (2013), we also include a noise measure of OAT€ bond prices to control for variation in the amount of arbitrage capital available in this market.¹⁸ Finally, we add the euro overnight interbank rate to proxy for the opportunity cost of holding money and the associated liquidity premia of French government bonds, including OAT€ bonds, as explained in Nagel (2016). Combining these four explanatory variables tied to market liquidity and functioning produces the results reported in regression (1) in Table 5. We note a relatively modest adjusted R^2 of 0.30. The average OAT€ bond age, the one-month realized volatility of the ten-year OAT€ bond yield, and the overnight rate all have statistically significant negative coefficients. This implies that an increase in the liquidity risk of OAT€ bonds is associated with lower average estimated bond-specific risk premia. Moreover, the noise measure, which serves as a proxy for financial frictions in the market for OAT€s, has a positive, but insignificant coefficient in

¹⁷The ten-year OAT€ bond yield is the ten-year fitted real yield implied by the AFNS model estimated using our sample of daily OAT€ prices.

¹⁸The noise measure is the mean absolute fitted error from the estimated daily AFNS model, where each error is calculated as the difference between the observed OAT€ price converted into yield to maturity and the fitted OAT€ price also converted into yield to maturity.

this regression. Hence, we take these results to show that our average estimated bond-specific risk premia in the OAT€ prices behave more like convenience premia than liquidity premia.

After having explored the role of liquidity factors, we examine the effects of factors reflecting risk sentiment domestically and globally on the average estimated bond-specific risk premia. This set of variables includes the VIX, which represents near-term uncertainty about the general stock market as reflected in options on the Standard & Poor’s 500 stock price index and is widely used as a gauge of investor fear and risk aversion. The set also contains the yield difference between seasoned (off-the-run) U.S. Treasury securities and the most recently issued (on-the-run) U.S. Treasury security of the same ten-year maturity. This on-the-run (OTR) premium is a frequently used measure of financial frictions in the U.S. Treasury market. To control for factors related to the uncertainty about the interest rate environment, we include the MOVE index. The fourth variable is the U.S. TED spread, which is calculated as the difference between the three-month U.S. LIBOR and the three-month U.S. T-bill interest rate. This spread represents a measure of the perceived general credit risk in global financial markets. As an additional indicator of credit risk and credit risk sentiment, we use the composite measure of the credit risk of French government bonds shown in Figure 5. The next variable in the set is the ten-year U.S. Treasury yield from the Federal Reserve’s H.15 database, which is included to control for reach-for-yield effects in advanced economies. This may be particularly relevant for our sample during the period between December 2008 and December 2015 and again in the 2020-2021 period when U.S. short-term interest rates were constrained by the zero lower bound. Finally, we include the West Texas Intermediate (WTI) Cushing crude oil price to proxy for energy prices, which represent a significant risk to the inflation outlook in many countries around the world, including many euro area member states. The results of the regression with these seven explanatory variables is reported in regression (2) in Table 5. This produces a modest adjusted R^2 of 0.27. We note that all seven variables have some explanatory power as their estimated coefficients are all statistically significant.

To assess the robustness of the results from the first two regressions, we include all variables with the results reported in column (3) in Table 5. This joint regression produces a high adjusted R^2 of 0.53. The significant increase in the adjusted R^2 suggests that there is little overlap between the two sets of explanatory variables. The first set is squarely focused on the liquidity in the OAT€ market, while the second set represents global risk sentiment and flight-to-safety effects.

With the systematic negative coefficients on the liquidity risk variables—and on the VIX and the MOVE Index in the full regression model—we feel that we can confidently reject the conjecture that our average estimated bond-specific risk premia in the OAT€ prices should represent liquidity risk premia. This is also consistent with the interpretation we offered in Section 4.1, when we contrasted our estimates with the estimated U.S. TIPS liquidity premia

Explanatory variables	(1)	(2)	(3)
Avg. bond age (yrs)	-3.039*** (0.379)		-4.367*** (0.391)
One-month realized volatility of ten-year real yield (bps)	-0.203*** (0.068)		-0.233*** (0.054)
Bond noise measure (bps)	0.385 (0.267)		-0.780*** (0.284)
Overnight rate (%)	-0.708* (0.420)		-1.421** (0.565)
VIX (%)		-0.322*** (0.068)	-0.070 (0.059)
Ten-year OTR premium (bps)		0.698*** (0.116)	0.525*** (0.070)
MOVE Index (bps)		-0.141*** (0.039)	-0.114*** (0.022)
TED spread (bps)		0.024* (0.013)	0.036*** (0.011)
Composite credit risk measure (bps)		0.068*** (0.013)	0.055*** (0.016)
Ten-year US Treasury yield (%)		1.960*** (0.422)	-2.738*** (0.609)
WTI (\$)		0.054*** (0.018)	0.159*** (0.019)
Constant	17.081*** (2.567)	-1.753 (3.189)	29.015*** (3.542)
N	4838	4838	4838
Adjusted R^2	0.30	0.27	0.53

Table 5: Regression Results for Average Estimated OAT€ Bond-Specific Risk Premium

The table reports the results of regressions with the average estimated bond-specific risk premium of French OAT€s as the dependent variable and 11 explanatory variables. Standard errors computed by the Newey-West estimator (with 13 lags) are reported in parentheses. Asterisks *, ** and *** indicate significance at the 10 percent, 5 percent, and 1 percent levels, respectively.

reported by CR. Hence, the trading dynamics in the OAT€ market seem to be fundamentally different from those prevailing in the U.S. TIPS market.

Finally, changes in perceived credit risk as reflected in either the TED spread or our composite credit risk measure are significantly positively correlated with changes in the bond-specific risk premia. Based on these results we conclude that some part of the bond-specific risk premia seems to reflect compensation for credit risk.

5 A New Normal for Euro-Area Interest Rates?

In this section, we first go through a careful model selection process to find a preferred specification of the AFNS-R model’s objective \mathbb{P} -dynamics. Second, we use this AFNS-R model to account for bond-specific risk and standard term premia in the OAT€ prices and obtain expected real short rates and the associated measure of the natural rate. We then proceed to assess the robustness of our natural rate estimate, examine the realism of the model-implied real rates, study its factor decomposition, and examine its ties to both U.S. and euro area monetary policy as well as any relationship to the demand for safe assets as revealed at U.S. Treasury auctions. Finally, we compare this estimate to other market- and macro-based estimates from the literature, and consider model projections to assess its likely path going forward.

5.1 Definition of the Natural Rate

Our working definition of the natural rate of interest r_t^* is

$$r_t^* = \frac{1}{5} \int_{t+5}^{t+10} E_t^{\mathbb{P}}[r_s^R] ds, \quad (8)$$

that is, the average expected real short rate over a five-year period starting five years ahead, where the expectation is with respect to the objective \mathbb{P} -probability measure. As noted in the introduction, this 5yr5yr forward average expected real short rate should be little affected by short-term transitory shocks. Alternatively, r_t^* could be defined as the expected real short-term interest rate at an infinite horizon. However, this quantity will depend crucially on whether the factor dynamics exhibit a unit root. As is well known, the typical spans of time series data that are available do not distinguish strongly between highly persistent stationary processes and nonstationary ones. Our model follows the finance literature and adopts the former structure, so strictly speaking, our infinite-horizon steady-state expected real rate is constant. However, we view our data sample as having insufficient information in the ten-year to infinite horizon range to definitively pin down that steady state, so we prefer our definition with a medium- to long-run horizon. Moreover, we examine the sensitivity of our results to

Alternative specifications	Goodness of fit statistics			
	$\log L$	k	p -value	BIC
(1) Unrestricted $K^{\mathbb{P}}$	234,604.3	65	n.a.	-468,651.7
(2) $\kappa_{34}^{\mathbb{P}} = 0$	234,603.0	64	0.11	-468,657.7
(3) $\kappa_{34}^{\mathbb{P}} = \kappa_{12}^{\mathbb{P}} = 0$	234,602.3	63	0.24	-468,664.8
(4) $\kappa_{34}^{\mathbb{P}} = \kappa_{12}^{\mathbb{P}} = \kappa_{31}^{\mathbb{P}} = 0$	234,601.7	62	0.27	-468,671.6
(5) $\kappa_{34}^{\mathbb{P}} = \dots = \kappa_{43}^{\mathbb{P}} = 0$	234,600.7	61	0.16	-468,678.6
(6) $\kappa_{34}^{\mathbb{P}} = \dots = \kappa_{42}^{\mathbb{P}} = 0$	234,599.5	60	0.12	-468,684.9
(7) $\kappa_{34}^{\mathbb{P}} = \dots = \kappa_{32}^{\mathbb{P}} = 0$	234,598.8	59	0.24	-468,692.1
(8) $\kappa_{34}^{\mathbb{P}} = \dots = \kappa_{41}^{\mathbb{P}} = 0$	234,593.8	58	< 0.01	-468,690.7
(9) $\kappa_{34}^{\mathbb{P}} = \dots = \kappa_{14}^{\mathbb{P}} = 0$	234,589.9	57	< 0.01	-468,691.5
(10) $\kappa_{34}^{\mathbb{P}} = \dots = \kappa_{13}^{\mathbb{P}} = 0$	234,584.9	56	< 0.01	-468,690.0
(11) $\kappa_{34}^{\mathbb{P}} = \dots = \kappa_{21}^{\mathbb{P}} = 0$	234,579.1	55	< 0.01	-468,687.0
(12) $\kappa_{34}^{\mathbb{P}} = \dots = \kappa_{24}^{\mathbb{P}} = 0$	234,577.4	54	0.07	-468,692.2
(13) $\kappa_{34}^{\mathbb{P}} = \dots = \kappa_{23}^{\mathbb{P}} = 0$	234,570.8	53	< 0.01	-468,687.5

Table 6: **Evaluation of Alternative Specifications of the AFNS-R Model**

There are 13 alternative estimated specifications of the AFNS-R model. Each specification is listed with its maximum log likelihood ($\log L$), number of parameters (k), the p -value from a likelihood ratio test of the hypothesis that it differs from the specification above with one more free parameter, and the Bayesian information criterion (BIC). The period analyzed covers daily data from October 31, 2002, to December 30, 2022.

using alternative integration intervals in the definition r_t^* and find them to be robust.

5.2 Model Selection

For estimation of the natural rate and associated real term premia, the specification of the mean-reversion matrix $K^{\mathbb{P}}$ is crucial as noted earlier. To select the best-fitting specification of the model's real-world dynamics, we use a general-to-specific modeling strategy in which the least significant off-diagonal parameter of $K^{\mathbb{P}}$ is restricted to zero and the model is re-estimated. This strategy of eliminating the least significant coefficient is carried out down to the most parsimonious specification, which has a diagonal $K^{\mathbb{P}}$ matrix. The final specification choice is based on the value of the Bayesian information criterion (BIC), as in Christensen et al. (2014).¹⁹

The summary statistics of the model selection process are reported in Table 6. The BIC

¹⁹The Bayesian information criterion is defined as $\text{BIC} = -2 \log L + k \log T$, where k is the number of model parameters and $T = 5,258$ is the number of daily data observations.

$K^{\mathbb{P}}$	$K^{\mathbb{P}}_{\cdot,1}$	$K^{\mathbb{P}}_{\cdot,2}$	$K^{\mathbb{P}}_{\cdot,3}$	$K^{\mathbb{P}}_{\cdot,4}$	$\theta^{\mathbb{P}}$		Σ
$K^{\mathbb{P}}_{1,\cdot}$	0.0448 (0.0785)	0	0	0	0.0388 (0.0249)	σ_{11}	0.0054 (0.0000)
$K^{\mathbb{P}}_{2,\cdot}$	0	1.0132 (0.3200)	0.8448 (0.2718)	0	-0.0260 (0.0105)	σ_{22}	0.0117 (0.0002)
$K^{\mathbb{P}}_{3,\cdot}$	0	0	0.5067 (0.2678)	0	-0.0200 (0.0123)	σ_{33}	0.0184 (0.0003)
$K^{\mathbb{P}}_{4,\cdot}$	0	0	0	0.0817 (0.1420)	-0.0287 (0.0441)	σ_{44}	0.0189 (0.0025)

Table 7: **Estimated Dynamic Parameters of the Preferred AFNS-R Model**

The table shows the estimated parameters of the $K^{\mathbb{P}}$ matrix, $\theta^{\mathbb{P}}$ vector, and diagonal Σ matrix for the preferred AFNS-R model according to the BIC. The estimated value of λ is 0.3245 (0.0013), while $\kappa_R^{\mathbb{Q}} = 7.5228$ (0.9785), and $\theta_R^{\mathbb{Q}} = 0.0002$ (0.0000). The maximum log likelihood value is 234,577.4. The numbers in parentheses are the estimated parameter standard deviations.

is minimized by specification (12), which has a $K^{\mathbb{P}}$ -matrix given by

$$K^{\mathbb{P}}_{BIC} = \begin{pmatrix} \kappa_{11}^{\mathbb{P}} & 0 & 0 & 0 \\ 0 & \kappa_{22}^{\mathbb{P}} & \kappa_{23}^{\mathbb{P}} & 0 \\ 0 & 0 & \kappa_{33}^{\mathbb{P}} & 0 \\ 0 & 0 & 0 & \kappa_{44}^{\mathbb{P}} \end{pmatrix}.$$

This specification shows that the model's \mathbb{P} -dynamics preferred by the data have a structure similar to the one assumed under the risk-neutral \mathbb{Q} -dynamics used for pricing to achieve the Nelson-Siegel factor loading structure, which is comforting.

The estimated parameters of the preferred specification are reported in Table 7. The estimated \mathbb{Q} -dynamics used for pricing and determined by $(\Sigma, \lambda, \kappa_R^{\mathbb{Q}}, \theta_R^{\mathbb{Q}})$ are very close to those reported in Table 4 for the AFNS-R model with diagonal $K^{\mathbb{P}}$. This implies that both model fit and the estimated OAT€ bond-specific risk premia from the preferred AFNS-R model are very similar to those already reported and therefore not shown. Furthermore, the estimated objective \mathbb{P} -dynamics in terms of $\theta^{\mathbb{P}}$ and Σ are also qualitatively similar to those reported in Table 4.

Still, to understand the role played by the mean-reversion matrix $K^{\mathbb{P}}$ for estimates of the natural rate, we will later analyze the most flexible model with unrestricted mean-reversion matrix $K^{\mathbb{P}}$ and the most parsimonious model with diagonal $K^{\mathbb{P}}$, in addition to our preferred specification described above.

5.3 Estimates of the Natural Rate

Our market-based measure of the natural rate is the average expected real short rate over a five-year period starting five years ahead. This 5yr5yr forward average expected real short rate should be little affected by short-term transitory shocks and well positioned to capture the persistent trends in the natural rate.

To illustrate the decomposition underlying our definition of r_t^* , recall that the real term premium is defined as

$$TP_t(\tau) = y_t(\tau) - \frac{1}{\tau} \int_t^{t+\tau} E_t^{\mathbb{P}}[r_s] ds.$$

That is, the real term premium is the difference in expected real returns between a buy-and-hold strategy for a τ -year real bond and an instantaneous rollover strategy at the risk-free real rate r_t . Note that $y_t(\tau)$ in this definition is the *frictionless* yield clean of any bond-specific risk premia. Figure 14 shows the preferred AFNS-R model decomposition of the 5yr5yr forward frictionless real yield based on this definition. The solid gray line is the 5yr5yr forward real term premium, which, although volatile, has fluctuated around a fairly stable level since the early 2000s. As suggested by theory, this premium is countercyclical and elevated during economic recessions. In contrast, the estimate of the natural rate of interest implied by the AFNS-R model—the black line—shows a gradual decline from above 1.5 percent in the early 2000s to well below -1.5 percent by late 2021, with a partial retracing of that decline during the last year of our sample. Importantly, the vast majority of the persistent trends in the 5yr5yr forward real yield is driven by similar trends in this measure of r_t^* .

To examine the sensitivity of our r_t^* estimate to our choice to define r_t^* as the average expected real short rate over a five-year period starting five years ahead, we consider three alternative definitions that all embed a longer view about the time it takes for the euro area economy to reach steady state. The first assumes that this takes seven years and then measures the neutral real rate as the average expected real short over the following three years. It is referred to as the 7yr3yr r_t^* estimate. The second alternative takes an even longer view and assumes that it takes nine years to reach steady state and then measures the neutral real rate as the average expected real short rate over a short one-year period. It is referred to as the 9yr1yr r_t^* estimate. Finally, the third alternative takes the longest view and assumes that it takes ten years for the economy to reach steady state and then measures r_t^* as the average expected real short rate over a five-year horizon as in our benchmark definition. It is referred to as the 10yr5yr r_t^* estimate. Figure 15 shows all four r_t^* estimates, which are very close to each other thanks to the high estimated persistence of the state variables within our preferred AFNS-R model. Hence, our r_t^* estimate of the neutral real rate for the euro area has very little sensitivity to the specific definition of r_t^* used. Thus, our reported results are very robust from that perspective.

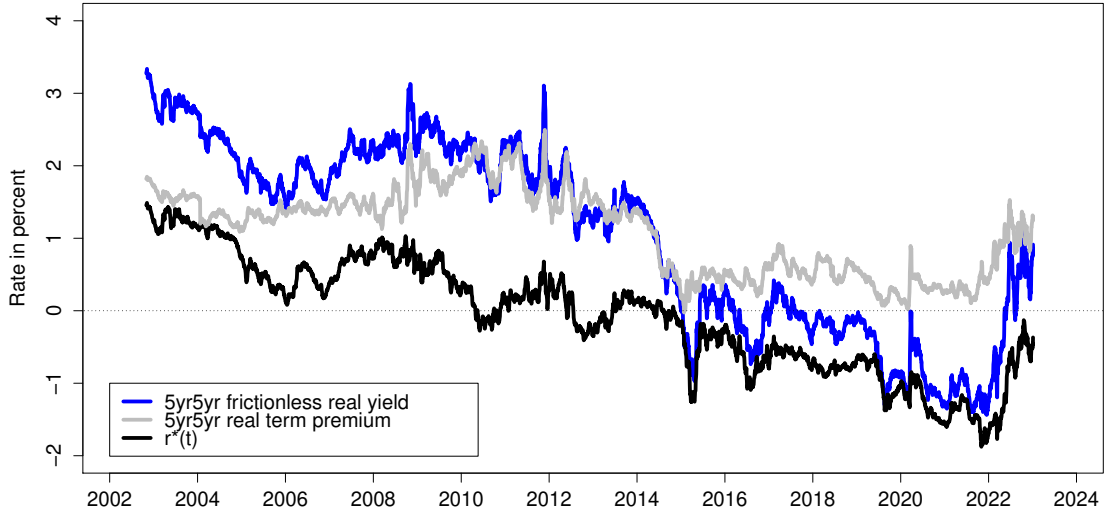


Figure 14: AFNS-R Model 5yr5yr Real Yield Decomposition

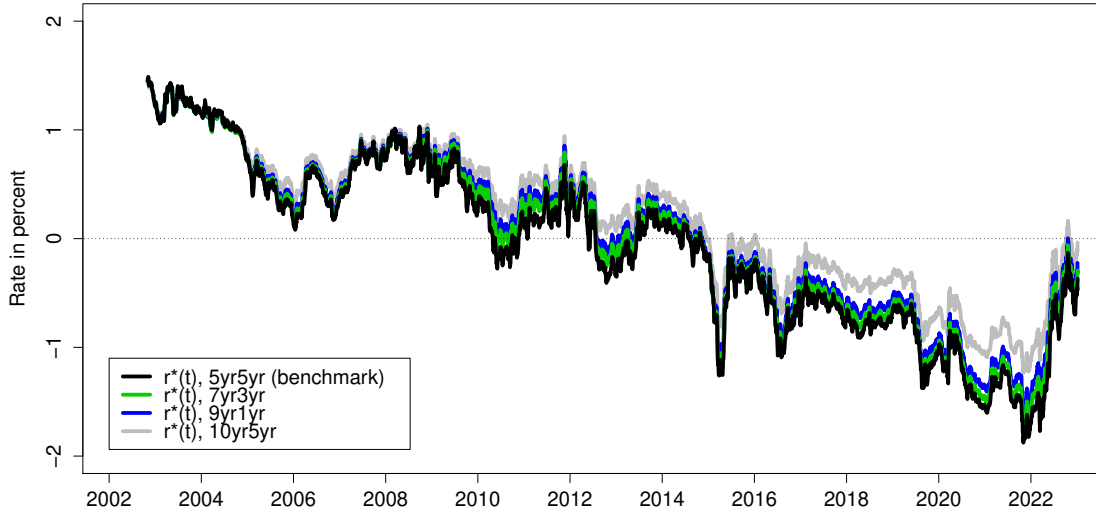


Figure 15: The Sensitivity of r^* Estimate to Alternative Definitions

To assess the sensitivity of our r_t^* estimate to the specification of the mean-reversion matrix $K^{\mathbb{P}}$, we compare it in Figure 16 to the estimates from the AFNS-R models with unrestricted and diagonal $K^{\mathbb{P}}$ matrix, respectively. As noted in Figure 16, our r_t^* estimate is indeed very sensitive to this model choice, but parsimonious specifications like our preferred

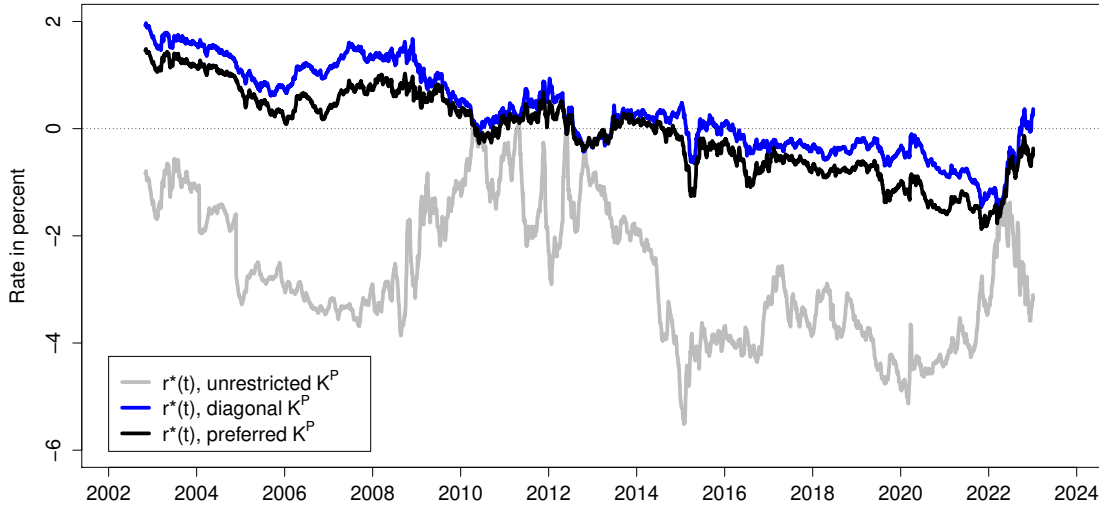


Figure 16: **The Sensitivity of r^* Estimate to $K^{\mathbb{P}}$ Specification**

AFNS-R model specification favored by the data tend to give fairly similar r_t^* estimates. Still, these results demonstrate how insignificant off-diagonal parameters in the specification of the mean-reversion $K^{\mathbb{P}}$ matrix can materially distort estimates of r_t^* . Hence, the results underscore the importance of our careful model selection procedure needed to identify appropriate specifications of $K^{\mathbb{P}}$ supported by the bond price data.

The effect on the estimated natural rate from accounting for the bond-specific risk premia in OAT€ prices is the subject of Figure 17. The black line is the estimate of r_t^* from the AFNS-R model, while the gray line is the estimate from the AFNS model, which does not account for time-varying bond-specific risk premium effects in OAT€ prices.²⁰ Accounting for the bond-specific risk premia in OAT€ prices leads to a persistent and diverging difference in the two natural rate estimates. Thus, even though both average close to zero during our sample period, it is crucial to account for the bond-specific risk premia to produce reliable estimates of the natural rate of interest.

Next, we vary the data cutoff used to censor the data for each OAT€ that approaches maturity from zero months (i.e. no censoring of any observations) up to 30 months in six month increments with the 12-month cutoff being our benchmark. Figure 18 shows the resulting six r_t^* estimates. We note that our r_t^* estimate is sensitive to the cutoff choice to some extent. Importantly, cutoff choices in the 12- to 24-month range produce very similar r_t^* estimates, while either very early or very late cutoff points produce more meaningful

²⁰For the AFNS model, we also go through a careful model selection process and use the BIC to determine a preferred specification, as described in online Appendix A.

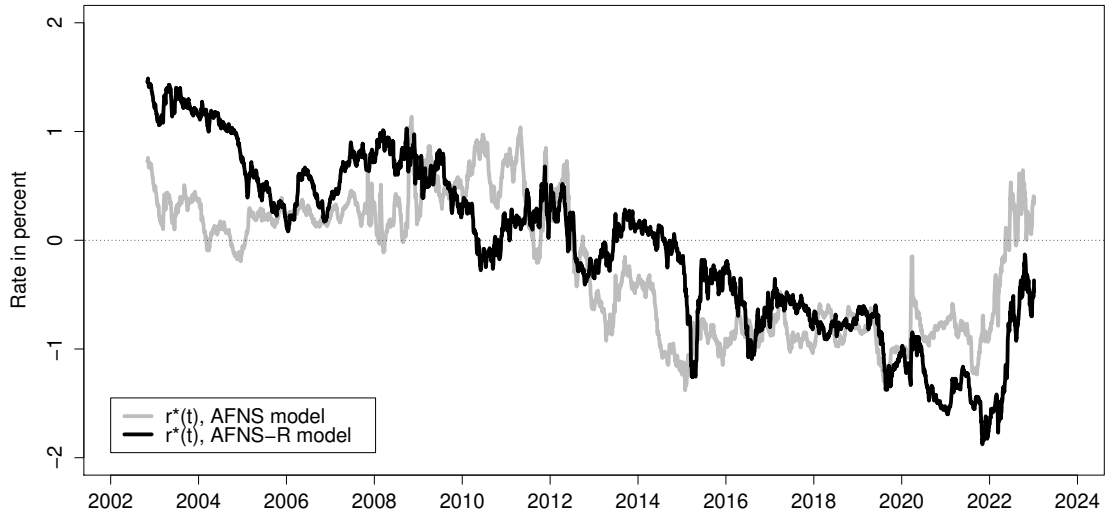


Figure 17: **Effect of the Bond-Specific Risk Adjustment on Estimates of r^***

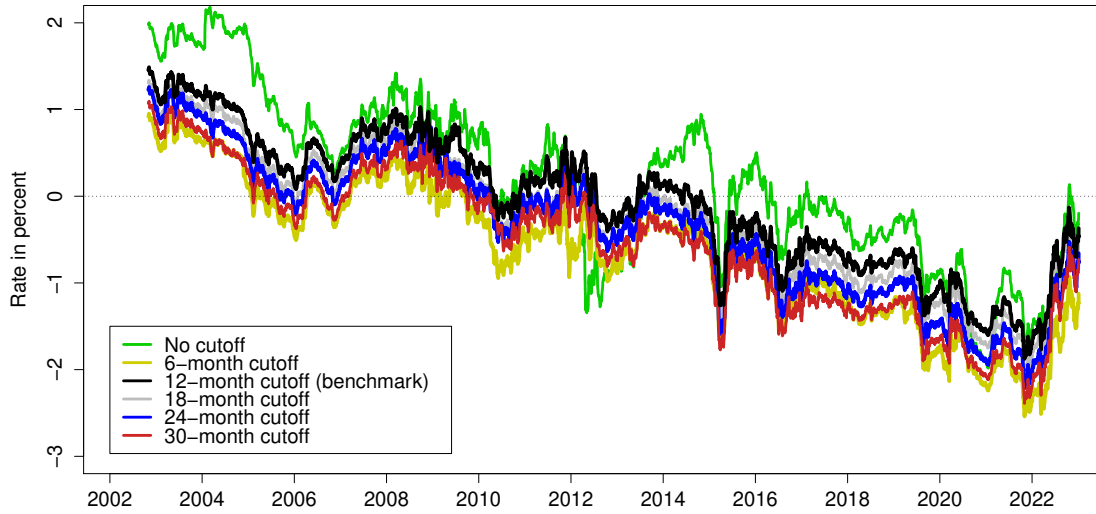


Figure 18: **The Sensitivity of r^* Estimate to Data Cutoff**

differences. Overall, we consider our choice to use a 12-month cutoff as recommended by ACR to strike a sensible balance between including as much data as possible and the robustness of our r_t^* estimate to this particular implementation choice.

As a final robustness check, we examine the role of the data frequency. Figure 19 shows

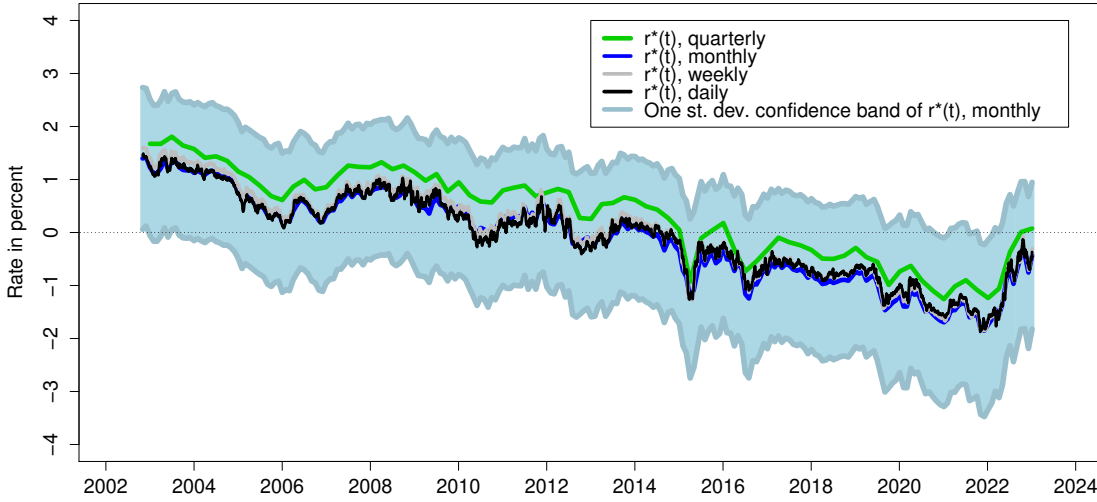


Figure 19: **The Sensitivity of r^* Estimate to Data Frequency**

the r_t^* estimates implied by our preferred AFNS-R model estimated at daily, weekly, monthly, and quarterly frequency. The results show that our estimate has little sensitivity to our choice to focus on high-frequency daily data. This also underscores the usefulness of our model for real-time analysis as we also demonstrate later on in Section 6.2.

To assess the statistical uncertainty surrounding our r_t^* estimate, we perform a classic parametric bootstrap simulation study. To facilitate this, we focus on our monthly preferred AFNS-R model and use it to simulate $N = 40$ samples for the four states at a monthly frequency for 243 months, which corresponds to the number of observations in our monthly sample.²¹ We then use the simulated states to compute N panels of coupon-bond prices that match those observed in the monthly sample in terms of available bonds and their characteristics. These bond prices are computed using the formula in equation (5)

$$P_t^i(t_0^i, \tau^i)^{obs} = P_t^i(t_0^i, \tau^i)^{sim} + \varepsilon_t^i D_t^i(t_0^i, \tau^i),$$

where $P_t^i(t_0^i, \tau^i)^{sim}$ is the true simulated price for bond i at time t , $D_t^i(t_0^i, \tau^i)$ is its duration, and $\varepsilon_t^i \sim \mathcal{NID}(0, (\sigma_\varepsilon)^2)$ are simulated errors with σ_ε equal to its estimated value based on the observed monthly data.

These simulated monthly samples are used as input into estimations of our preferred AFNS-R model. This produces N alternative parameter vectors with each being statistically as likely as the one obtained from the observed bond data. The N parameter vectors are then

²¹See Andreasen et al. (2019) for the details of the model simulations.

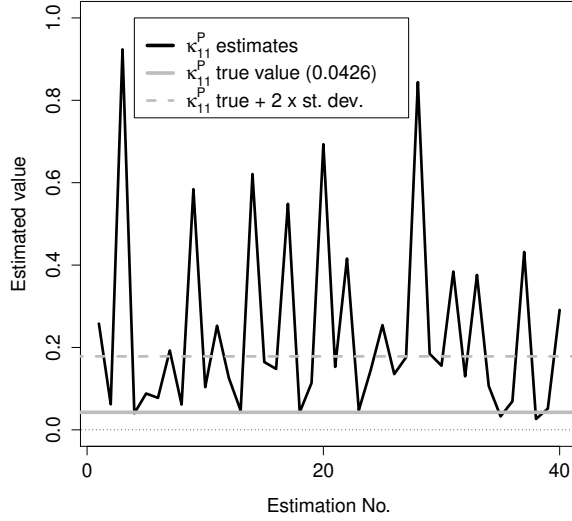


Figure 20: **Estimates of $\kappa_{11}^{\mathbb{P}}$ in Simulation Study**

Illustration of the N estimates of $\kappa_{11}^{\mathbb{P}}$ produced in our simulation study.

used to filter the observed bond sample and calculate the associated r_t^* series.

Finally, we calculate the standard deviation of the N values of r_t^* for each observation date and add and subtract it from our estimated monthly r_t^* series. This produces the one standard deviation confidence band shown in Figure 19, which is about ± 1.5 percent. Moreover, because of the high quality of the bond data and the good fit of the AFNS-R model, filtering adds very little uncertainty. Instead, the entire confidence band is due to uncertainty about the estimated mean vector $\theta^{\mathbb{P}}$ and mean-reversion matrix $K^{\mathbb{P}}$, while λ and the volatility parameters in Σ are extremely well identified from the cross section of bond prices; see also Andreasen et al. (2019).

Based on our simulation study it is possible to identify the main source of the large width of the reported one standard deviation confidence band for our r_t^* estimate. As we show in the section below, practically all variation in r_t^* in our preferred AFNS-R model is due to variation in the level factor L_t thanks to the low estimated value of its mean-reversion $\kappa_{11}^{\mathbb{P}}$.

In the following, we therefore focus on the estimates of this particular parameter. Figure 20 shows the individual $\kappa_{11}^{\mathbb{P}}$ estimates obtained with the N simulated bond samples, while the true value used to produce the simulated samples is shown with a solid grey line. For reference, we also show with a dashed grey line the critical level that is 2 times the estimated standard deviation of $\kappa_{11}^{\mathbb{P}}$ above the true value based on the observed monthly data. Note that only about 20 percent of the estimates are near the grey horizontal line, while the majority of the estimates are significantly higher and well above the 2 standard deviation critical line,

meaning that they are unlikely estimates based on the observed data. This is the finite-sample upward bias phenomenon discussed at length in Bauer et al. (2012) and is tied to the fact that each simulated sample is only 20 years in length. Crucially, high values for $\kappa_{11}^{\mathbb{P}}$ entails low persistence of the level factor in our preferred AFNS-R model. As a result, when we use those parameter vectors to filter the observed OAT€ data, we get overly stable estimated r_t^* series as opposed to the “true” trending r_t^* estimates shown in Figure 19. This dispersion in the implied r_t^* due to the significantly upward biased estimates of $\kappa_{11}^{\mathbb{P}}$ is the mechanism behind the large reported confidence bands of our r_t^* estimate. As a consequence, we view our reported confidence band as a very conservative upper bound of the true uncertainty surrounding our reported r_t^* estimates. Clearly, we got the low $\kappa_{11}^{\mathbb{P}}$ value of 0.0426 from the actual OAT€ data. Thus, the observed data is not of the nature that leads to the upward biased estimates of $\kappa_{11}^{\mathbb{P}}$. Instead, it is characterized by very persistent trends as is evident in Figure 3, and our estimated AFNS-R model parameters reflect that.

Importantly, despite the likely overstatement, the estimated confidence bands of our r_t^* estimate are narrower than those reported for many macro-based r_t^* estimates, including the widely followed Laubach and Williams (2003) model.²² This highlights an additional benefit of using high quality bond market data for the estimation of r_t^* .

5.3.1 Factor Decomposition of Natural Rate Estimate

Having established the robustness of our r_t^* estimate, we now examine the contribution to its persistent changes the past twenty years made by each factor within the preferred AFNS-R model.²³

To proceed, we note that the analytical formula for r_t^* in the preferred specification of the AFNS-R model is given by²⁴

$$\begin{aligned} r_t^* &= \frac{1}{5} \int_{t+5}^{t+10} E_t^{\mathbb{P}}[r_s] ds \\ &= \theta_1^{\mathbb{P}} + \theta_2^{\mathbb{P}} + (L_t - \theta_1^{\mathbb{P}}) \frac{e^{-\kappa_{11}^{\mathbb{P}} 5} - e^{-\kappa_{11}^{\mathbb{P}} 10}}{5\kappa_{11}^{\mathbb{P}}} + (S_t - \theta_2^{\mathbb{P}}) \frac{e^{-\kappa_{22}^{\mathbb{P}} 5} - e^{-\kappa_{22}^{\mathbb{P}} 10}}{5\kappa_{22}^{\mathbb{P}}} \\ &\quad - \frac{1}{5} \frac{\kappa_{23}^{\mathbb{P}}}{\kappa_{22}^{\mathbb{P}} - \kappa_{33}^{\mathbb{P}}} (C_t - \theta_3^{\mathbb{P}}) \left(\frac{e^{-\kappa_{33}^{\mathbb{P}} 5} - e^{-\kappa_{33}^{\mathbb{P}} 10}}{\kappa_{33}^{\mathbb{P}}} - \frac{e^{-\kappa_{22}^{\mathbb{P}} 5} - e^{-\kappa_{22}^{\mathbb{P}} 10}}{\kappa_{22}^{\mathbb{P}}} \right). \end{aligned}$$

This shows that the r_t^* estimate implied by our preferred AFNS-R model is an affine function of the frictionless level, slope, and curvature factors, while the bond-specific risk factor plays no role for our r_t^* estimate as it is independent of the other three factors in the model.

Given the estimated parameters reported in Table 7, the fixed loadings on the frictionless

²²See Figure 3 in Laubach and Williams (2001) for the 70 percent confidence band in their model.

²³We thank Simon Lloyd for suggesting this analysis.

²⁴See Online Appendix D for details of the derivation.

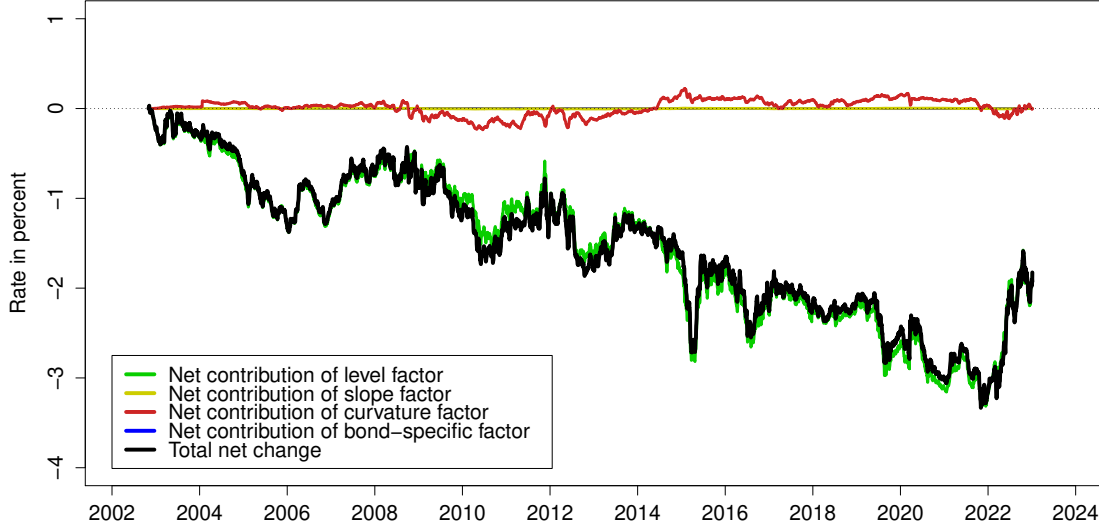


Figure 21: **Factor Contribution to Net Change in r^* Estimate**

level, slope, and curvature factors are 0.716, 0.001, and -0.046, respectively. Thus, based on the estimated parameters of our preferred model, the level factor will be the primary factor driving variation in our r_t^* estimate with a minor secondary role for the curvature factor, while the slope factor plays essentially no role.

In Figure 21, we plot the net change in our r_t^* estimate since the start of our sample, i.e., we are plotting $r_t^* - r_{t_0}^*$, where $r_{t_0}^*$ is the estimated natural rate at the start of our sample. Figure 21 also shows the net contribution from each of the four state variables implied by the factor loadings listed above. The level factor accounts for 100.2 percent of the net decline in our r_t^* estimate as the net contribution of the curvature factor provides a tiny positive offset, while the slope factor has essentially no impact on our r_t^* estimate.

5.3.2 Realism of the Model-Implied Real Rates

To build further confidence around our r_t^* estimate, we aim to assess the realism of the model-implied short-term real rates, which is the key building block in our finance-based definition of the natural rate.²⁵

To begin, for each month from December 2002 to December 2022, we combine the twelve-month ahead Consensus Forecasts of the three-month French government bond yield with their forecasts of HICP inflation for the current calendar year to produce a survey-based

²⁵We thank Min Wei for suggesting this exercise.

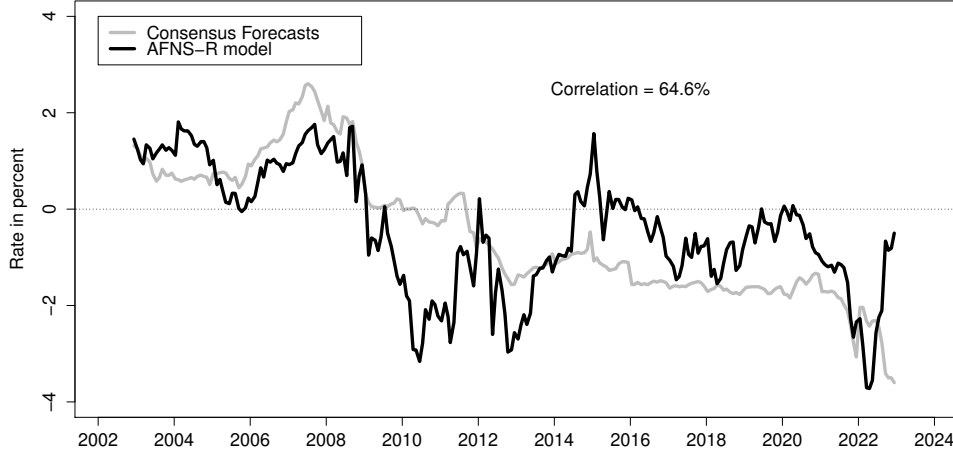


Figure 22: **Survey-Based and Model-Implied Expected Real Yields**

measure of the three-month real yield expected to prevail 12 months ahead. Although there is a mild mismatch between the two survey forecast horizons, any potential issues arising from that discrepancy are significantly tempered by the stability of the survey inflation forecasts.

To produce the matching model output, we calculate the model-implied three-month frictionless real yield (i.e. without any bond-specific risk premia) expected to prevail 12 months later. As a consequence, the model-implied real yield expectations are for a horizon exactly identical to that of the survey-based real yield forecasts.

Figure 22 shows these survey-based and model-implied expected three-month real yield series. We note both their general closeness and reasonably high positive correlation (65%). Based on this evidence, we conclude that our model is able to generate realistic levels of shorter-term real yields that track the information in the Consensus Forecasts surveys even though none of that information is used in the model estimation.

5.4 Comparison of Estimates of the Natural Rate

In this section, we compare our estimate of the natural rate to other existing estimates of the natural interest rate in the literature. To start, we compare our r_t^* estimate from the preferred AFNS-R model to the U.S. market-based estimate reported by CR using solely the prices of U.S. TIPS. These two market-based estimates of the natural rate are shown in Figure 23. Their high positive correlation and similar downward trend are both evident. Also, they share the common feature that their most pronounced declines over the past two decades happened before and after, but not *during* the GFC. These observations combined suggest

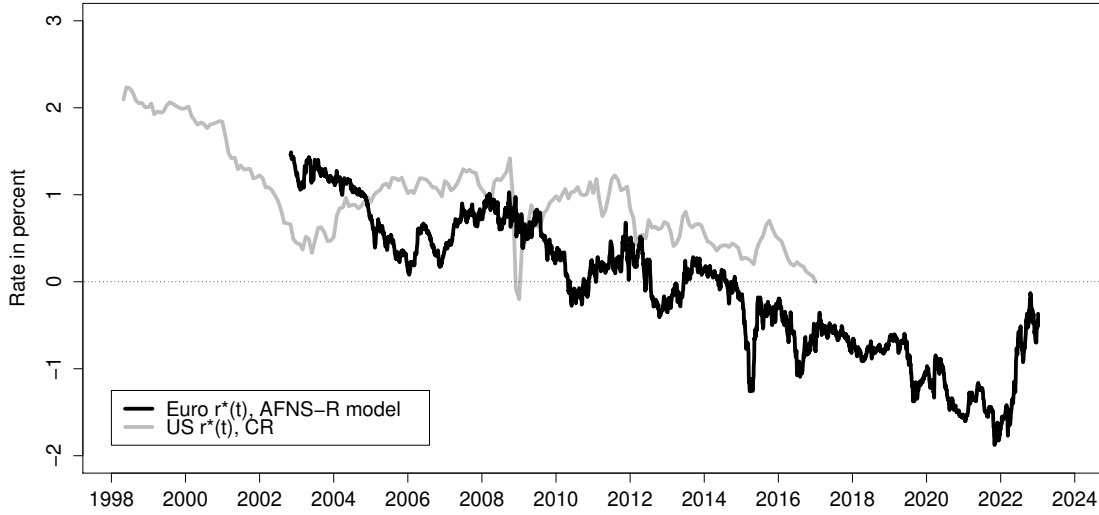


Figure 23: **Comparison with Foreign Market-Based Estimate of r^***

that the factors depressing U.S. and euro-area interest rates are likely to be global in nature and are not particularly tied to developments surrounding the GFC.

Now, we turn to the crucial comparison of our finance-based estimate of r_t^* with estimates based on macroeconomic data. Figure 24 shows the r_t^* estimate from our preferred AFNS-R model, along with the macro-based estimate of r_t^* from Holston et al. (2017, henceforth HLW), which is the filtered estimate generated by applying the approach described in Laubach and Williams (2003) to euro-area macroeconomic series. The r_t^* estimate from HLW starts in 1972. However, until the onset of the GFC, this macro-based estimate appears to be stationary and remains close to 2.5 percent the whole time. This is consistent with the received wisdom of that era in monetary economics that viewed the natural rate as effectively constant—for example, as assumed in the large Taylor rule literature. It is only in the aftermath of the GFC that we see a persistent large downward movement in the macro-based r_t^* estimate, which is much later and smaller than the sizable drop in our market-based estimate. Importantly, at the end of our sample, this macro-based estimate is -0.68 percent and hence close to our market-based estimate.

The second macro-based estimate of r_t^* is taken from Del Negro et al. (2019, henceforth DGGT). They estimate a flexible vector autoregression model with common trends for a sample of data from 7 advanced economies, including Germany, France, and Italy, covering the period from 1870 to 2016 and here extended through the end of 2020.²⁶ They use annual data

²⁶We thank Marco Del Negro for sharing the updated data.

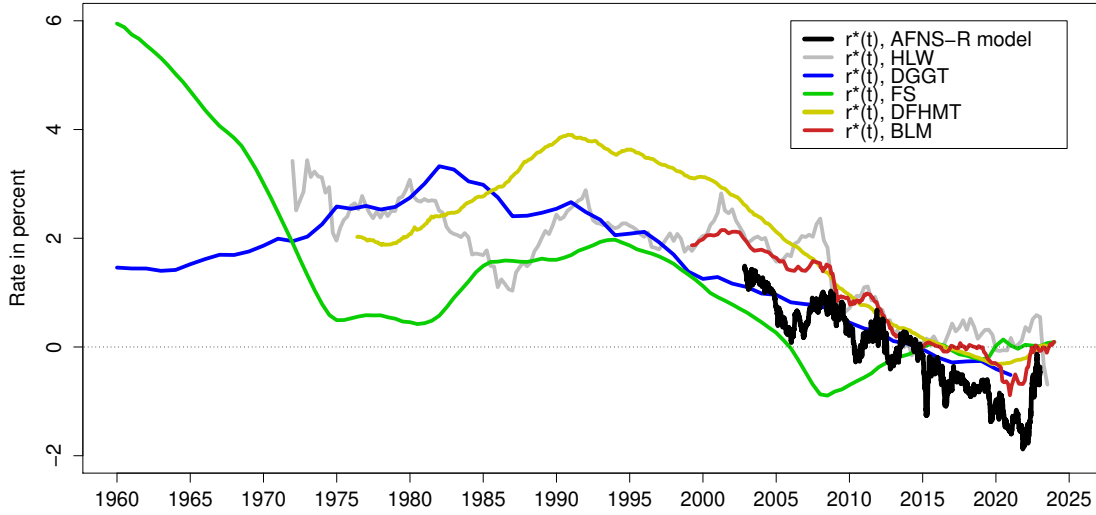


Figure 24: **Comparison with Macro-Based Estimates of r^***

on short- and long-term government bond yields, consumer prices, and real consumption per capita in addition to Moody's Baa corporate bond yields. In their analysis, it is an assumption of no arbitrage in the long run that implies a factor structure for the trend of real interest rates across countries. They find that real interest rates across these 7 countries share a global common trend that has been particularly pronounced since the 1970s. Moreover, using regression analysis, they find that declining consumption growth and increasing convenience yields from the safety and liquidity offered by government bonds from these countries are the main drivers of declining real rates the past 40 years. We calculate the average of their r_t^* estimates for Germany, France, and Italy to get a representative estimate for the euro area. This series is shown with a solid blue line in Figure 24. Note that their r_t^* estimate for the euro area was increasing back in the 1960s and 1970s before starting a pronounced secular decline in the early 1980s. The trend lower continues through the end of the shown sample and leaves it below zero by 2020 not much above our market-based r_t^* estimate.

The third macro-based estimate of r_t^* is taken from Ferreira and Shousha (2023, henceforth FS) and shown with a solid green line in Figure 24. They consider a panel of 11 advanced economies and estimate the longer-run neutral real interest rates while accounting for changes in the global supply of safe assets and their convenience yields in addition to productivity and demographics and global spillovers from their developments. Their r_t^* estimate for the euro area starts in 1960 and fell steadily until the mid-1970s. It reversed some of the decline in the early 1980s and remained fairly stable until the late 1990s. It then steadily declined

until 2008 when it reached a historic low of -0.89 percent. Since then it has gradually trended higher and stood at 0.1 percent by the end of 2023. This upward trend the past 15 years with a net increase of about 1 percentage point sets it apart from the other estimates, which mostly trend lower during this period.

The fourth and final macro-based estimate of r_t^* comes from Davis et al. (2024, henceforth DFHMT). They introduce a unified no-arbitrage macro-finance model with two trend factors used to estimate the natural rate r_t^* for 10 advanced economies, including Germany, France, and Spain. Using a multitude of data sources on trend growth and inflation in addition to risk premium series, DFHMT also underscore the need for a coherent model approach like ours. Importantly, the interpretation of their natural rate r_t^* is consistent with Laubach and Williams (2003) of representing a medium-run real rate anchor for monetary policy. Our finance-based definition taken from CR is intended to capture the same concept. Hence, the DFHMT r_t^* estimate should be comparable to ours. One notable difference, though, is that, by relying on a single average yield equation, their estimation is not fully exploiting all the information in the yield curve unlike our approach.

To get a representative estimate for the euro area, we calculate the average of their r_t^* estimates for Germany, France, and Italy. The resulting r_t^* series is shown with a solid yellow line in Figure 24. While increasing in the 1970s and 1980s, the DFHMT r_t^* estimate peaked in late 1989. In the subsequent more than 30 years, r_t^* fell more than 4 percentage points according to their estimate and ends the sample slightly below zero. For the overlapping period this entails a close similarity between their r_t^* estimate for the euro area and our market-based r_t^* estimate. Overall, this pattern aligns well with the observed OAT€ yields shown in Figure 3. Moreover, using panel regressions, DFHMT relate their r_t^* estimates to economic growth and demographic variables and find that slowing growth and population aging have been significant factors in driving down the natural rate r_t^* globally, and in their three European countries in particular. Given the similarity of our market-based r_t^* to their estimate, we speculate that our estimate is likely influenced by those same factors.

The final series shown in Figure 24 is the median of a variety of r_t^* estimates reported by Brand et al. (2024, henceforth BLM). They include both macro- and market- as well as survey-based estimates of r_t^* for the euro area.²⁷ The similarities in both the declining trend and the general level of their median r_t^* estimate and our market-based r_t^* estimate are striking. In particular, they both suggest that the natural rate experienced a significant decline early on during the COVID-19 pandemic and a fairly sharp recovery of that decline in early 2022. As a result, both series suggest that r_t^* in the euro area has changed little on net since before the pandemic. Still, all six considered measures suggest that r_t^* in the euro area has declined notably the past 20-30 years and remains close to zero at the end of

²⁷We thank Claus Brand for sharing this series.

our sample despite the recent sharp increases in long-term interest rates in the euro area and other major advanced economies. This obviously matters for judgments about the stance of monetary policy, as we will discuss later on.

5.5 Monetary Policy and the Natural Rate of Interest

In a recent influential paper, Hillenbrand (2025) shows that most of the decline in U.S. long-term interest rates during the decades before the pandemic occurred in narrow windows around FOMC meetings. The most straightforward interpretation of his results is that accommodative U.S. monetary policy left seemingly permanent or at least very long lasting marks on U.S. long-term interest rates. Hanson and Stein (2015) is another influential paper providing evidence of a causal effect flowing from U.S. monetary policy to U.S. long-term real rates.

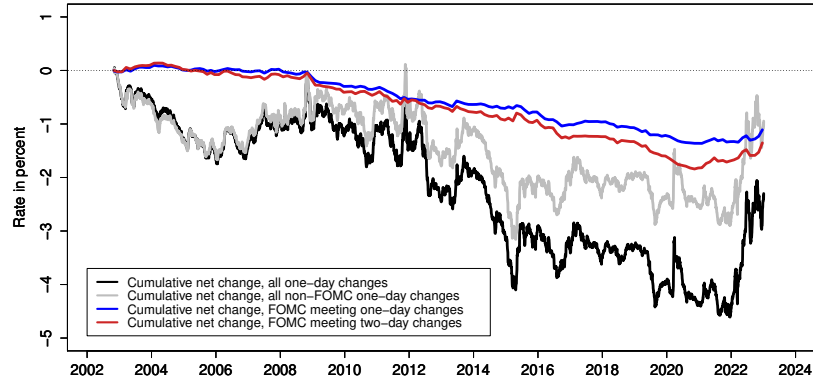
Hoffmann et al. (2024) extend the analysis of Hillenbrand (2025) to long-term bond yields from ten advanced economies and document that non-U.S. long-term interest rates have been affected in much the same way during that same set of narrow time windows. They interpret this as U.S. monetary policy having large and lasting spillover effects on fixed-income markets in other advanced economies, presumably for similar reasons.

Motivated by this evidence we are interested in examining how monetary policy announcements affect our r_t^* estimate for the euro area. Given that the literature above is centered around U.S. monetary policy, we begin by examining its role for our r_t^* estimate before we proceed to a similar analysis of the changes in our r_t^* estimate following the governing council meetings at the ECB.

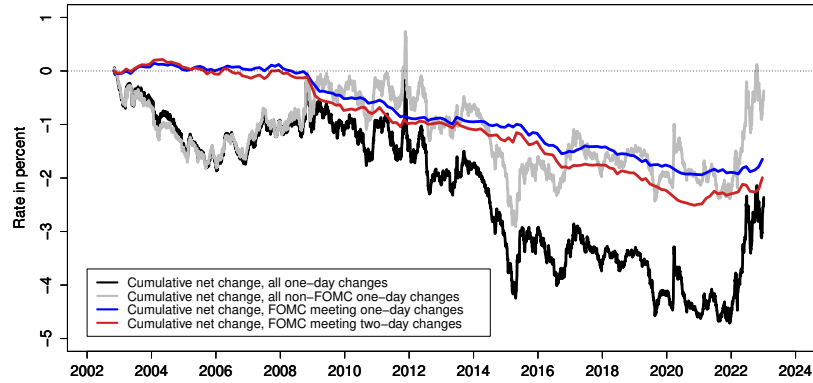
5.5.1 The Role of U.S. Monetary Policy

In the following, we exploit the fact that we are executing our analysis at daily frequency. This allows us to use our euro-area r_t^* estimate and the associated 5yr5yr real yield decomposition to speak to the question about spillover effects of U.S. monetary policy onto euro-area long-term real yields. Specifically, we focus on the scheduled FOMC meeting dates listed in Hoffmann et al. (2024) and limit the analysis to the ones since October 2002 that overlap with our sample. Given that European markets are closed when the FOMC statements are released to the public, usually around 2 pm New York time, we calculate one-day changes as the change in yields between the day *after* an FOMC meeting and the day *of* the FOMC meeting, while two-day changes add one day to the calculation to get the more complete response of European bond markets to each FOMC meeting.

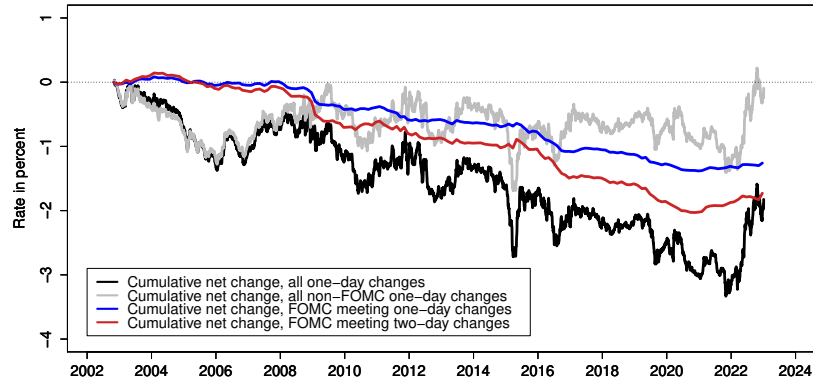
We then proceed as in Hillenbrand (2025) and piece together all the one- and two-day responses and contrast those cumulative changes with the cumulative one-day changes on all



(a) Fitted 5yr5yr real yield



(b) Fitted 5yr5yr frictionless real yield



(c) r_t^* estimate

Figure 25: U.S. Monetary Policy Effects on 5yr5yr Real Yields and r^* Estimate

the remaining non-FOMC days. In Figure 25, we plot the results of these response cumulations for the raw 5yr5yr fitted real yield without any adjustments, the 5yr5yr frictionless real yield implied by our preferred AFNS-L model, and our r_t^* estimate that adjusts the latter for the term premium component. We make several noteworthy observations based on the resulting series. First, in the 2002-2008 period, there is a very limited role for U.S. monetary policy in driving the variation in euro-area long-term real yields, and this conclusion is insensitive to the 5yr5yr real yield measure used.

Second, in the 2009-2016 period when U.S. monetary policy was constrained by the ZLB for an extended period and a variety of unconventional monetary policies and strategies were employed, it seems that narrow FOMC windows can account for about one third of the decline in long-term real yields in the euro area.

Third, for the remaining part of our sample period, it appears that U.S. monetary policy had again close to zero net effect on long-term real yields in the euro area. Of particular note, windows around FOMC meetings account for very little of the sizable sharp increase in both long-term real yields and our r_t^* estimate since early 2022.

Thus, while measured in net changes between October 2002 and December 2022—in particular with a two-day event window—the data can be construed to show that U.S. monetary policy can explain almost 100 percent of the net decline in r_t^* in the euro area, a more detailed breakdown clearly reveals that FOMC windows account for very little of the full variation in our euro-area r_t^* estimate.

Finally and importantly, a two-day response window nearly doubles the measurement of the spillover effect from U.S. monetary policy onto our r_t^* estimate compared with the strict academically sounder one-day response windows. Significant delayed responses of this magnitude raise questions about the appropriateness of relying on narrow one-day event windows for measuring financial market reactions in the euro area as done in the high-frequency literature (see, e.g., Nakamura and Steinsson 2018), but we leave it for future research to examine that important question further.

5.5.2 The Role of ECB Monetary Policy

As the U.S. analysis above left much variation in our r_t^* estimate for the euro area unexplained, we next examine the effects of the ECB’s monetary policy decisions. To do so, we follow the approach of Hillenbrand (2025) and register the net change in our r_t^* estimate during narrow one- and three-day event windows around each governing council (GC) meeting since November 2002.

The resulting cumulative changes in our r_t^* estimate during the one- and three-day event windows are shown in Figure 26 with a green and gray line, respectively. Figure 26 also shows the cumulative net change in our r_t^* estimate for all days in the sample.

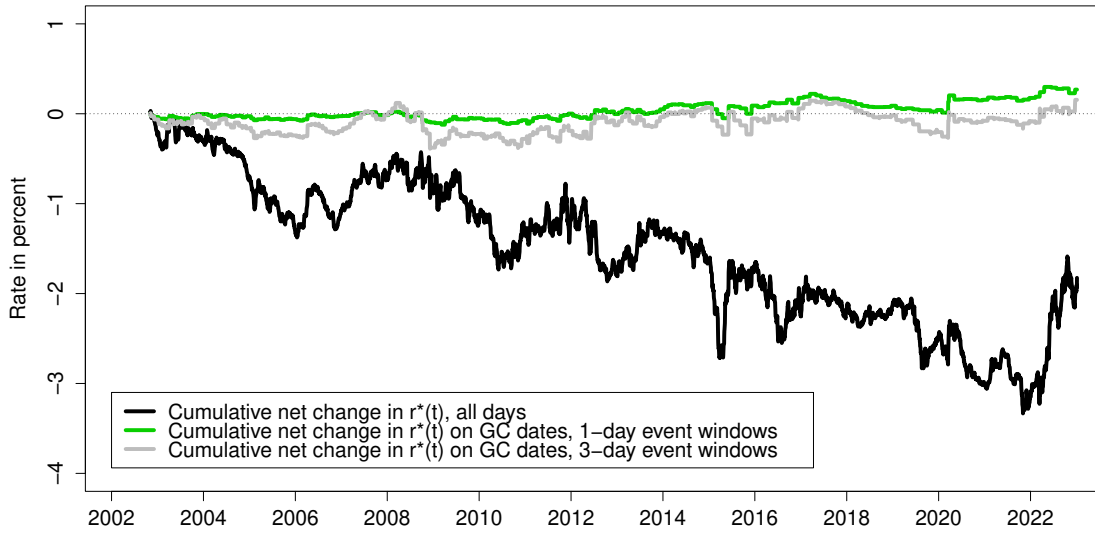


Figure 26: **ECB Monetary Policy Effects on r^* Estimate**

In light of the overwhelming evidence cited earlier about the strong effects of U.S. monetary policy on U.S. long-term real interest rates, the results for the effects of the ECB's monetary policy are surprising in that ECB's monetary policy announcements have at best small, short-lived effects on our estimate of r_t^* for the euro area. Importantly, this conclusion applies to all 20 years of our sample and is independent of the length of the event window. Even more strikingly, there is not a single subperiod that resembles the strong monetary policy effects reported for the U.S. Thus, this is one place where there seems to be a stark difference in the effects of monetary policy between the U.S. and the euro area. We leave it for future research to explore whether this difference in the impact on long-term real rates matters for the overall transmission of monetary policy to the real economy.

Moreover, as a practical matter, this independence result implies that our estimate of r_t^* can be used for real-time policy analysis in the euro area. For example, it can serve as a conditioning variable in monetary policy rules such as the one described in Taylor (1993). However, we leave an exploration of that avenue for future research.

Finally, the finding of independence between our r_t^* estimate and the ECB's monetary policy also provides an answer to the question posed in the introduction regarding why the ECB ended up employing negative monetary policy rates for an extended period in the years after the European Sovereign Debt Crisis. Our analysis indicates that it was the low level of the natural rate in the euro area that ended up forcing the ECB to use negative policy rates to achieve a sufficiently accommodative stance of monetary policy. Based on the presented

Explanatory variables	(1)	(2)	(3)
$\mathbf{1}_{GC} \times \text{MPS}$	0.2039** (0.0885)		
MPS		0.1974** (0.0907)	0.1947** (0.0889)
$\mathbf{1}_{GC}$			0.0006 (0.0016)
N	5,257	210	5,257
Adjusted R^2	0.0035	0.0647	0.0031

Table 8: **Regression Results for Changes in r_t^* on ECB Monetary Policy Shocks**

The table reports the results of regressions with daily changes in r_t^* on ECB monetary policy shocks. MPS is the euro-area monetary policy shocks from Jarocinski and Karadi (2020), while $\mathbf{1}_{GC}$ takes a value of 1 on a Governing Council day and a 0 otherwise. For regressions (1) and (3), all changes are daily. For regression (2), all changes are at a Governing Council frequency. All regressions include an intercept and lagged values of the dependent variable. Standard errors are in parentheses. Asterisks *, ** and *** indicate significance at the 10 percent, 5 percent, and 1 percent levels, respectively.

evidence, we feel that we can relatively safely rule out the alternative story that r_t^* in the euro area became significantly negative as a consequence of the ECB’s conventional and unconventional monetary policies since the global financial crisis. We find very little evidence supporting that interpretation.

To examine the effect of ECB monetary policy on our r_t^* estimate further, we again leverage the fact that our r_t^* estimate is daily and examine its relationship to the high-frequency monetary policy shocks for the euro area constructed by Jarocinski and Karadi (2020). We regress daily changes of r_t^* on these shocks both based on our full sample by interacting the shocks with an indicator variable and for the subsample just containing the GC meeting dates. The results are reported in the first two columns of Table 8. Both regressions produce a statistically significant positive coefficient with a value around 0.2. To explore whether this effect is due to the monetary shock or just represent event-day effects tied to GC meetings, we include both as separate variables with the results reported in the third column of Table 8. The results indicate that it is the size of the monetary policy shocks that matter while GC meeting dummy variable on its own is entirely insignificant.

To summarize, ECB monetary policy shocks do have a positive effect on r_t^* in the euro area, but our replication of the Hillenbrand (2025) exercise shown in Figure 26 indicates that these effects are very transitory.

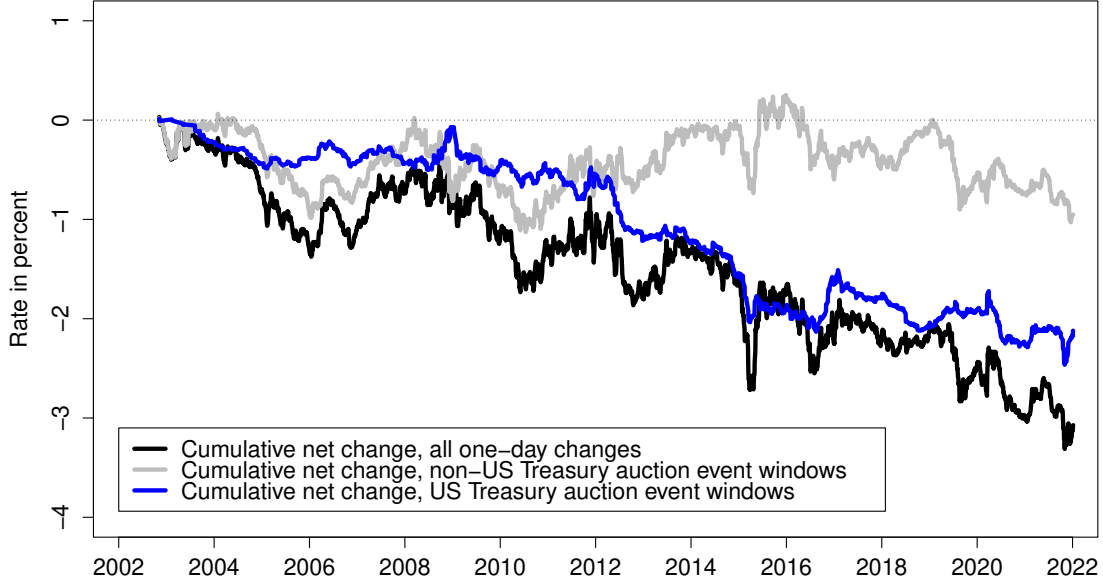


Figure 27: U.S. Treasury Auction Effects on r^* Estimate

5.6 U.S. Treasury Auctions and the Natural Rate of Interest

In a recent paper, Somogyi et al. (2025) find that most of the decline in U.S. long-term interest rates during the decades before the pandemic occurred in narrow windows around U.S. Treasury auctions, seemingly competing with the analysis of Hillenbrand (2025) in terms of explaining the persistent long-term yield declines. Their interpretation is that U.S. Treasury auctions offer investors evidence of the global demand for safe assets.²⁸

If true, this mechanism could potentially also matter for the pricing of safe assets in the euro area, including the French OATs in our sample. To explore that conjecture, we piece together all the changes in our r_t^* estimate during the U.S. Treasury auction event windows examined in Somogyi et al. (2025) and contrast those cumulative changes with the cumulative changes on all the remaining non-auction days. In Figure 27, we plot the results of these response cumulations for our r_t^* estimate. We make several noteworthy observations based on the resulting series. First, in the 2002-2008 period, there is a limited role for U.S. Treasury auctions in driving the variation in euro-area long-term real yields. However, starting in 2009, most of the decline in our euro r_t^* estimate since then has occurred in narrow windows coinciding with U.S. Treasury auctions. Hence, on net between 2002 and 2021 when

²⁸Given that about half of U.S. government debt is held by foreigners, the auction results can be interpreted as reflecting safe asset demand on a global scale.

the sample analyzed by Somogyi et al. (2021) ends, more than two percentage points of the decline in our euro r_t^* estimate appear to be associated with news tied to U.S. Treasury auctions. Equally importantly, the changes in r_t^* on non-auction days are smaller and appear to be mostly transitory in nature.

The takeaway seems to be that part of the decline in long-term real rates in the euro area during our sample period reflects increasing demand for safe assets. Given that this effect started to materialize in 2009 coinciding with the launch of large-scale asset purchase programs in the U.S. and the U.K.,²⁹ we speculate that global safe asset demands may have been persistently affected by the unconventional policies pursued by the world’s largest central banks. This interpretation provides a way to reconcile the findings of Hillenbrand (2025) and Somogyi et al. (2025), but we leave it for future research to examine that conjecture further. Crucially, though, our results in the previous section show that any effects on r_t^* flowing from the ECB’s asset purchases did not materialize around GC meetings, but whether other ECB communications such as speeches could play a role is beyond the scope of our paper and also left for future research.

5.7 Projections of the Natural Rate

In light of the intense debate among researchers, investors, and policymakers about whether there is a new normal for interest rates, we end our analysis in this section by presenting the outlook for the natural rate based on our preferred AFNS-R model. We follow the approach of Christensen et al. (2015) and simulate 10,000 factor paths over a ten-year horizon conditioned on the shape of the OAT€ yield curve and investors’ embedded forward-looking expectations as of the end of our sample (that is, using estimated state variables and factor dynamics as of December 30, 2022). The simulated factor paths are then converted into forecasts of r_t^* . Figure 28 shows the median projection and the 5th and 95th percentile values for the simulated natural rate over a ten-year forecast horizon.³⁰

First, we note that our r_t^* estimate experienced some reversal of the declines from the past two decades during the last year of our sample, which left it at -0.37 percent at its end. The median r_t^* projection shows a persistent, but very gradual further reversal throughout the ten-year projection period that would put it close to 0.2 percent by 2032. The upper 95th percentile rises more rapidly and moves slightly above 2 percent by the end of the projection period, while the lower 5th percentile represents outcomes with the natural rate trending persistently lower into negative territory and remaining there over the entire forecast horizon. Although stationary, these results show that a highly persistent model like our preferred

²⁹See Christensen and Rudebusch (2012) for an analysis of the early U.S. and U.K. QE programs.

³⁰Note that the lines do not represent short rate paths from a single simulation run over the forecast horizon; instead, they delineate the distribution of all simulation outcomes at a given point in time.

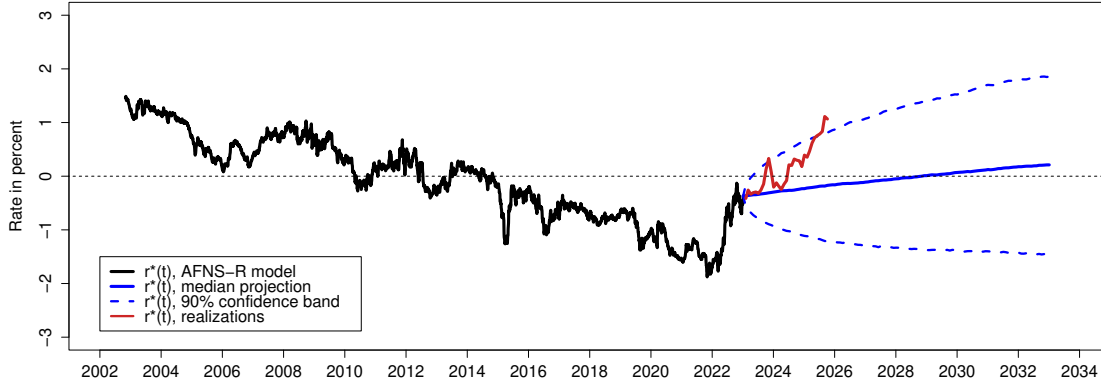


Figure 28: **Ten-Year Projections of r^* from AFNS-R Model**

AFNS-R model can deviate from the estimated mean for several decades. Thus, nonstationary dynamics such as unit roots or trending shifting end points are not necessary to satisfactorily model the secular persistent decline of interest rates observed in the OAT€ market the past two decades. Of course, like most estimates of persistent dynamics, the model may still suffer from some finite-sample bias in the estimated parameters of its mean-reversion matrix $K^{\mathbb{P}}$, which would imply that it does not exhibit a sufficient amount of persistence—as described in Bauer et al. (2012). In turn, this would suggest (all else being equal) that the outcomes below the median are more likely than a straight read of the simulated probabilities indicate, and correspondingly those above the median are less likely than indicated. As a consequence, we view the projections in Figure 28 as an upper bound estimate of the true probability distribution of the future path for the natural rate.

As an out-of-sample robustness exercise and to assess the reasonableness of the projections, we examine the results from real-time updates of our model during the post-pandemic reopening and its aftermath. This represents an alternative way to both stress test the model and assess the robustness of our findings and conclusions. To achieve this, we update our data each month from January 2023 to September 2025 and re-estimate our preferred AFNS-R model. These updated estimates of r_t^* are shown in Figure 28 with a solid red line. We note that the subsequent realizations of our r_t^* estimates have trended up persistently since 2023 and much more so than our median projection. As a result, it moved up above the 95th percentile by spring 2025 and sits at 1.07 percent as of September 30, 2025, slightly above the 98th percentile of our simulated outcomes for that horizon. Whether this elevated level of r_t^* will persist remains to be seen. Part of the recent uptick in the r_t^* estimate seems to be related to on-going political turmoil in France combined with persistent large government

deficits. However, we leave it for future research to examine any such ties further. Still, against that background, it is maybe not all that surprising that the 90% confidence band surrounding the r_t^* projections is narrower than the subsequent realizations. In fact, we take it as suggestive evidence that the model’s estimated factor dynamics imply a realistic amount of uncertainty about investors’ long-term real rate expectations in the euro area.

Importantly, this exercise demonstrates how a dynamic term structure model like ours can be used to assign probabilities to both future risks as well as historical realizations. This is crucial from a risk management perspective as emphasized by Christensen et al. (2015) in the context of stress testing the U.S. Federal Reserve’s balance sheet.

6 The Stance of ECB Monetary Policy

In this section, as a final application of our market-based estimate of r_t^* , we use it to construct measures of the stance of the ECB’s monetary policy.

In theory, the stance of monetary policy would be given by the difference between the current real instantaneous short rate and its natural level as reflected in r_t^* , i.e., it would be defined as

$$\zeta_t = r_t - r_t^*.$$

The intuition behind this definition is straightforward. When the current real short rate is above its natural level, interest rates of all kinds are likely to be above their steady-state level and will provide some headwind for economic activity through higher borrowing costs and help slowdown the economy. And vice versa, when the current real short rate is below its natural level, the general interest rate level is likely to be below what is needed to maintain trend growth, and businesses and households may take advantage of that by making investments in new projects or housing at cheap financing rates, which will help boost economic activity.

Unfortunately, the instantaneous real short rate is not directly observable because we do not have a continuous measure of the very short end of the OAT€ yield curve, given that individual OAT€s reach maturity infrequently as noted in Figure 2(b). Furthermore, as explained earlier, OAT€s, like other inflation-indexed bonds, tend to have rather erratic prices close to maturity thanks to both low liquidity and the unpredictability of the final inflation adjustments to be earned—the sudden and very sharp spike in HICP inflation in 2022 is very illustrative in this regard.³¹ Thus, to make the definition above operational, we consider instead three proxies that we think of as reasonable substitutes for r_t . The first is given by the one-year fitted real OAT€ yield from an estimation of the AFNS model without

³¹For comparison, a standard fixed-coupon bond pays a principal of 1 and fixed coupons C . Thus, there is no uncertainty about its final cash flow in the months leading up to its maturity date, which helps maintain the liquidity of such securities.

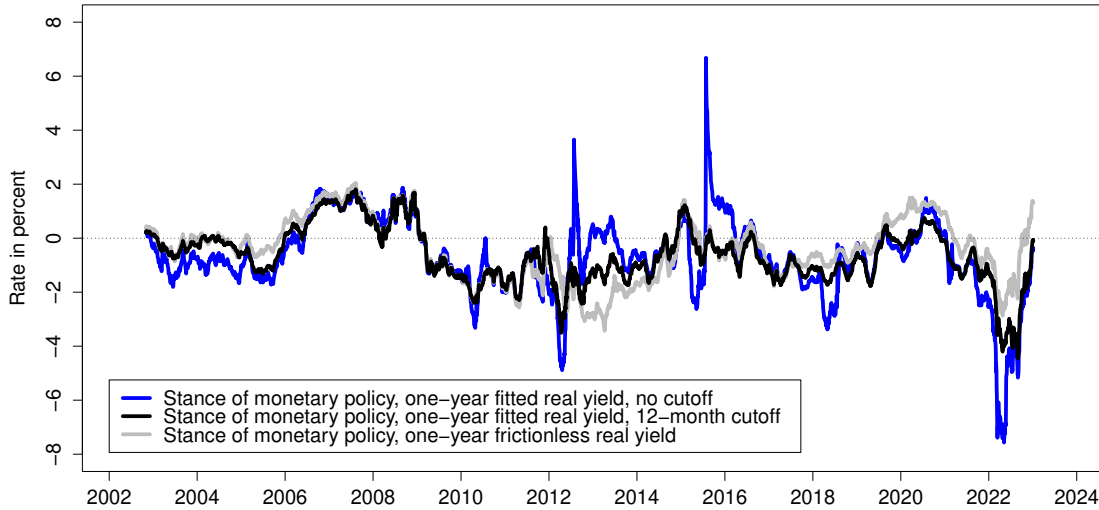


Figure 29: **Market-Based Measures of the Stance of Monetary Policy**

censoring any bond price information, that is, OAT€ prices remain in the sample until they mature. This provides the best possible coverage around the one-year maturity point but comes at the cost of adding significant noise from the prices of OAT€s close to maturity. Still, one can argue that this yield measures the full actual real yields observed in financial markets—including noise and frictions—and hence represents the most realistic real-world equivalent to the textbook short-term real rate embedded in the definition of ζ_t . To limit the noise and erratic behavior while preserving the desirable economic interpretation, we consider a second proxy for the stance of monetary policy calculated using instead the one-year fitted real yield from an estimation of the AFNS model imposing our baseline censoring of price information when bonds have less than one year to maturity. The third and final proxy is the one-year frictionless real yield implied by our preferred AFNS-R model. This is a cleaner and more stable measure of the one-year real yield as it adjusts for the noise from the bond-specific risk premia. However, in doing so, it may be different from the textbook concept of the real short rate r_t appearing in the original definition of ζ_t . Moreover, as OAT€ bond prices with less than one year to maturity are censored in the estimation of our preferred AFNS-R model, it may capture the short end of the OAT€ real yield curve less accurately similar to our second proxy.

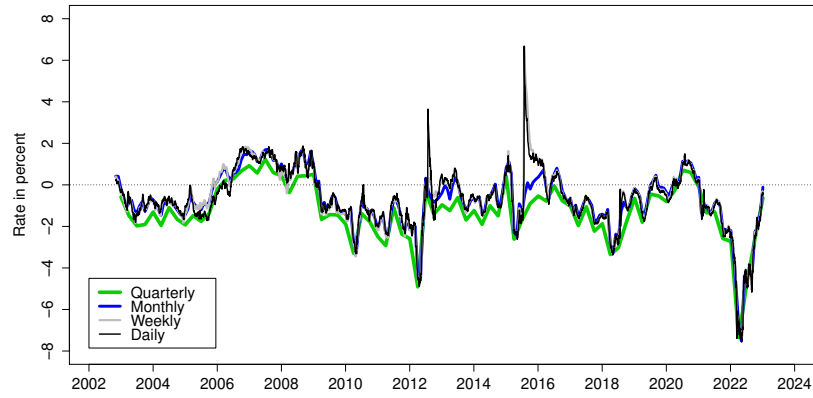
The resulting three empirical measures of the ECB’s stance of monetary policy are shown in Figure 29. In general, the three measures are quite similar and highly positively correlated, although there are important differences to note. Allowing for no data cutoff in the estimation

that produces the short-term real yields, provides a stance measure with sharp spikes up or down whenever a bond in the sample approaches maturity. Crucially, these sharp short-lived gyrations are uncorrelated with the stance of monetary policy, which leads us to reject this measure. In comparison, using frictionless real yields to construct our measure of the stance of monetary policy, provides a more smooth and stable estimate. Unfortunately, as we demonstrate in Figure 30 below, this measure of the stance of monetary policy is very sensitive in the first decade of our sample to the data frequency used in the model estimation, which is an undesirable feature. In contrast, using fitted real yields based on our baseline approach with censoring of the bond prices with less than one year to maturity, provides a stance measure that is both relatively stable *and* robust to the data frequency used in the model estimation. As a consequence, this is our preferred measure of the stance of monetary policy in the euro area.³²

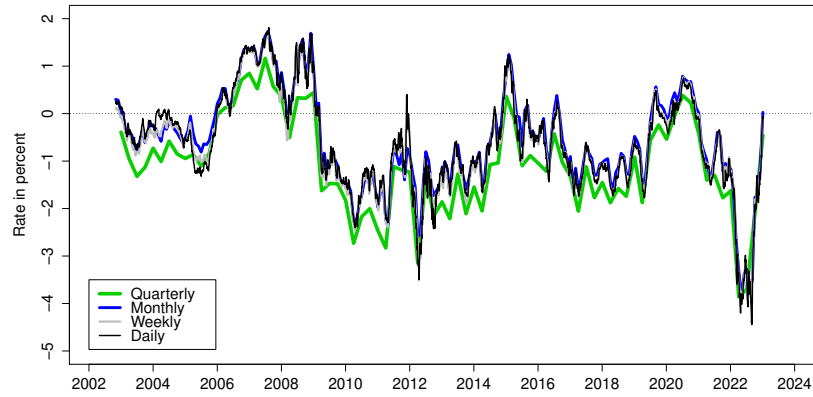
Comfortingly, there are several important commonalities across the three measures worth highlighting. First, monetary policy in the euro area was tight going into the GFC in 2007 and remained above neutral into 2009 before finally reaching an accommodative level. Second, in the 2015-2018 period, quantitative easing and other unconventional measures along with forward guidance managed to push the stance of monetary policy into accommodative territory and keep it there for several years according to all three measures. Third, at the peak of the COVID-19 pandemic in spring 2020, monetary policy reached a tightening stance and did not become accommodative until early 2021. Finally and similar to the United States, the ECB response to the spike in inflation following the global economic reopening after the pandemic was delayed, which had the implication that monetary policy remained very accommodative for an extended period of time and did not reach a tightening posture until the very end of our sample, and only according to one of our three measures. This may have contributed to prolonging the spell of high inflation in the euro area during this period, but it falls well outside the focus of this paper to make any determinations to that effect, so we leave it for future research to explore that question further.

Based on these observations we think of our empirical market-based measures of the ECB's monetary policy stance as realistic and representative. Moreover, as demonstrated by our analysis, they can be estimated at daily frequency and hence used for truly real-time policy analysis. This represents a major advantage relative to existing macro-based estimates, which are only available with a lag and may be subject to significant data revisions.

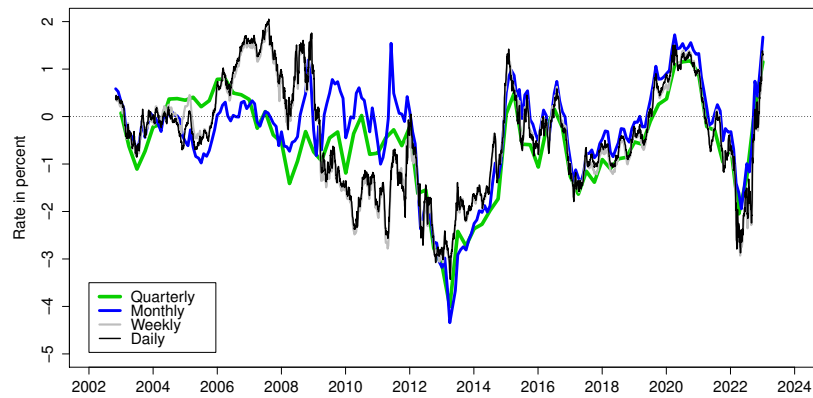
³²In online Appendix F, we establish the high quality of the estimated short-term real yields used in the calculation of our preferred measure of the stance of monetary policy by comparing them with corresponding fitted OAT€ real yields reported in a recent paper by Grishchenko et al. (2025).



(a) Stance of monetary policy, one-year fitted real yield, no cutoff



(b) Stance of monetary policy, one-year fitted real yield, 12-month cutoff



(c) Stance of monetary policy, one-year frictionless real yield, 12-month cutoff

Figure 30: Sensitivity of Measures of the Stance of Monetary Policy to Data Frequency

6.1 Comparison with a Text-Based Policy Stance Measure

To validate our market-based measures of the stance of ECB’s monetary policy, we focus on Hubert and Portier (2024, henceforth HP), who construct a text-based measure of the ECB’s stance of monetary policy. Specifically, they use textual analysis techniques to identify words that are either dovish or hawkish in the policy statement and during the press conference following each ECB governing council meeting. By subtracting the dovish count from the hawkish count and divide by the total word count, they obtain a measure of the net hawkish signal or stance conveyed after each policy meeting since 2001.

For this comparison, we use our preferred measure of the stance of ECB monetary policy based on the one-year fitted real yield using 12-month censoring in the model estimation. In Figure 31, we compare our chosen market-based measure of the stance of monetary policy in the euro area to the text-based ECB stance measure reported by HP. We note that, although broadly similar in the 2003-2008 period and again in the 2015-2019 period, the two measures imply sharply different assessments of ECB’s monetary policy stance during the European Sovereign Debt Crisis in 2010-2013, during the COVID-19 pandemic in 2020-2021, *and* during the post-pandemic spike in inflation. Interestingly, the text-based measure suggests that ECB policy was neutral-to-net hawkish during the sovereign debt crisis, while our market-based measure suggests that monetary policy in the euro area was accommodative during this period by historical standards. During the COVID-19 pandemic we see the opposite pattern whereby ECB policymakers tried to convey an accommodative stance, but the market-based measure indicates that this was not achieved until after the pandemic when inflation spiked up. During this latter, equally interesting period the measures again flip sign. While ECB policymakers were trying to send very strong hawkish signals, the market-based measure suggests that monetary policy was very accommodative initially as short-term real rates were very negative due to the high inflation. As a consequence, monetary policy only reached a restrictive stance by late 2022 according to our market-based measure.

What explains this very different pattern for the text-based measure during these crucial periods? To offer an answer, we note that HP’s measure reflects—in a very direct way—the monetary policy stance communicated by ECB officials in the statement and through the answers to questions during the press conference. However, by design, it fails to capture to what extent the messaging is actually registered by financial market participants. In contrast, our market-based measure is designed to exactly capture the information investors have priced into the deep and liquid OAT€ bond market. Under the assumption that investors are forward looking and have every monetary incentive to use what they deem to be the best available information in devising their trading strategies, this “best available” information gets reflected in the bond prices. Under the additional assumption that our model is well specified, it should

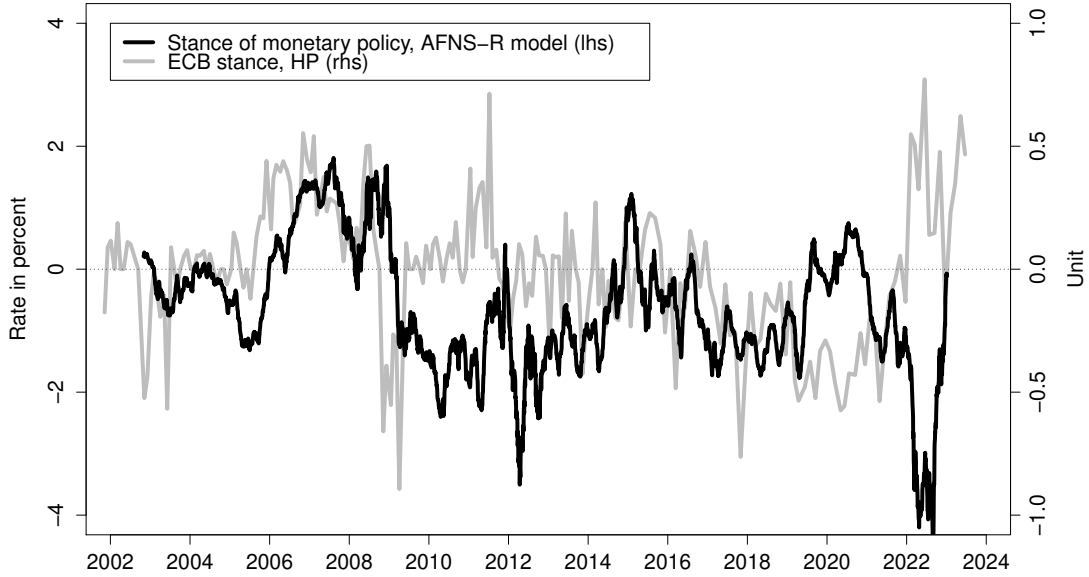


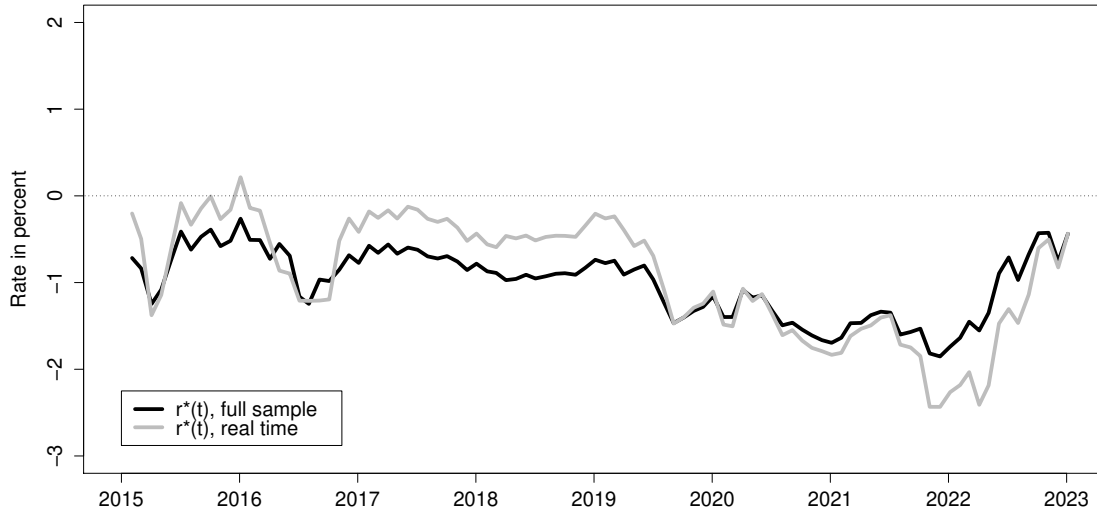
Figure 31: **Comparison with a Text-Based Measure of the Stance of Monetary Policy**

extract this information and the embedded investor expectations in a reliable manner. This is the theoretical and econometric argument for why our market-based measure of the stance of monetary policy should be preferable to the text-based measure produced by HP. This also explains why they may be different and not necessarily highly positively correlated.

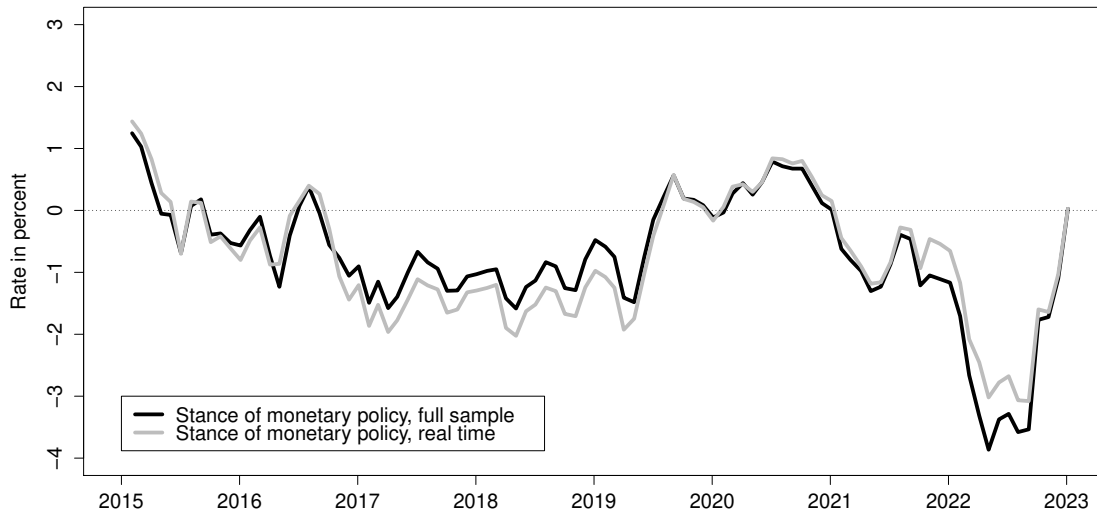
6.2 Real-Time Analysis

As a final exercise, we examine the real-time behavior of both our r_t^* estimate and our proposed measure of the stance of ECB's monetary policy. Given the documented robustness of both measures to the data frequency used, we choose to perform the exercise at the monthly frequency, in part to save on computing time and in part because this is the frequency conventionally used in macro-based policy analysis. Practically, we start the model estimation on January 31, 2015, add one month of data to our sample, re-estimate our preferred AFNS-R model, and continue this process until we reach our full sample that ends on December 30, 2022. This allows us to study the real-time model performance before, during, and after the COVID-19 pandemic.

Figure 32 shows the resulting real-time estimates with a comparison with the corresponding full-sample estimates. We note that the real-time estimates of both r_t^* and the policy stance measure are very close to their full-sample counterparts. Furthermore, Christensen



(a) r_t^*



(b) Stance of monetary policy

Figure 32: **Real-Time Estimates of r_t^* and the Stance of Monetary Policy**

and Mouabbi (2025) provide updated estimates of r_t^* through the end of March 2025 that preserve the robust pattern documented above for the overlapping period. Overall, we take this evidence to demonstrate that our model can be reliably used for real-time analysis.

7 Conclusion

Given the historic downtrend in yields in recent decades, many researchers have investigated the factors pushing down the steady-state level of the safe short-term real interest rate. However, all of this empirical work has been based on *macroeconomic* models and data, and uncertainty about the correct macroeconomic specification has led some to question the resulting macro-based estimates of the natural rate. We avoid this debate by introducing a market-based measure of the natural rate derived from an empirical dynamic term structure model estimated solely on the prices of bonds issued by the French government and indexed to the HICP—known as OAT€s. By adjusting for both OAT€ bond-specific risk premia and real term premia, we uncover investors’ expectations for the underlying frictionless real short rate for the five-year period starting five years ahead. This measure of the natural rate of interest exhibits a gradual decline over the past two decades that accounts for about 75 percent of the general decline in euro-area bond yields. Specifically, as of the end of December 2022, the AFNS-R model estimate of r_t^* is -0.37 percent, with a net decline of slightly less than 2 percentage points since the early 2000s.

Given that our measure of the natural rate of interest is based on the forward-looking information priced into the active inflation-indexed OAT€ market and can be updated at a daily frequency as we demonstrate, it could serve as an important input for real-time monetary policy analysis. Our related empirical measures of the stance of monetary policy would seem to be particularly relevant to examine further in this regard. For future research, our methods could also be expanded along an international dimension. With a significant degree of capital mobility, the natural rate will depend on global saving and investment, so the joint modeling of inflation-indexed bonds in several countries could be informative (see HLW for an international discussion of the natural rate). Finally, our measure could be incorporated into an expanded joint macroeconomic and finance analysis—particularly with an eye towards further understanding the determinants of changes in the natural rate.

References

- Abrahams, Michael, Tobias Adrian, Richard K. Crump, Emanuel Moench, and Rui Yu, 2016, “Decomposing Real and Nominal Yield Curves,” *Journal of Monetary Economics*, Vol. 84, 182-200.
- Andreasen, Martin M., Jens H. E. Christensen, and Simon Riddell, 2021, “The TIPS Liquidity Premium,” *Review of Finance*, Vol. 25, No. 6, 1639-1675.
- Andreasen, Martin M., Jens H. E. Christensen, and Glenn D. Rudebusch, 2019, “Term Structure Analysis with Big Data: One-Step Estimation Using Bond Prices,” *Journal of Econometrics*, Vol. 212, 26-46.
- Bauer, Michael D., Glenn D. Rudebusch, and Jing (Cynthia) Wu, 2012, “Correcting Estimation Bias in Dynamic Term Structure Models,” *Journal of Business and Economic Statistics*, Vol. 30, No. 3, 454-467.
- Beaudry, Paul, Paolo Cavallino, and Tim Willems, 2025, “Monetary Policy along the Yield Curve: Why Can Central Banks Affect Long-Term Real Rates?,” Staff Working Paper No. 1,117, Bank of England.
- Bernanke, Ben, 2005, “The Global Saving Glut and the U.S. Current Account Deficit,” Sandridge Lecture, Richmond VA, March 10.
- Blanchard, Olivier, 2023, *Fiscal Policy under Low Interest Rates*. MIT Press: Cambridge, Massachusetts.
- Brand, Claus, Noémie Lisack, and Falk Mazelis, 2024, “Estimates of the Natural Interest Rate for the Euro Area: An Update,” European Central Bank, Economic Bulletin Issue 1.
- Cardozo, Cristhian H. R. and Jens H. E. Christensen, 2025, “The Benefit of Inflation-Indexed Debt: Evidence from an Emerging Market,” Working Paper 2023-04, Federal Reserve Bank of San Francisco.
- Carriero, Andrea, Sarah Mouabbi, and Elisabetta Vangelista, 2018, “U.K. Term Structure Decompositions at the Zero Lower Bound,” *Journal of Applied Econometrics*, Vol. 33, 643-661.
- Carvalho, Carlos, Andrea Ferrero, and Fernanda Nechio, 2016, “Demographics and Real Interest Rates: Inspecting the Mechanism,” *European Economic Review*, Vol. 88, 208-226.

- Christensen, Jens H. E., Francis X. Diebold, and Glenn D. Rudebusch, 2011, “The Affine Arbitrage-Free Class of Nelson-Siegel Term Structure Models,” *Journal of Econometrics*, Vol. 164, No. 1, 4-20.
- Christensen, Jens H. E., Jose A. Lopez, and Glenn D. Rudebusch, 2010, “Inflation Expectations and Risk Premiums in an Arbitrage-Free Model of Nominal and Real Bond Yields,” *Journal of Money, Credit and Banking*, Supplement to Vol. 42, No. 6, 143-178.
- Christensen, Jens H. E., Jose A. Lopez, and Glenn D. Rudebusch, 2014, “Do Central Bank Liquidity Facilities Affect Interbank Lending Rates?,” *Journal of Business and Economic Statistics*, Vol. 32, No. 1, 136-151.
- Christensen, Jens H. E., Jose A. Lopez, and Glenn D. Rudebusch, 2015, “A Probability-Based Stress Test of Federal Reserve Assets and Income,” *Journal of Monetary Economics*, Vol. 73, 26-43.
- Christensen, Jens H. E. and Nikola Mirkov, 2022, “The Safety Premium of Safe Assets,” Working Paper 2019-28, Federal Reserve Bank of San Francisco.
- Christensen, Jens H. E. and Sarah Mouabbi, 2023, “Pre- and Post-Pandemic Inflation Expectations in France: A Bond Market Perspective,” Manuscript, Federal Reserve Bank of San Francisco.
- Christensen, Jens H. E. and Sarah Mouabbi, 2025, “A Rising Star: The Natural Interest Rate in the Euro Area,” *FRBSF Economic Letter*, 2025-11.
- Christensen, Jens H. E., Sarah Mouabbi, and Caroline Paulson, 2025, “German Inflation-Linked Bonds: Overpriced, yet Undervalued,” Working Paper 2025-03, Federal Reserve Bank of San Francisco.
- Christensen, Jens H. E. and Glenn D. Rudebusch, 2012, “The Response of Interest Rates to U.S. and U.K. Quantitative Easing,” *Economic Journal*, Vol. 122, F385-F414.
- Christensen, Jens H. E. and Glenn D. Rudebusch, 2015, “Estimating Shadow-Rate Term Structure Models with Near-Zero Yields,” *Journal of Financial Econometrics*, Vol. 13, No. 2, 226-259.
- Christensen, Jens H. E. and Glenn D. Rudebusch, 2019, “A New Normal for Interest Rates? Evidence from Inflation-Indexed Debt,” *Review of Economics and Statistics*, Vol. 101, No. 5, 933-949.
- Clarida, Richard, 2014, “Navigating the New Neutral,” *Economic Outlook*, PIMCO, November.

- Dai, Qiang and Kenneth J. Singleton, 2000, "Specification Analysis of Affine Term Structure Models," *Journal of Finance*, Vol. 55, No. 5, 1943-1978.
- Dai, Qiang, Kenneth J. Singleton, and Wei Yang, 2004, "Predictability of Bond Risk Premia and Affine Term Structure Models," manuscript, Stanford University.
- D'Amico, Stefania, Don H. Kim, and Min Wei, 2018, "Tips from TIPS: The Informational Content of Treasury Inflation-Protected Security Prices," *Journal of Financial and Quantitative Analysis* Vol. 53, 243-268.
- Davis, Josh, Cristian Feunzalida, Leon Huetsch, Benjamin Mills, and Alan M. Taylor, 2024, "Global Natural Rates in the Long Run: Postwar Macro Trends and the Market-Implied r^* in 10 Advanced Economies," *Journal of International Economics*, Vol. 149, 103919.
- Del Negro, Marco, Domenico Giannone, Marc P. Giannoni, and Andrea Tambalotti, 2019, "Global Trends in Interest Rates," *Journal of International Economics*, Vol. 118, 248-262.
- Duffee, Gregory R., 2002, "Term Premia and Interest Rate Forecasts in Affine Models," *Journal of Finance*, Vol. 57, No. 1, 405-443.
- Ejsing, Jacob, Juan Angel Garcia, and Thomas Werner, 2007, "The Term Structure of Euro Area Break-Even Inflation Rates: The Impact of Seasonality," European Central Bank Working Paper Series No. 830.
- Favero, Carlo A., Arie E. Gozluklu, and Haoxi Yang, 2016, "Demographics and the Behavior of Interest Rates," *IMF Economic Review* Vol. 64, No. 4, 732-776.
- Ferreira, Thiago R. T. and Samer Shousha, 2023, "Determinants of Global Neutral Interest Rates," *Journal of International Economics*, Vol. 145, 103833.
- Finlay, Richard and Sebastian Wende, 2012, "Estimating Inflation Expectations with a Limited Number of Inflation-Indexed Bonds," *International Journal of Central Banking*, Vol. 8, No. 2, 111-142.
- Fontaine, Jean-Sébastien and René Garcia, 2012, "Bond Liquidity Premia," *Review of Financial Studies*, Vol. 25, No. 4, 1207-1254.
- Gagnon, Etienne, Benjamin K. Johansson, and David Lopez-Salido, 2016, "Understanding the New Normal: The Role of Demographics," Finance and Economics Discussion Series 2016-080. Washington: Board of Governors of the Federal Reserve System, <http://dx.doi.org/10.17016/FEDS.2016.080>.

- Greenspan, Alan, 2005, Federal Reserve Board’s Semiannual Monetary Policy Report to the Congress, Testimony to the U.S. Senate, February 16.
- Grishchenko, Olesya V. and Jing-Zhi Huang, 2013, “Inflation Risk Premium: Evidence from the TIPS Market,” *Journal of Fixed Income*, Vol. 22, No. 4, 5-30.
- Grishchenko, Olesya V., Franck Moraux, and Olga Pakulyak, 2025, “How Stable Inflation Expectations are in the Euro Area? Evidence from the French Bond Market,” Manuscript, Banque de France.
- Gürkaynak, Refet S., Brian Sack, and Jonathan H. Wright, 2010, “The TIPS Yield Curve and Inflation Compensation,” *American Economic Journal: Macroeconomics*, Vol. 2, No. 1, 70-92.
- Hanson, Sam G. and Jeremy C. Stein, 2015, “Monetary Policy and Long-Term Real Rates,” *Journal of Financial Economics*, Vol. 115, 429-448.
- Hillenbrand, Sebastian, 2025, “The Fed and the Secular Decline in Interest Rates,” *Review of Financial Studies*, Vol. 38, No. 4, 981-1013.
- Hoffmann, Boris, Zehao Li, and Steve Pak Yeung Wu, 2024, “Monetary Policy and the Secular Decline in Long-Term Interest Rates: A Global Perspective,” Manuscript, Bank for International Settlements.
- Holston, Kathryn, Thomas Laubach, and John C. Williams, 2017, “Measuring the Natural Rate of Interest: International Trends and Determinants,” *Journal of International Economics*, Vol. 108, 559-575.
- Houweling, Patrick, Albert Mentink, and Ton Vorst, 2005, “Comparing Possible Proxies of Corporate Bond Liquidity,” *Journal of Banking and Finance*, Vol. 29, No. 6, 1331-1358.
- Hu, Grace Xing, Jun Pan, and Jiang Wang, 2013, “Noise as Information for Illiquidity,” *Journal of Finance*, Vol. 68, No. 6, 2341-2382.
- Hubert, Paul and Rose Portier, 2024, “Monetary Policy and the Slope of the Yield Curve,” Manuscript, Banque de France.
- Joyce, Michael A. S., Iryna Kaminska, and Peter Lildholdt, 2012, “Understanding the Real Rate Conundrum: An Application of No-Arbitrage Models to the U.K. Real Yield Curve,” *Review of Finance*, Vol. 16, 837-866.
- Joyce, Michael, Peter Lildholdt, and Steffen Sørensen, 2010, “Extracting Inflation Expectations and Inflation Risk Premia from the Term Structure: A Joint Model of the U.K. Nominal and Real Yield Curves,” *Journal of Banking and Finance*, Vol. 34, 281-294.

- Kim, Don H. and Kenneth J. Singleton, 2012, "Term Structure Models and the Zero Bound: An Empirical Investigation of Japanese Yields," *Journal of Econometrics*, Vol. 170, No. 1, 32-49.
- Laubach, Thomas and John C. Williams, 2003, "Measuring the Natural Rate of Interest," *Review of Economics and Statistics*, Vol. 85, No. 4, 1063-1070.
- Laubach, Thomas and John C. Williams, 2016, "Measuring the Natural Rate of Interest Redux," *Business Economics*, Vol. 51, No. 2, 57-67.
- Nagel, Stefan, 2016, "The Liquidity Premium of Near-Money Assets," *Quarterly Journal of Economics*, Vol. 131, No. 4, 1927-1971.
- Nakamura, Emi and Jón Steinsson, 2018, "High-Frequency Identification of Monetary Non-Neutrality: The Information Effect," *Quarterly Journal of Economics*, Vol. 133, No. 3, 1283-1330.
- Nelson, Charles R. and Andrew F. Siegel, 1987, "Parsimonious Modeling of Yield Curves," *Journal of Business*, Vol. 60, No. 4, 473-489.
- Pflueger, Carolin E. and Luis M. Viceira, 2016, "Return Predictability in the Treasury Market: Real Rates, Inflation, and Liquidity," in *Handbook of Fixed-Income Securities*, edited by P. Veronesi, Wiley, Hoboken, N.J., pp. 191-209 (Chapter 10).
- Sack, Brian and Robert Elsasser, 2004, "Treasury Inflation-Indexed Debt: A Review of the U.S. Experience," *Federal Reserve Bank of New York Economic Policy Review*, Vol. 10, No. 1, 47-63.
- Somogyi, Fabricius, Jonathan Wallen, and Lingdi Xu, 2025, "Treasury Auctions and Long-Term Bond Yields," Manuscript, Northeastern University.
- Speck, Christian, 2021, "Market Microstructure of Inflation-Indexed Bonds and Technical Biases in Market-Based Inflation Indicators," Deutsche Bundesbank Internal Note.
- Summers, Lawrence H., 2014, "U.S. Economic Prospects: Secular Stagnation, Hysteresis, and the Zero Lower Bound," *Business Economics*, Vol. 49, No. 2, 65-73.
- Summers, Lawrence H., 2015, "Demand Side Secular Stagnation," *American Economic Review, Papers and Proceedings*, Vol. 105, No. 5, 60-65.
- Summers, Lawrence H., 2023, "Back to Secular Stagnation?," Speech at the Annual Meeting of the American Economic Association, January 7, 2023.

Swanson, Eric T. and John C. Williams, 2014, “Measuring the Effect of the Zero Lower Bound on Medium- and Longer-Term Interest Rates,” *American Economic Review*, Vol. 104, No. 10, 3154-3185.

Taylor, John B., 1993, “Discretion versus Policy Rules in Practice,” *Carnegie-Rochester Conference Series on Public Policy*, Vol. 39, 195-214.

Online Appendix

The Natural Rate of Interest in the Euro Area: Evidence from Inflation-Indexed Bonds

Jens H. E. Christensen

Federal Reserve Bank of San Francisco

jens.christensen@sf.frb.org

and

Sarah Mouabbi

Banque de France

sarah.mouabbi@banque-france.fr

The views in this paper are solely the responsibility of the authors and should not be interpreted as reflecting the views of the Federal Reserve Bank of San Francisco or the Federal Reserve System, or those of the Banque de France or the Eurosystem.

This version: October 30, 2025.

Contents

A	Sensitivity of Estimated State Variables to Data Frequency	2
B	Sensitivity of Estimated State Variables to Data Cutoff	3
C	German Inflation-Indexed Bond Analysis	5
D	Model Selection in the Daily AFNS Model	7
E	Formulas for r_t^* and Real Term Premia in the Preferred AFNS-R Model	10
F	Comparison of Fitted OAT€ Zero-Coupon Yields	14

A Sensitivity of Estimated State Variables to Data Frequency

In this appendix, we examine the sensitivity of the estimated state variables within the AFNS-R model to the data frequency. To do so, we focus on the most parsimonious specification of the model with diagonal $K^{\mathbb{P}}$ mean-reversion matrix and diagonal Σ volatility matrix estimated at daily, weekly, monthly, and quarterly frequency, respectively.

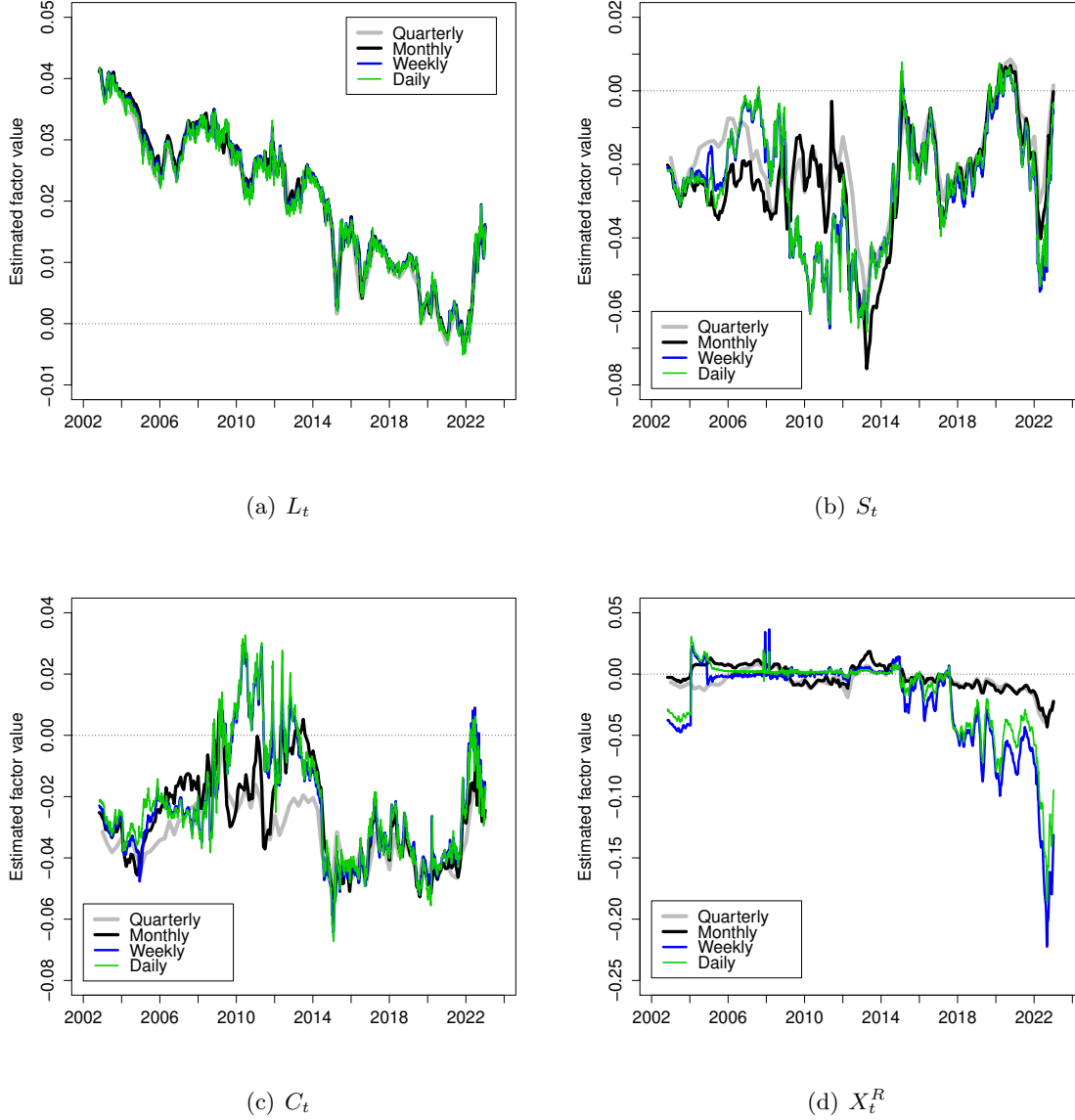


Figure 1: **Estimated State Variables: Data Frequency**

Illustration of the estimated state variables from the AFNS-R model when estimated using daily, weekly, monthly, and quarterly data.

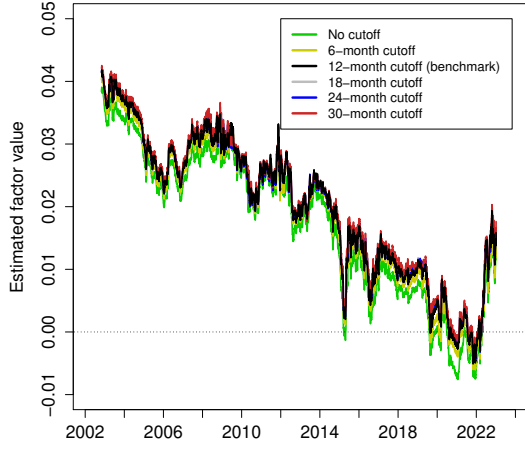
Figure 1 shows the estimated paths for all four state variables from the four estimations.

We note that, due to the limited number of observed bond prices in the early years of our sample, all state variables are not fully identified during that period. As a consequence, we do see some differences in the filtered state variables depending on the frequency of the data used in the model estimation. Importantly, though, the dominating level factor *is* well identified and its filtered path is insensitive to the data frequency. Moreover, roughly starting in 2012 the filtered paths for the frictionless level, slope, and curvature factors become insensitive to the data frequency thanks to the sufficiently large number of observed bond prices during the remaining part of the sample. Furthermore, we do see some differences in the estimated bond-specific risk factor X_t^R depending on the data frequency even after 2012. However, these differences do not translate into differences in the average estimated bond-specific risk premium series during the last 10 years of our sample as demonstrated in Figure 12 in the main text. Finally and most importantly, we stress that it follows from Figure 18 in the main text that the r_t^* estimates from our preferred AFNS-R model estimated at different data frequencies are very similar and all exhibit the same trending patterns. Hence, the crucial r_t^* output for our analysis has little sensitivity to the data frequency used, which supports our choice to focus on the highest possible daily data frequency for our analysis.

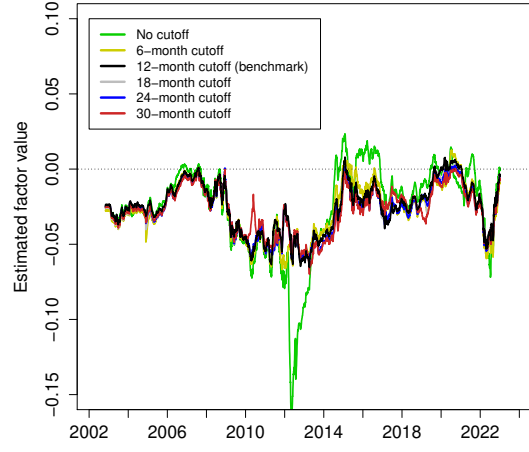
B Sensitivity of Estimated State Variables to Data Cutoff

In this appendix, we examine the sensitivity of the estimated state variables within the AFNS-R model to the data censoring cutoff used in the model estimation. To do so, we focus on our preferred specification of the AFNS-R model given that we are interested in the impact of this choice on our r_t^* estimate in addition to its impact on estimated bond-specific risk premia. In the exercise, we consider alternative cutoff censoring choices ranging from no cutoff to 30 months in 6-month increments with the 12-month cutoff being our benchmark as in the main text.

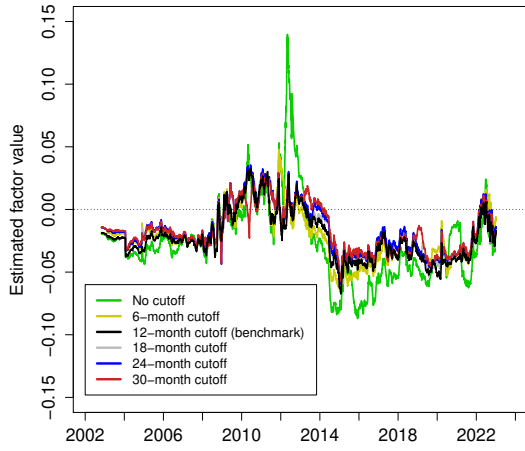
Figure 2 shows the estimated paths for all four state variables from the six estimations. We note that, in general, the estimated state variables have relatively little sensitivity to the cutoff choice except when there is no cutoff imposed. In that case, the estimated slope, curvature, and bond-specific risk factors can be affected during the time windows when there are OAT€s in the sample approaching maturity.



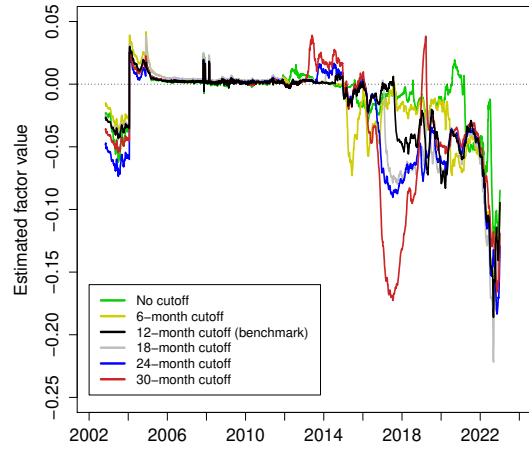
(a) L_t



(b) S_t



(c) C_t



(d) X_t^R

Figure 2: Estimated State Variables: Data Cutoff

Illustration of the estimated state variables from the AFNS-R model when estimated with varying data cutoff choices ranging from no censoring up to censoring with 30 months to maturity.

C German Inflation-Indexed Bond Analysis

In this appendix, we describe the analysis of German inflation-indexed bond prices with cash flows adjusted based on the harmonized index of consumer prices (HICP) in the euro area. These prices were used in the construction of the 5yr5yr Franco-German real yield spread appearing in Section 2.1 in the main text.

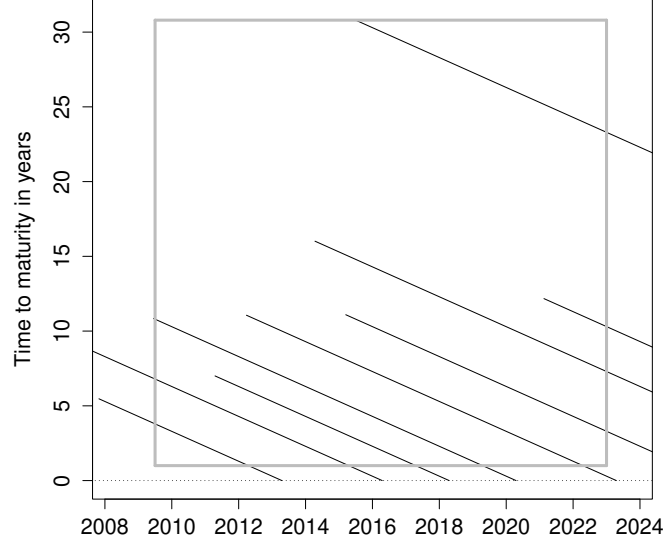


Figure 3: **Maturity Distribution of German Inflation-Indexed Bonds**

Illustration of the maturity distribution of the available universe of German inflation-indexed bonds with cash flows adjusted based on the HICP (ex tobacco). The solid grey rectangle indicates the sample used in the empirical analysis, where the sample is restricted to start on June 12, 2009, and end on December 30, 2022.

The German federal government issued its first inflation-indexed bond referencing HICP on March 15, 2006. However, it is not until June 12, 2009, that the third such bond was issued and started trading. This determines the start date for our analysis of this market as we need a minimum three bond observations to be able to reliably estimate the 5yr5yr German real yield using a standard arbitrage-free Nelson-Siegel (AFNS) model as recommended by Andreasen et al. (2019).

Figure 3 shows the distribution of the available universe of German inflation-indexed bonds, where we note a repeated, although somewhat infrequent, issuance of ten-year bonds

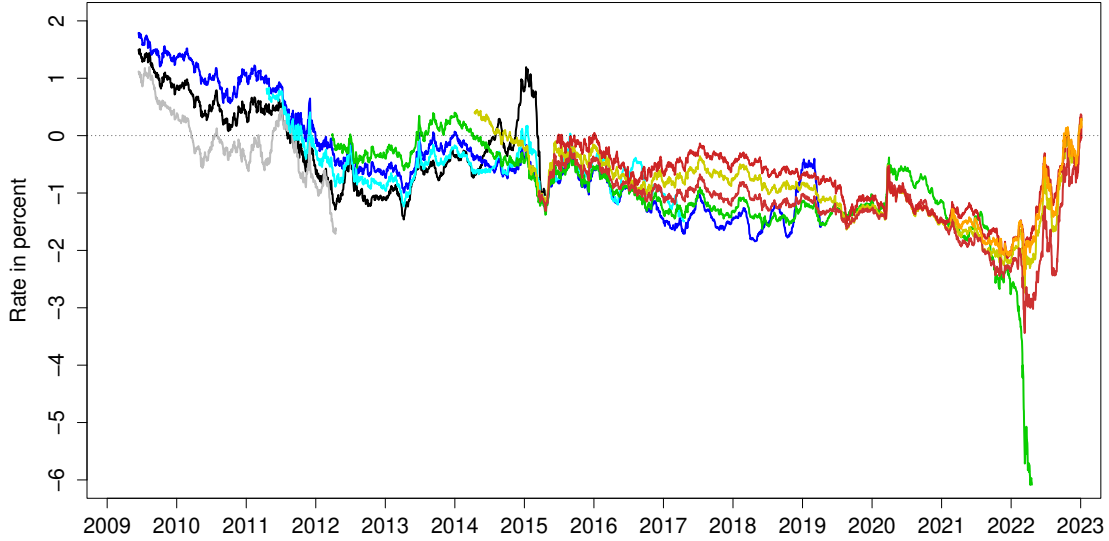


Figure 4: **Yield to Maturity of German Inflation-Indexed Bonds**

mixed with a 15-year and a 30-year bond. This implies that there is good coverage in the 5- to 10-year maturity range that is of importance to the construction of the key 5yr5yr forward yield that we are interested in. It is also this cross-sectional dispersion that provides the econometric identification of the factors within our model.

Figure 4 shows the yields to maturity for all nine German inflation-indexed bonds in our sample at daily frequency from June 12, 2009, to December 30, 2022. Note that, with the exception of the first couple of years, the bond yields have remained in negative territory.

Based on the AFNS model estimated using the daily data, we calculate the fitted 5yr5yr German real yield shown with a solid grey line in Figure 5. We then repeat this for the AFNS model estimated using the French OAT€ bond prices as described in Appendix D. This produces the 5yr5yr French real yield shown with a solid black line in Figure 5. Now, the 5yr5yr Franco-German yield spread described in Section 2.1 in the main text is simply the difference between these two yield series and shown with a solid red line in Figure 5.

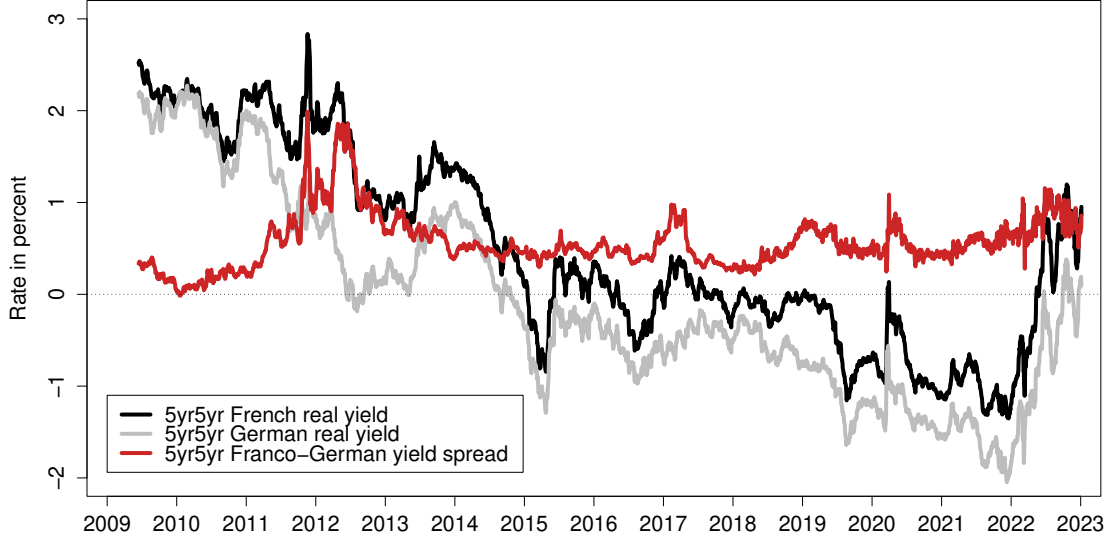


Figure 5: **5yr5yr French and German Real Yields and Their Yield Spread**

D Model Selection in the Daily AFNS Model

In this appendix, we go through a careful model selection procedure for the AFNS model estimated at daily frequency similar to the one described in the main text for the AFNS-R model.

For estimates of r_t^* based on our definition, the specification of the mean-reversion matrix $K^{\mathbb{P}}$ is critical. To select the best fitting specification of the AFNS model's real-world dynamics, we use a general-to-specific modeling strategy in which the least significant off-diagonal parameter of $K^{\mathbb{P}}$ is restricted to zero and the model is re-estimated. This strategy of eliminating the least significant coefficient is carried out down to the most parsimonious specification, which has a diagonal $K^{\mathbb{P}}$ matrix. As in the main text, the final specification choice is based on the value of the Bayesian information criterion (BIC).

The summary statistics of the model selection process are reported in Table 1. The BIC is minimized by specification (6), which has a $K^{\mathbb{P}}$ matrix given by

$$K_{BIC}^{\mathbb{P}} = \begin{pmatrix} \kappa_{11}^{\mathbb{P}} & 0 & \kappa_{13}^{\mathbb{P}} \\ 0 & \kappa_{22}^{\mathbb{P}} & 0 \\ 0 & 0 & \kappa_{33}^{\mathbb{P}} \end{pmatrix}.$$

Alternative Specifications	Goodness of fit statistics			
	$\log L$	k	p -value	BIC
(1) Unrestricted $K^{\mathbb{P}}$	217,252.5	17	n.a.	-434,359.4
(2) $\kappa_{31}^{\mathbb{P}} = 0$	217,252.5	16	1.00	-434,367.9
(3) $\kappa_{31}^{\mathbb{P}} = \kappa_{21}^{\mathbb{P}} = 0$	217,251.9	15	0.27	-434,375.3
(4) $\kappa_{31}^{\mathbb{P}} = \kappa_{21}^{\mathbb{P}} = \kappa_{32}^{\mathbb{P}} = 0$	217,250.8	14	0.14	-434,381.7
(5) $\kappa_{31}^{\mathbb{P}} = \dots = \kappa_{23}^{\mathbb{P}} = 0$	217,248.6	13	0.04	-434,385.8
(6) $\kappa_{31}^{\mathbb{P}} = \dots = \kappa_{12}^{\mathbb{P}} = 0$	217,247.3	12	0.11	-434,391.8
(7) $\kappa_{31}^{\mathbb{P}} = \dots = \kappa_{13}^{\mathbb{P}} = 0$	217,238.6	11	< 0.01	-434,383.0

Table 1: **Evaluation of Alternative Specifications of the AFNS Model**

There are seven alternative estimated specifications of the AFNS model. Each specification is listed with its maximum log likelihood ($\log L$), number of parameters (k), the p -value from a likelihood ratio test of the hypothesis that it differs from the specification above with one more free parameter, and the Bayesian information criterion (BIC). The period analyzed covers daily data from October 31, 2002, to December 30, 2022.

$K^{\mathbb{P}}$	$K_{\cdot,1}^{\mathbb{P}}$	$K_{\cdot,2}^{\mathbb{P}}$	$K_{\cdot,3}^{\mathbb{P}}$	$\theta^{\mathbb{P}}$		Σ
$K_{1,\cdot}^{\mathbb{P}}$	0.1709 (0.0732)	0	-0.1702 (0.0392)	0.0318 (0.0169)	$\Sigma_{1,1}$	0.0036 (0.0000)
$K_{2,\cdot}^{\mathbb{P}}$	0	0.3863 (0.2018)	0	-0.0242 (0.0115)	$\Sigma_{2,2}$	0.0129 (0.0002)
$K_{3,\cdot}^{\mathbb{P}}$	0	0	0.2717 (0.2361)	0.0073 (0.0177)	$\Sigma_{3,3}$	0.0183 (0.0003)

Table 2: **Estimated Parameters in the Preferred AFNS Model**

The estimated parameters for the mean-reversion matrix $K^{\mathbb{P}}$, the mean vector $\theta^{\mathbb{P}}$, and the volatility matrix Σ in the AFNS model preferred according to the BIC. The \mathbb{Q} -related parameter is estimated at $\lambda = 0.3861$ (0.0012). The maximum log likelihood value is 217,247.3. The numbers in parentheses are the estimated standard deviations.

The estimated parameters of this preferred specification are reported in Table 2. We note that most of the parameters are very close to those reported in the main text for the AFNS model with diagonal $K^{\mathbb{P}}$ matrix, which seems reasonable given that only the off-diagonal $\kappa_{13}^{\mathbb{P}}$ parameter separates the two models.

Figure 6 shows the 5yr5yr real yield decomposition implied by the preferred AFNS model. Its estimate of the natural real rate r_t^* is stable with persistent fluctuations around zero. As a result, the model implies that the lower trend in the 5yr5yr real yield is driven by declines in the 5yr5yr real term premium.

To examine the sensitivity of the estimated r_t^* from the preferred AFNS model to the specification of the $K^{\mathbb{P}}$ matrix, we consider the AFNS models with unrestricted and diagonal $K^{\mathbb{P}}$ matrix. The resulting r_t^* estimates are shown in 7 where we note that the estimates

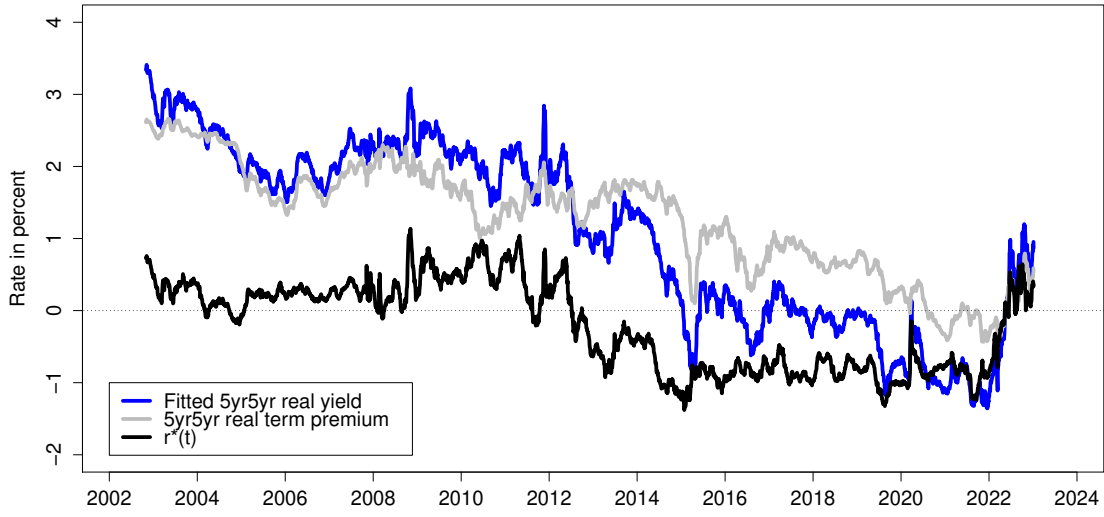


Figure 6: 5yr5yr Real Yield Decomposition

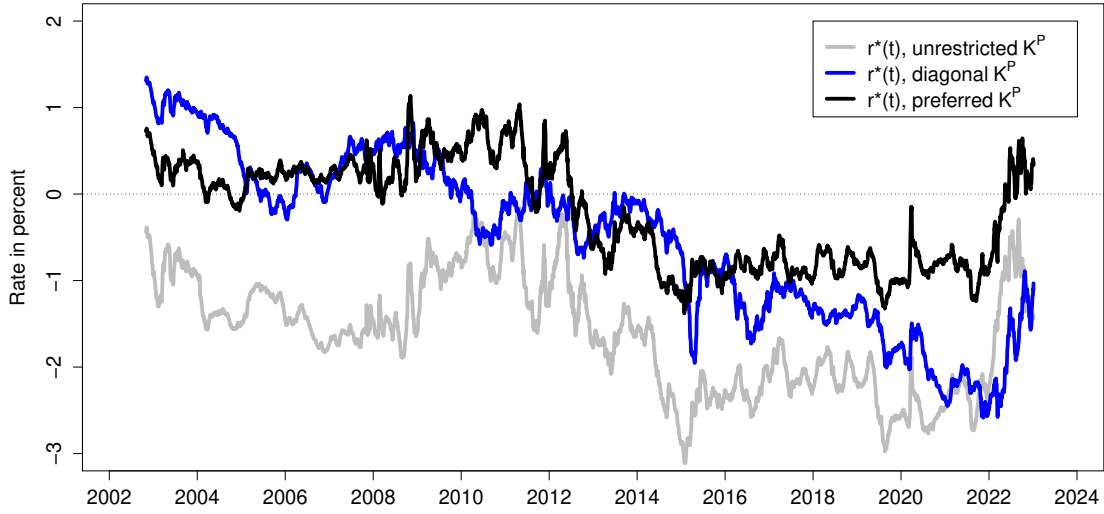


Figure 7: Sensitivity of r^* Estimate to $K^{\mathbb{P}}$ Specification

are indeed very sensitive to this choice. This underscores the importance of going through a careful model selection procedure like the one described above.

E Formulas for r_t^* and Real Term Premia in the Preferred AFNS-R Model

In this appendix, we derive the analytical formulas for real short rate expectations, including r_t^* , and real term premia within the preferred AFNS-R model of French OAT€ prices.

For a start, we note that the τ -year real term premium is defined as

$$TP_t(\tau) = y_t(\tau) - \frac{1}{\tau} \int_t^{t+\tau} E_t^{\mathbb{P}}[r_s] ds,$$

where $y_t(\tau)$ refers to the frictionless real yield within the AFNS-R model.

In the preferred AFNS-R model, as in any AFNS model, the instantaneous real short rate is defined as

$$r_t = L_t + S_t,$$

while the specification of the \mathbb{P} -dynamics is given by

$$\begin{pmatrix} dL_t \\ dS_t \\ dC_t \\ dX_t^R \end{pmatrix} = \begin{pmatrix} \kappa_{11}^{\mathbb{P}} & 0 & 0 & 0 \\ 0 & \kappa_{22}^{\mathbb{P}} & \kappa_{23}^{\mathbb{P}} & 0 \\ 0 & 0 & \kappa_{33}^{\mathbb{P}} & 0 \\ 0 & 0 & 0 & \kappa_{44}^{\mathbb{P}} \end{pmatrix} \left[\begin{pmatrix} \theta_1^{\mathbb{P}} \\ \theta_2^{\mathbb{P}} \\ \theta_3^{\mathbb{P}} \\ \theta_4^{\mathbb{P}} \end{pmatrix} - \begin{pmatrix} L_t \\ S_t \\ C_t \\ X_t^R \end{pmatrix} \right] dt + \begin{pmatrix} \sigma_{11} & 0 & 0 & 0 \\ 0 & \sigma_{22} & 0 & 0 \\ 0 & 0 & \sigma_{33} & 0 \\ 0 & 0 & 0 & \sigma_{44} \end{pmatrix} \begin{pmatrix} dW_t^{L,\mathbb{P}} \\ dW_t^{S,\mathbb{P}} \\ dW_t^{C,\mathbb{P}} \\ dW_t^{R,\mathbb{P}} \end{pmatrix}.$$

Thus, the mean-reversion matrix is given by

$$K^{\mathbb{P}} = \begin{pmatrix} \kappa_{11}^{\mathbb{P}} & 0 & 0 & 0 \\ 0 & \kappa_{22}^{\mathbb{P}} & \kappa_{23}^{\mathbb{P}} & 0 \\ 0 & 0 & \kappa_{33}^{\mathbb{P}} & 0 \\ 0 & 0 & 0 & \kappa_{44}^{\mathbb{P}} \end{pmatrix}.$$

Its matrix exponential can be calculated analytically and is given by

$$\exp(-K^{\mathbb{P}}\tau) = \begin{pmatrix} e^{-\kappa_{11}^{\mathbb{P}}\tau} & 0 & 0 & 0 \\ 0 & e^{-\kappa_{22}^{\mathbb{P}}\tau} & -\kappa_{23}^{\mathbb{P}} \frac{e^{-\kappa_{33}^{\mathbb{P}}\tau} - e^{-\kappa_{22}^{\mathbb{P}}\tau}}{\kappa_{22}^{\mathbb{P}} - \kappa_{33}^{\mathbb{P}}} & 0 \\ 0 & 0 & e^{-\kappa_{33}^{\mathbb{P}}\tau} & 0 \\ 0 & 0 & 0 & e^{-\kappa_{44}^{\mathbb{P}}\tau} \end{pmatrix}.$$

Thus, the conditional mean of the state variables is

$$\begin{aligned}
E_t^{\mathbb{P}}[X_{t+\tau}] &= \theta^{\mathbb{P}} + \begin{pmatrix} e^{-\kappa_{11}^{\mathbb{P}}\tau} & 0 & 0 & 0 \\ 0 & e^{-\kappa_{22}^{\mathbb{P}}\tau} & -\kappa_{23}^{\mathbb{P}} \frac{e^{-\kappa_{33}^{\mathbb{P}}\tau} - e^{-\kappa_{22}^{\mathbb{P}}\tau}}{\kappa_{22}^{\mathbb{P}} - \kappa_{33}^{\mathbb{P}}} & 0 \\ 0 & 0 & e^{-\kappa_{33}^{\mathbb{P}}\tau} & 0 \\ 0 & 0 & 0 & e^{-\kappa_{44}^{\mathbb{P}}\tau} \end{pmatrix} \begin{pmatrix} L_t - \theta_1^{\mathbb{P}} \\ S_t - \theta_2^{\mathbb{P}} \\ C_t - \theta_3^{\mathbb{P}} \\ X_t^R - \theta_4^{\mathbb{P}} \end{pmatrix} \\
&= \begin{pmatrix} \theta_1^{\mathbb{P}} + e^{-\kappa_{11}^{\mathbb{P}}\tau}(L_t - \theta_1^{\mathbb{P}}) \\ \theta_2^{\mathbb{P}} + e^{-\kappa_{22}^{\mathbb{P}}\tau}(S_t - \theta_2^{\mathbb{P}}) - \kappa_{23}^{\mathbb{P}} \frac{e^{-\kappa_{33}^{\mathbb{P}}\tau} - e^{-\kappa_{22}^{\mathbb{P}}\tau}}{\kappa_{22}^{\mathbb{P}} - \kappa_{33}^{\mathbb{P}}}(C_t - \theta_3^{\mathbb{P}}) \\ \theta_3^{\mathbb{P}} + e^{-\kappa_{33}^{\mathbb{P}}\tau}(C_t - \theta_3^{\mathbb{P}}) \\ \theta_4^{\mathbb{P}} + e^{-\kappa_{44}^{\mathbb{P}}\tau}(X_t^R - \theta_4^{\mathbb{P}}) \end{pmatrix}.
\end{aligned}$$

In order to get back to the real term premium formula, we note that the conditional expectation of the instantaneous real short rate process is:

$$\begin{aligned}
E_t^{\mathbb{P}}[r_s] &= E_t^{\mathbb{P}}[L_s + S_s] \\
&= \theta_1^{\mathbb{P}} + e^{-\kappa_{11}^{\mathbb{P}}(s-t)}(L_t - \theta_1^{\mathbb{P}}) + \theta_2^{\mathbb{P}} + e^{-\kappa_{22}^{\mathbb{P}}(s-t)}(S_t - \theta_2^{\mathbb{P}}) - \kappa_{23}^{\mathbb{P}} \frac{e^{-\kappa_{33}^{\mathbb{P}}(s-t)} - e^{-\kappa_{22}^{\mathbb{P}}(s-t)}}{\kappa_{22}^{\mathbb{P}} - \kappa_{33}^{\mathbb{P}}}(C_t - \theta_3^{\mathbb{P}}).
\end{aligned}$$

Now, we integrate the expected real short rate over the time interval from t to $t + \tau$ as in the definition of the real term premium:

$$\begin{aligned}
\int_t^{t+\tau} E_t^{\mathbb{P}}[r_s] ds &= \int_t^{t+\tau} \left(\theta_1^{\mathbb{P}} + e^{-\kappa_{11}^{\mathbb{P}}(s-t)}(L_t - \theta_1^{\mathbb{P}}) + \theta_2^{\mathbb{P}} + e^{-\kappa_{22}^{\mathbb{P}}(s-t)}(S_t - \theta_2^{\mathbb{P}}) - \kappa_{23}^{\mathbb{P}} \frac{e^{-\kappa_{33}^{\mathbb{P}}(s-t)} - e^{-\kappa_{22}^{\mathbb{P}}(s-t)}}{\kappa_{22}^{\mathbb{P}} - \kappa_{33}^{\mathbb{P}}}(C_t - \theta_3^{\mathbb{P}}) \right) ds \\
&= (\theta_1^{\mathbb{P}} + \theta_2^{\mathbb{P}})\tau + (L_t - \theta_1^{\mathbb{P}}) \int_t^{t+\tau} e^{-\kappa_{11}^{\mathbb{P}}(s-t)} ds + (S_t - \theta_2^{\mathbb{P}}) \int_t^{t+\tau} e^{-\kappa_{22}^{\mathbb{P}}(s-t)} ds \\
&\quad - \frac{\kappa_{23}^{\mathbb{P}}}{\kappa_{22}^{\mathbb{P}} - \kappa_{33}^{\mathbb{P}}}(C_t - \theta_3^{\mathbb{P}}) \int_t^{t+\tau} (e^{-\kappa_{33}^{\mathbb{P}}(s-t)} - e^{-\kappa_{22}^{\mathbb{P}}(s-t)}) ds \\
&= (\theta_1^{\mathbb{P}} + \theta_2^{\mathbb{P}})\tau + (L_t - \theta_1^{\mathbb{P}}) \left[\frac{-1}{\kappa_{11}^{\mathbb{P}}} e^{-\kappa_{11}^{\mathbb{P}}(s-t)} \right]_t^{t+\tau} + (S_t - \theta_2^{\mathbb{P}}) \left[\frac{-1}{\kappa_{22}^{\mathbb{P}}} e^{-\kappa_{22}^{\mathbb{P}}(s-t)} \right]_t^{t+\tau} \\
&\quad - \frac{\kappa_{23}^{\mathbb{P}}}{\kappa_{22}^{\mathbb{P}} - \kappa_{33}^{\mathbb{P}}}(C_t - \theta_3^{\mathbb{P}}) \left[\frac{-1}{\kappa_{33}^{\mathbb{P}}} e^{-\kappa_{33}^{\mathbb{P}}(s-t)} + \frac{1}{\kappa_{22}^{\mathbb{P}}} e^{-\kappa_{22}^{\mathbb{P}}(s-t)} \right]_t^{t+\tau} \\
&= (\theta_1^{\mathbb{P}} + \theta_2^{\mathbb{P}})\tau + (L_t - \theta_1^{\mathbb{P}}) \frac{1 - e^{-\kappa_{11}^{\mathbb{P}}\tau}}{\kappa_{11}^{\mathbb{P}}} + (S_t - \theta_2^{\mathbb{P}}) \frac{1 - e^{-\kappa_{22}^{\mathbb{P}}\tau}}{\kappa_{22}^{\mathbb{P}}} \\
&\quad - \frac{\kappa_{23}^{\mathbb{P}}}{\kappa_{22}^{\mathbb{P}} - \kappa_{33}^{\mathbb{P}}}(C_t - \theta_3^{\mathbb{P}}) \left[\frac{1 - e^{-\kappa_{33}^{\mathbb{P}}\tau}}{\kappa_{33}^{\mathbb{P}}} - \frac{1 - e^{-\kappa_{22}^{\mathbb{P}}\tau}}{\kappa_{22}^{\mathbb{P}}} \right].
\end{aligned}$$

For the calculation of r_t^* , we need

$$\begin{aligned}
\int_{t+5}^{t+10} E_t^{\mathbb{P}}[r_s]ds &= \int_t^{t+10} E_t^{\mathbb{P}}[r_s]ds - \int_t^{t+5} E_t^{\mathbb{P}}[r_s]ds \\
&= (\theta_1^{\mathbb{P}} + \theta_2^{\mathbb{P}})10 + (L_t - \theta_1^{\mathbb{P}}) \frac{1 - e^{-\kappa_{11}^{\mathbb{P}}10}}{\kappa_{11}^{\mathbb{P}}} + (S_t - \theta_2^{\mathbb{P}}) \frac{1 - e^{-\kappa_{22}^{\mathbb{P}}10}}{\kappa_{22}^{\mathbb{P}}} \\
&\quad - \frac{\kappa_{23}^{\mathbb{P}}}{\kappa_{22}^{\mathbb{P}} - \kappa_{33}^{\mathbb{P}}} (C_t - \theta_3^{\mathbb{P}}) \left[\frac{1 - e^{-\kappa_{33}^{\mathbb{P}}10}}{\kappa_{33}^{\mathbb{P}}} - \frac{1 - e^{-\kappa_{22}^{\mathbb{P}}10}}{\kappa_{22}^{\mathbb{P}}} \right] \\
&\quad - \left[(\theta_1^{\mathbb{P}} + \theta_2^{\mathbb{P}})5 + (L_t - \theta_1^{\mathbb{P}}) \frac{1 - e^{-\kappa_{11}^{\mathbb{P}}5}}{\kappa_{11}^{\mathbb{P}}} + (S_t - \theta_2^{\mathbb{P}}) \frac{1 - e^{-\kappa_{22}^{\mathbb{P}}5}}{\kappa_{22}^{\mathbb{P}}} \right. \\
&\quad \left. - \frac{\kappa_{23}^{\mathbb{P}}}{\kappa_{22}^{\mathbb{P}} - \kappa_{33}^{\mathbb{P}}} (C_t - \theta_3^{\mathbb{P}}) \left(\frac{1 - e^{-\kappa_{33}^{\mathbb{P}}5}}{\kappa_{33}^{\mathbb{P}}} - \frac{1 - e^{-\kappa_{22}^{\mathbb{P}}5}}{\kappa_{22}^{\mathbb{P}}} \right) \right] \\
&= (\theta_1^{\mathbb{P}} + \theta_2^{\mathbb{P}})5 + (L_t - \theta_1^{\mathbb{P}}) \frac{e^{-\kappa_{11}^{\mathbb{P}}5} - e^{-\kappa_{11}^{\mathbb{P}}10}}{\kappa_{11}^{\mathbb{P}}} + (S_t - \theta_2^{\mathbb{P}}) \frac{e^{-\kappa_{22}^{\mathbb{P}}5} - e^{-\kappa_{22}^{\mathbb{P}}10}}{\kappa_{22}^{\mathbb{P}}} \\
&\quad - \frac{\kappa_{23}^{\mathbb{P}}}{\kappa_{22}^{\mathbb{P}} - \kappa_{33}^{\mathbb{P}}} (C_t - \theta_3^{\mathbb{P}}) \left(\frac{e^{-\kappa_{33}^{\mathbb{P}}5} - e^{-\kappa_{33}^{\mathbb{P}}10}}{\kappa_{33}^{\mathbb{P}}} - \frac{e^{-\kappa_{22}^{\mathbb{P}}5} - e^{-\kappa_{22}^{\mathbb{P}}10}}{\kappa_{22}^{\mathbb{P}}} \right).
\end{aligned}$$

The analytical formula for r_t^* in the preferred specification of the AFNS-R model is then given by

$$\begin{aligned}
r_t^* &= \frac{1}{5} \int_{t+5}^{t+10} E_t^{\mathbb{P}}[r_s]ds \\
&= \theta_1^{\mathbb{P}} + \theta_2^{\mathbb{P}} + (L_t - \theta_1^{\mathbb{P}}) \frac{e^{-\kappa_{11}^{\mathbb{P}}5} - e^{-\kappa_{11}^{\mathbb{P}}10}}{5\kappa_{11}^{\mathbb{P}}} + (S_t - \theta_2^{\mathbb{P}}) \frac{e^{-\kappa_{22}^{\mathbb{P}}5} - e^{-\kappa_{22}^{\mathbb{P}}10}}{5\kappa_{22}^{\mathbb{P}}} \\
&\quad - \frac{1}{5} \frac{\kappa_{23}^{\mathbb{P}}}{\kappa_{22}^{\mathbb{P}} - \kappa_{33}^{\mathbb{P}}} (C_t - \theta_3^{\mathbb{P}}) \left(\frac{e^{-\kappa_{33}^{\mathbb{P}}5} - e^{-\kappa_{33}^{\mathbb{P}}10}}{\kappa_{33}^{\mathbb{P}}} - \frac{e^{-\kappa_{22}^{\mathbb{P}}5} - e^{-\kappa_{22}^{\mathbb{P}}10}}{\kappa_{22}^{\mathbb{P}}} \right).
\end{aligned}$$

Moreover, the key term appearing in the formula for the real term premium is given by

$$\frac{1}{\tau} \int_t^{t+\tau} E_t^{\mathbb{P}}[r_s]ds = \theta_1^{\mathbb{P}} + \theta_2^{\mathbb{P}} + (L_t - \theta_1^{\mathbb{P}}) \frac{1 - e^{-\kappa_{11}^{\mathbb{P}}\tau}}{\kappa_{11}^{\mathbb{P}}\tau} + (S_t - \theta_2^{\mathbb{P}}) \frac{1 - e^{-\kappa_{22}^{\mathbb{P}}\tau}}{\kappa_{22}^{\mathbb{P}}\tau} - \frac{\kappa_{23}^{\mathbb{P}}}{\kappa_{22}^{\mathbb{P}} - \kappa_{33}^{\mathbb{P}}} (C_t - \theta_3^{\mathbb{P}}) \left[\frac{1 - e^{-\kappa_{33}^{\mathbb{P}}\tau}}{\kappa_{33}^{\mathbb{P}}\tau} - \frac{1 - e^{-\kappa_{22}^{\mathbb{P}}\tau}}{\kappa_{22}^{\mathbb{P}}\tau} \right].$$

The final analytical formula for the τ -year real term premium within the preferred speci-

fication of the AFNS-R model is then given by

$$\begin{aligned}
TP_t(\tau) &= y_t(\tau) - \frac{1}{\tau} \int_t^{t+\tau} E_t^P[r_s] ds \\
&= L_t + \frac{1 - e^{-\lambda\tau}}{\lambda\tau} S_t + \left(\frac{1 - e^{-\lambda\tau}}{\lambda\tau} - e^{-\lambda\tau} \right) C_t - \frac{A(\tau)}{\tau} \\
&\quad - \theta_1^{\mathbb{P}} - \theta_2^{\mathbb{P}} - (L_t - \theta_1^{\mathbb{P}}) \frac{1 - e^{-\kappa_{11}^{\mathbb{P}}\tau}}{\kappa_{11}^{\mathbb{P}}\tau} - (S_t - \theta_2^{\mathbb{P}}) \frac{1 - e^{-\kappa_{22}^{\mathbb{P}}\tau}}{\kappa_{22}^{\mathbb{P}}\tau} \\
&\quad + \frac{\kappa_{23}^{\mathbb{P}}}{\kappa_{22}^{\mathbb{P}} - \kappa_{33}^{\mathbb{P}}} (C_t - \theta_3^{\mathbb{P}}) \left[\frac{1 - e^{-\kappa_{33}^{\mathbb{P}}\tau}}{\kappa_{33}^{\mathbb{P}}\tau} - \frac{1 - e^{-\kappa_{22}^{\mathbb{P}}\tau}}{\kappa_{22}^{\mathbb{P}}\tau} \right] \\
&= \left(1 - \frac{1 - e^{-\kappa_{11}^{\mathbb{P}}\tau}}{\kappa_{11}^{\mathbb{P}}\tau} \right) (L_t - \theta_1^{\mathbb{P}}) + \left(\frac{1 - e^{-\lambda\tau}}{\lambda\tau} - \frac{1 - e^{-\kappa_{22}^{\mathbb{P}}\tau}}{\kappa_{22}^{\mathbb{P}}\tau} \right) S_t - \left(1 - \frac{1 - e^{-\kappa_{22}^{\mathbb{P}}\tau}}{\kappa_{22}^{\mathbb{P}}\tau} \right) \theta_2^{\mathbb{P}} \\
&\quad + \left(\frac{1 - e^{-\lambda\tau}}{\lambda\tau} - e^{-\lambda\tau} \right) C_t + \frac{\kappa_{23}^{\mathbb{P}}}{\kappa_{22}^{\mathbb{P}} - \kappa_{33}^{\mathbb{P}}} (C_t - \theta_3^{\mathbb{P}}) \left[\frac{1 - e^{-\kappa_{33}^{\mathbb{P}}\tau}}{\kappa_{33}^{\mathbb{P}}\tau} - \frac{1 - e^{-\kappa_{22}^{\mathbb{P}}\tau}}{\kappa_{22}^{\mathbb{P}}\tau} \right] - \frac{A(\tau)}{\tau}.
\end{aligned}$$

Next, we provide the formulas for the decomposition of real forward rates in the preferred AFNS-R model, where we recall that the frictionless yields within the AFNS-R model have the standard AFNS structure.

In AFNS models, in general, the instantaneous forward rate is given by

$$f_t(\tau) = L_t + e^{-\lambda\tau} S_t + \lambda\tau e^{-\lambda\tau} C_t + A^f(\tau),$$

where the yield-adjustment term in the instantaneous forward rate function is:

$$\begin{aligned}
A^f(\tau) &= -\frac{\partial A(\tau)}{\partial \tau} \\
&= -\frac{1}{2} \sigma_{11}^2 \tau^2 - \frac{1}{2} (\sigma_{21}^2 + \sigma_{22}^2) \left(\frac{1 - e^{-\lambda\tau}}{\lambda} \right)^2 \\
&\quad - \frac{1}{2} (\sigma_{31}^2 + \sigma_{32}^2 + \sigma_{33}^2) \left[\frac{1}{\lambda^2} - \frac{2}{\lambda^2} e^{-\lambda\tau} - \frac{2}{\lambda} \tau e^{-\lambda\tau} + \frac{1}{\lambda^2} e^{-2\lambda\tau} + \frac{2}{\lambda} \tau e^{-2\lambda\tau} + \tau^2 e^{-2\lambda\tau} \right] \\
&\quad - \sigma_{11} \sigma_{21} \tau \frac{1 - e^{-\lambda\tau}}{\lambda} - \sigma_{11} \sigma_{31} \left[\frac{1}{\lambda} \tau - \frac{1}{\lambda} \tau e^{-\lambda\tau} - \tau^2 e^{-\lambda\tau} \right] \\
&\quad - (\sigma_{21} \sigma_{31} + \sigma_{22} \sigma_{32}) \left[\frac{1}{\lambda^2} - \frac{2}{\lambda^2} e^{-\lambda\tau} - \frac{1}{\lambda} \tau e^{-\lambda\tau} + \frac{1}{\lambda^2} e^{-2\lambda\tau} + \frac{1}{\lambda} \tau e^{-2\lambda\tau} \right].
\end{aligned}$$

The instantaneous real forward rate term premium in the preferred AFNS-R model then

becomes

$$\begin{aligned}
TP_t^f(\tau) &= f_t(\tau) - E_t^{\mathbb{P}}[r_{t+\tau}] \\
&= L_t + e^{-\lambda\tau} S_t + \lambda\tau e^{-\lambda\tau} C_t + A^f(\tau) \\
&\quad - \theta_1^{\mathbb{P}} - e^{-\kappa_{11}^{\mathbb{P}}\tau} (L_t - \theta_1^{\mathbb{P}}) - \theta_2^{\mathbb{P}} - e^{-\kappa_{22}^{\mathbb{P}}\tau} (S_t - \theta_2^{\mathbb{P}}) + \kappa_{23}^{\mathbb{P}} \frac{e^{-\kappa_{33}^{\mathbb{P}}\tau} - e^{-\kappa_{22}^{\mathbb{P}}\tau}}{\kappa_{22}^{\mathbb{P}} - \kappa_{33}^{\mathbb{P}}} (C_t - \theta_3^{\mathbb{P}}) \\
&= \left(1 - e^{-\kappa_{11}^{\mathbb{P}}\tau}\right) (L_t - \theta_1^{\mathbb{P}}) + \left(e^{-\lambda\tau} - e^{-\kappa_{22}^{\mathbb{P}}\tau}\right) S_t - \left(1 - e^{-\kappa_{22}^{\mathbb{P}}\tau}\right) \theta_2^{\mathbb{P}} \\
&\quad + \lambda\tau e^{-\lambda\tau} C_t + \kappa_{23}^{\mathbb{P}} \frac{e^{-\kappa_{33}^{\mathbb{P}}\tau} - e^{-\kappa_{22}^{\mathbb{P}}\tau}}{\kappa_{22}^{\mathbb{P}} - \kappa_{33}^{\mathbb{P}}} (C_t - \theta_3^{\mathbb{P}}) + A^f(\tau).
\end{aligned}$$

Finally, we note that the formulas above nest the case of the independent-factors AFNS-R model, while r_t^* and real term premia for the unconstrained and unrestricted AFNS-R models have to be calculated numerically.

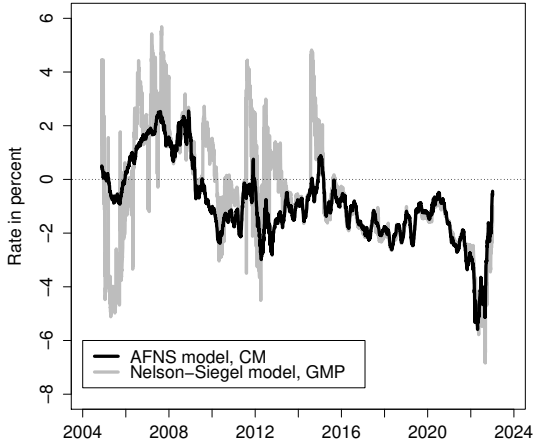
F Comparison of Fitted OAT€ Zero-Coupon Yields

In this appendix, we examine the quality of the fitted real yields implied by the standard AFNS model estimated using our sample of daily French OAT€ prices. Given that these are the yields used in the construction of our preferred measure of the stance of monetary policy in the euro area described in Section 6 of the paper, it is crucial to establish their appropriateness for that purpose.

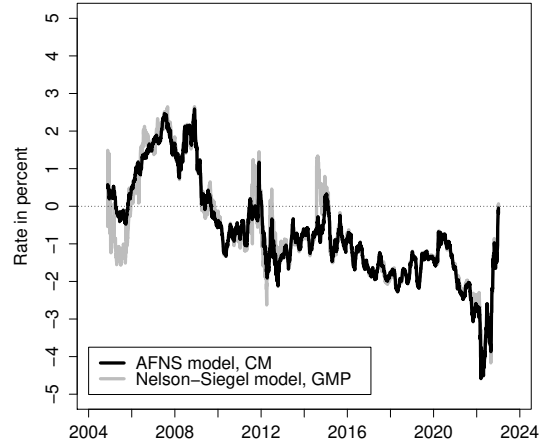
To proceed, we compare them to the fitted OAT€ zero-coupon yields constructed in a recent paper by Grishchenko et al. (2025, henceforth CMP).¹ For their yield curve construction, CMP use a standard Nelson and Siegel (1987) yield curve with four parameters fitted to the observed OAT€ prices for each day in isolation. They consider the same 19 French OAT€s that we have in our sample, and they report fitted yield curves for the period from November 17, 2004, to February 21, 2023, for integer maturities from one year up to twenty years. Aligning our constructed yield data with theirs, we get matching yield curves for a total of 4,723 days covering the period from November 17, 2004, to December 30, 2022.

In Figure 8, we compare the fitted real yields at four representative maturities: one year, two years, five years, and ten years. For the one-year real yield series shown in Figure 8(a), we see persistent major differences between the two yield estimates during the first ten years until 2015. Visually, it is clear that the series estimated by GMP is the source of the

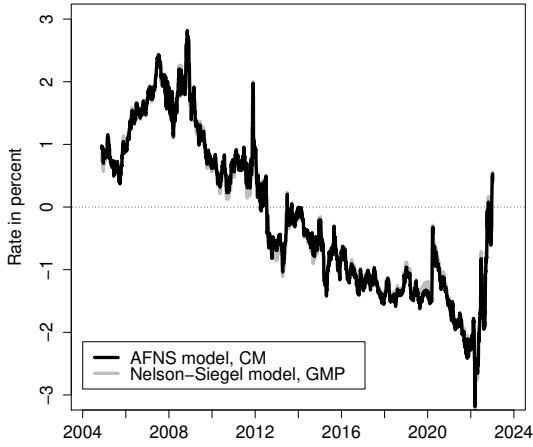
¹We thank Olesya Grishchenko for sharing the data.



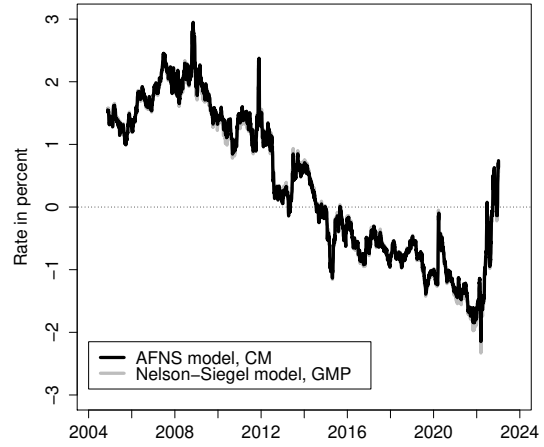
(a) One-year yield



(b) Two-year yield



(c) Five-year yield



(d) Ten-year yield

Figure 8: Comparison of Fitted OAT€ Zero-Coupon Yields

Illustration of the fitted zero-coupon yields implied by the independent-factors AFNS model described in Appendix D estimated based on our benchmark sample of daily data covering the period from October 31, 2002, to December 30, 2022. Also shown are the fitted real zero-coupon yields constructed by GMP using a standard Nelson and Siegel (1987) yield curve model based on daily prices for the same 19 French OAT€s included in our sample. In both cases, the shown period covers data from November 17, 2004, to December 30, 2022, a total of 4,723 daily observations.

difference as it has a correlation of 70.5 percent with the difference series, while the series estimated by the AFNS model has a low correlation of 3.8 percent with the one-year difference series. This difference between the constructed zero-coupon yields is also visible at the two-year maturity shown in Figure 8(b), but much less pronounced. Importantly, there are no

Maturity	Mean difference	MAD	Minimum difference	Maximum difference	Correlation in levels	Correlation in changes
1-year	-26.71	83.04	-500.26	459.08	0.736	0.058
2-year	0.00	20.01	-181.85	154.10	0.965	0.312
3-year	1.91	9.26	-53.82	77.47	0.995	0.667
4-year	0.57	6.29	-27.47	42.11	0.999	0.771
5-year	-0.32	4.74	-25.56	36.19	0.999	0.802
6-year	-0.47	3.87	-25.68	35.82	0.999	0.823
7-year	-0.15	3.46	-24.15	35.75	0.999	0.838
8-year	0.39	3.33	-22.12	34.73	0.999	0.848
9-year	0.98	3.34	-20.14	33.32	0.999	0.853
10-year	1.51	3.45	-18.34	31.72	0.999	0.856
11-year	1.93	3.53	-16.89	30.26	0.999	0.858
12-year	2.23	3.54	-16.64	29.13	0.999	0.858
13-year	2.39	3.48	-18.14	27.98	0.999	0.859
14-year	2.41	3.38	-19.65	26.85	0.999	0.858
15-year	2.31	3.24	-21.01	25.68	1.000	0.858
16-year	2.10	3.10	-22.33	24.50	1.000	0.857
17-year	1.78	2.97	-26.20	23.33	1.000	0.856
18-year	1.37	2.88	-30.12	22.18	0.999	0.854
19-year	0.87	2.84	-34.03	22.64	0.999	0.851
20-year	0.29	2.87	-38.02	23.07	0.999	0.848

Table 3: Summary Statistics of Fitted OAT€ Zero-Coupon Yield Comparison

The table reports the summary statistics of daily yield difference series of constructed real zero-coupon yields at integer maturities from one year to twenty years. The first data set contains the fitted real zero-coupon yields implied by the independent-factors AFNS model described in Appendix D estimated based on our benchmark sample of daily data covering the period from October 31, 2002, to December 30, 2022. The second data set contains the fitted real zero-coupon yields constructed by GMP using a standard Nelson and Siegel (1987) yield curve model based on daily prices for the same 19 French OAT€s included in our sample. In both cases, the considered period covers data from November 17, 2004, to December 30, 2022, a total of 4,723 daily observations.

material differences between the constructed yield series at the five- and ten-year maturities as documented in Figures 8(c) and 8(d). Finally, we note that the differences are greatly diminished after 2015 when a sufficient number of OAT€s are trading. At that point, CMP’s approach for construction yield curves with data for each trading day used in isolation starts to become comparable to our one-step approach that leverages the information in the full panel of OAT€ prices, which is strongly recommended based on the analysis in Andreasen et al. (2019).

Comparing the constructed yields for all twenty available maturities produces the summary statistics reported in Table 3. The main differences pertain to the short end of the

yield curve, while the constructed yields at the four-year maturity and up are very similar and highly positively correlated both in daily yield levels and in daily yield changes. This comparison also represents a useful sanity test: CMP and we are clearly relying on the same sample of OAT€ prices; otherwise the constructed yield curves would not be similar to the extent documented in Table 3.

Crucially, the one-step estimation of the AFNS model provides not only a close fit in the important five- to ten-year range widely used to construct medium- and long-term breakeven inflation rates, but also for the estimates of the shorter-term real yields that we rely upon in the construction of our market-based measure of the stance of monetary policy.

In summary, we conclude that our one-step estimation approach based on the AFNS model produces fitted real zero-coupon yields of very high quality.

References

- Andreasen, Martin M., Jens H. E. Christensen, and Glenn D. Rudebusch, 2019, “Term Structure Analysis with Big Data: One-Step Estimation Using Bond Prices,” *Journal of Econometrics*, Vol. 212, 26-46.
- Grishchenko, Olesya V., Franck Moraux, and Olga Pakulyak, 2025, “How Stable Inflation Expectations are in the Euro Area? Evidence from the French Bond Market,” Manuscript, Banque de France.
- Nelson, Charles R. and Andrew F. Siegel, 1987, “Parsimonious Modeling of Yield Curves,” *Journal of Business*, Vol. 60, No. 4, 473-489.